Trinity College Dublin
Coláiste na Tríonóide, Baile Átha Cliath
The University of Dublin

Investigating Failure Mechanisms, Defect Tolerance and Repair of Plant Stems for Practical Applications

A thesis submitted to

the Department of Mechanical & Manufacturing Engineering

Trinity College Dublin, the University of Dublin

in partial fulfilment of the requirements for the degree of

Doctor of Philosophy

By

Timothy Hone

Supervisor:

Professor David Taylor

2022

Declaration

I declare that this thesis has not been submitted as an exercise for a degree at this or any other university and it is entirely my own work.

I agree to deposit this thesis in the University's open access institutional repository or allow the Library to do so on my behalf, subject to Irish Copyright Legislation and Trinity College Library conditions of use and acknowledgement.

I consent to the examiner retaining a copy of the thesis beyond the examining period, should they so wish (EU GDPR May 2018).

_____

Timothy Hone

Signed on this the_____ day of _____ 2022

Timothy Hone

Abstract

Plants are complex in their biological composition and can provide inspiration for man-made engineering products. Designing bio-inspired products involves understanding the intricacies of plants' mechanical properties and response mechanisms to damage. There has been considerable work executed on investigating fully lignified trees, but little research has been performed on less lignified bushy species or young stems which have not yet lignified. This work presents four studies investigating mechanical properties and responses of plant stems when subject to three-point bending and complimented by a variety of staining and imaging techniques.

The research focused on fuchsia (*Fuchsia magellanica* var. *gracilis*) though tests were also carried out on elder (*Sambucus nigra*) and ash (*Fraxinus excelsior*). It was demonstrated that fuchsia could fail in one of two ways when subjected to three-point bending; a *greenstick fracture* or a *plastic hinge*. Phloroglucinol staining of the stems revealed that a greenstick failure is likely to occur in stems with relatively high density and stiffness. Further reasons for these complex failure mechanisms include the fact that the tensile strength of the stems is greater than the compressive and transverse strength. Mathematical and Finite Element modelling of these stems during three-point bending provided a method of quantifying the mechanical properties responsible. During three-point bending, MicroCT scans revealed that in failed stems an internal crack occurs before any external damage was visible. This internal crack provided inspiration for the development of a bio-mimetic self-healing structure. A common issue with modern self-healing structures is their inability to restrict healing agents from leaking out of the crack once it occurs. This research has demonstrated that developing a structure that intentionally fails from the inside out has the potential to mitigate this obstacle. The result was near perfect self-healing. Finite Element Analysis of the part of the structure under compression successfully predicted the early-stage deformation and the initiation of damage.

Defect tolerance is a prominent concern when developing modern engineering structures made of complex material such as carbon fibre and similar composite materials. Investigating how the mechanical properties of plants are impacted by damage can provide inspiration for the design of defect tolerant materials and structures. This study compared the defect tolerance of three species: fuchsia, ash and elder. Computational modelling of idealised engineering materials provided a framework in which to contrast the species against such materials. The

Timothy Hone

modelling further revealed that fuchsia was 39% more defect tolerant than a plastic, tough material such as steel. Self-repair is a ubiquitous process found in plant stems and has a magnitude of applications if replicated in modern materials. A pilot study on the repair of fuchsia revealed the self-healing capacity of a stem damaged from overloading in bending rather than cutting. Testing was made possible by the development of a portable three-point bending instrument which could be used on living plants in their natural environment. Healing mechanisms, including development of a callus and woundwood, were revealed using a combination of imaging techniques. Further data need to be gathered in the growing seasons of spring and summer before submitting the findings for publication, but an experimental protocol has been developed for future studies on plants of all species.

Timothy Hone

Timothy Hone

List of Publications

List of publications and conference presentations relevant to this work.

- T.Hone, M.Mylo et al. (2021) "Failure Mechanisms and Bending Strength of Fuschia magellanica Stems" J. R. Soc. Inter., 18(175).

- T.Hone, S.Kelehan et al. (2021) "Fracture and repair in a bio-inspired self-healing structure", Fatigue Frac EngMater Struct., 1:44, 3373-3383.

- T.Hone, D Taylor "Investigating defect tolerance and failure mechanisms in plant stems for practical applications", Society for Experimental Biology 2021 (Online)

- T.Hone, D Taylor "Investigating Defect Tolerance and Failure Mechanisms of Plant Stems for Practical Applications", Sir Bernard Crossland Symposium 2020 (Online)

- T.Hone, D Taylor "Investigating Defect Tolerance and Failure Mechanisms of Plant Stems", International Conference of Mechanics of Biomaterials and Tissues 2019 (Waikoloa Hawaii, U.S.)

Timothy Hone

Timothy Hone

Acknowledgements

First and foremost, I would like to thank my supervisor Professor David Taylor for providing me with the opportunity to undertake this exciting PhD topic. Professor Taylor was always available to offer new ideas, motivation, and guidance. I have learnt a vast amount from working with Professor Taylor and thoroughly enjoyed the entire process. I will be forever grateful for the experience.

I would like to thank Peter O'Reilly for all his time and insight into setting up imaging and mechanical testing equipment for a variety of experiments. To Mick Reilly thank you for all your help with so many aspects of the project. I would like to thank all of the workshop technicians JJ, Alex Kearns, Brendan Caffrey and Gabriel Nicholson for all the assistance with machining and developing custom testing equipment. Thank you to Paul Normoyle for all your help in developing the portable bending rig that was crucial to the project.

Thank you, Sarah Kelehan and Giulia Palomba, for all the assistance with experimentation. Many thanks to our friends in Freiburg University, Max Mylo, Olga Speck and Thomas Speck who have guided the biological side of the project which has added immense value.

Finally a big thank you to my parents and Sarah who not only provided uninterrupted support over the past three years, they helped with experimentation and documentation of results during the lockdown of 2020.

Timothy Hone

Timothy Hone

Contents

List of Figures

Timothy Hone

List of Tables

Chapter 1 Introduction

Plants have survived through millennia by means of evolution which has equipped them to endure the vast forces exerted by nature. Studying plants can provide inspiration for a magnitude of modern engineering materials and structures that can withstand large forces relative to their mass. One of the most prominent forces inflicted on plants is the bending moments exerted by wind. Therefore, loading stems in bending rather than other forms of mechanical testing is most likely to reveal a variety of responses that plants possess in their arsenal of defence mechanisms. Previous work has investigated how trees respond to loading and damage as timber is a commonly used material in traditional structures and modern engineering. However, little work has investigated the mechanisms behind how less lignified plant stems respond to loading and damage without catastrophic failure occurring.

This work was first inspired by that of Ennos & van Casteren [1-2] where a theoretical framework was developed to explain two main failure mechanisms observed during bending of plant stems, a *greenstick fracture* and *transverse buckling* (which I am calling a plastic hinge). Many of the conclusions were based on preliminary testing and data from the literature. This study builds on their work and employs rigorous mechanical testing, mathematical modelling, finite element analysis and a variety of imaging techniques to make detailed predictions surrounding the failure mechanisms of specific species.

Plants have complex structures being cellular, anisotropic and viscoelastic. While vascular channels are fundamentally responsible for the transport and delivery of food and water, they also provide structural durability to the plants, in a comparable way to fibres in fibre composites. The orthotropic properties primarily arise due to the orientation of different vascular channels combined with the composition of different cross-sectional tissue patterns. Studying the orientations of these vascular channels and cross-sectional tissue patterns has the potential to unlock an abundance of structural designs for modern fibre composite materials. Defect tolerance is an important concept to consider when developing modern engineering materials. What do I mean by defect tolerance? Defect tolerance is best described with an example. If we consider glass which is an elastic, brittle material, once a crack is inserted the mechanical properties are significantly compromised as the crack can rapidly propagate through the structure. However, if we take steel, being plastic and tough, once a crack is inserted it only has the effect of reducing the cross-sectional area by the length of the crack because steel has the ability to plastically deform. Plants, being fibre composites, are expected

to have impressive defect tolerance properties, however little research has been done to quantify these properties nor has an experimental protocol been developed.

Some living organisms are capable of self-repair. Self-repair has the potential to dramatically increase the lifespan of a material/object. In the literature, the focus of research has largely been in the response of plants to damage as a consequence of artificial cuts. Given that bending due to wind is expected to be the force most commonly experienced by plant stems, subjecting them to three-point bending should in large measure simulate bending caused by wind and cause similar effects. Using a combination of cross-sectional CT imaging of stem samples, mathematical modelling and FE analysis, enabled me to obtain a better understanding of how damage occurs and how plant stems self-repair. By modelling and analysing bending we also hope to provide inspiration for the design and manufacture of biomimetic materials. The findings are therefore of intrinsic interest to the biologist but also, very importantly, to the engineer. In the case of the engineer these include both obtaining a better understanding of the mechanical behaviour of natural materials and for designing and manufacturing biomimetic materials.

1.1 Thesis objectives

The overarching aim of this work is to provide bioinspiration to conventional engineering materials. This is achieved by understanding some of the complexities and intricacies of the structures found in nature, specifically those in plant stems. In order to achieve this goal, the following objectives are identified:

1. Observe and quantify the different failure mechanisms plants exhibit when their yield stress is exceeded during three-point bending.
2. Perform staining techniques and microscopy on the plant stems to determine their cross-sectional tissue patterns and material composition.
3. Model and replicate their failure mechanisms while accounting for complex non isotropic properties using both mathematical modelling and FE analysis.
4. Develop a methodology for quantifying defect tolerance in plant stems and compare to conventional engineering materials.
5. Create an experimental protocol to investigate and quantify the repair abilities of plant stems.

1.2 Thesis outline

This thesis is made up of four main chapters. The first three are journal papers and the fourth a pilot study presented in paper format.

Chapter 2	Is a published paper in the Journal of the Royal Society Interface that investigates failure mechanisms and bending strength of *Fuchsia magellanica var. gracilis* stems [3]. It presents new experimental data and makes use of a mathematical model and finite element analysis model to provide an in-depth understanding of the failure mechanism. Staining and microscopy from experienced botanists at Freiburg University provided an insight into the processes involved from a biological perspective.
Chapter 3	Is a paper published in Journal of Fatigue and Fracture of Engineering Material and Structures [4], describing a self-healing structure that took inspiration from the cellular structure of the fuchsia stems. This structure-level approach provides an innovative solution to introducing self-repair into engineering systems.
Chapter 4	Investigated defect tolerance of three plant species: Fuchsia magellanica var. gracilis (Fuchsia), Sambucus nigra (Elder) and Fraxinus excelsior (Ash). Here I created a novel methodology for quantifying defect tolerance in stems which could then be compared to idealised engineering materials. This paper has been submitted for publication in the Journal of the Royal Society Interface.
Chapter 5	Is a pilot study in developing an experimental protocol which can be used to ascertain the repair response of plant stems to damage caused by overloading in bending.
Chapter 6	Conclusions and outcomes of the work are summarised with impacts upon the field. Scope for future studies are then addressed where findings provide the most impact on the field of study.

1.3 Methodology

Selecting appropriate specimens:

Specimens were picked in Dublin, Ireland 2018-2020. Specimens were chosen that had diameters between 7-12mm and were roughly 1-2 years old. Young specimens were chosen as little work has been done on shrub type plant. Specimens that would be later subject to three-

point bend tests were chosen to have straight sections with no curves or bends. It was also ensured they had minimal ovality. This was all to ensure that the nominal bending moments could be calculated using conventional three-point bending formulae for a cylinder.

Preparing samples for testing and imaging:

For three point-bend tests, samples were cut to a length of 30cm, which was chosen as the span of the three-point testing rig was 15cm and therefore would therefore require additional length to allow for slippage during displacement. The ends of the specimens were immediately coated in Vaseline to minimise drying during transportation to the laboratory. Any nodes or flowers were removed and also coated in Vaseline. Specimens prepared for anatomical analysis were cut to short lengths (10-20mm) and either subject to Micro CT scans or staining and imaging techniques.

Subjecting specimens to three-point bend tests:

All plants were subject to three-point bend tests. Three-point bend tests were chosen as I feel it best resembles the forces experienced by plants in nature from wind and growing foliage. Many specimens had to be discarded from the results as they did not complete normal three-point bending. Reasons include, notches gripping the supports and causing horizontal forces and nonlinear displacement, specimens rotating on the supports during testing and specimens sliding out of the rig during bending. All three-point bend tests were performed on an Instron testing machine (type 3366, Norwood, MA, USA) equipped with a three-point bending apparatus. In some cases, further mechanical testing was required including tensile tests, compression test and Brazilian disk tests.

Performing anatomical analysis:

Micro CT was use to develop a 3D representation of the cross section of a stem before and after damage.
Toluidine blue staining and microscopy was used to provide a differentiation of the cell tissue. Phloroglucinol staining and microscopy provided an indication of the amount of lignification and vascular channels throughout the cross section.

Combining data for modelling:

Mechanical properties were extracted from the data from experimental testing, which were then used for modelling. This was assisted by the further understanding of the tissue composition in the stems from the microscopy.

Finite Element modelling:

The FE model involved creating a computational simulation of the three-point bend test in the laboratory. This was created in order to validate the experimental results and demonstrate the mechanical properties could be replicated. All FE modelling was performed on Ansys 19-21. The model for all experiments consisted of a constant circular cross section where symmetry was applied in two planes. All contacts between supports and stem were set to have a coefficient of friction of 0.15. A hexahedral-dominant mesh was applied and refined until mesh independence was achieved. This mesh type was chosen as it is best suited for bending applications. The model was assumed isotropic and homogenous and then solved statically.

Mathematical modelling:

Where possible mathematical modelling was performed to account for limiting factors of the FEA model which include complex non isotropic properties of the species. Models were then compared and combined to provide a more complete picture of the failure mechanism.

Conclusions:

Finally the experimental data was compared to the models in order to draw conclusions about the mechanical properties.

The methodology is illustrated in figure 1.1 by a flowchart.

1.4 References

1. Ennos AR, Van Casteren A. Transverse stresses and modes of failure in tree branches and other beams. Proc R Soc B Biol Sci. 2010;277(1685):1253–8.
2. van Casteren A, Sellers WI, Thorpe SKS, Coward S, Crompton RH, Ennos AR. Why don't branches snap? The mechanics of bending failure in three temperate angiosperm trees. Trees - Struct Funct. 2012;26(3):789–97.
3. Hone T, Mylo M, Speck O, Speck T, Taylor D. Failure mechanisms and bending strength of Fuchsia magellanica var. gracilis stems. *Journal of the Royal Society Interface.* 2021;18(175).
4. Hone T, Kelehan S, Taylor D. Fracture and repair in a bio-inspired self-healing structure. Fatigue Fract Eng Mater Struct. 2021 Dec 1;44(12):3373–83.
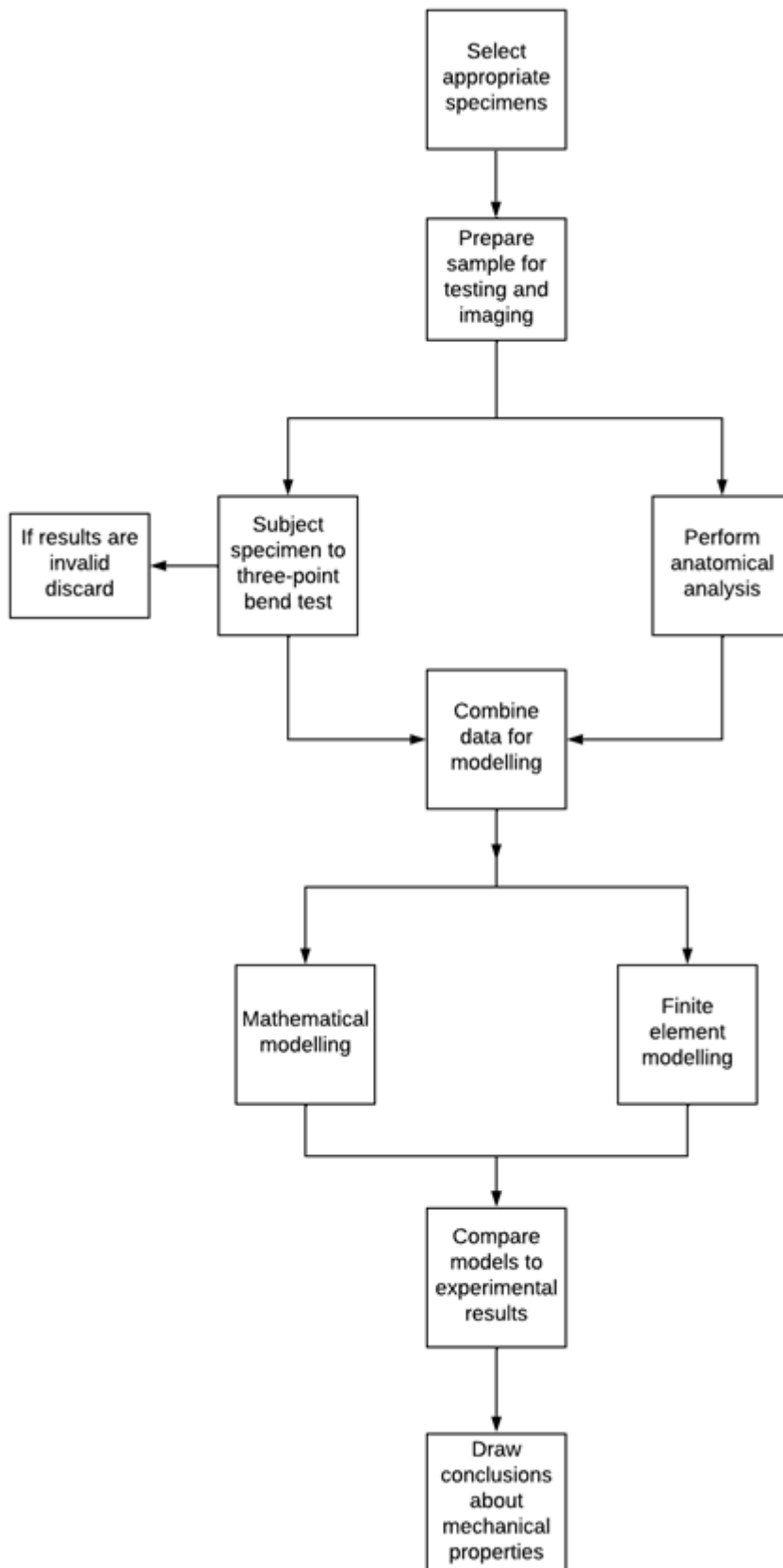
Figure 1.1: Flowchart of thesis.

Chapter 2 Failure Mechanisms and Bending Strength of *Fuchsia magellanica* var. *gracilis* Stems

Timothy Hone[1,], Max Mylo[2,3], Olga Speck[2,3], Thomas Speck[2,3] and David Taylor[1]*

[1]Trinity Centre for Biomedical Engineering, Department of Mechanical & Manufacturing Engineering, Trinity College Dublin, The University of Dublin, Ireland

[2]Plant Biomechanics Group, Botanic Garden, Faculty of Biology, University of Freiburg, Germany

[3]Cluster of Excellence *liv*MatS @ FIT—Freiburg Center for Interactive Materials and Bioinspired Technologies, University of Freiburg, Germany

Abstract

In the course of biological evolution, plant stems have evolved mechanical properties and an internal structure that makes them resistant to various types of failure. The mechanisms involved during damage development and failure in bending are complex and incompletely understood. The work presented builds on a theoretical framework outlined by Ennos and van Casteren, who applied engineering mechanics theory to explain why different woody stems fail in different ways. Our work has extended this approach, applying it to a detailed analysis of one particular species: *Fuchsia magellanica* var. *gracilis*. When subjected to three-point bending, stems of this species exhibited one of two failure mechanisms: a plastic hinge or a greenstick fracture. We developed a predictive model using a computer simulation and a mathematical analysis using the theory of plastic bending. Required material properties were obtained from tests, the literature and imaging techniques. We found that greenstick fractures are more likely to occur in more lignified stems with a higher density. We discovered a new failure mode: an internal crack caused by tensile transverse stress. This work helps in understanding how plants have evolved their bending resistance and may assist in the creation of novel engineering structures inspired by these principles.

Authors' contributions: TH carried out the mechanical and anatomical tests, the data analysis and carried out the FEA model, participated in the design of the study and drafted the manuscript. MM carried out the anatomical analyses, participated in the statistical analyses and critically revised the manuscript. OS and TS participated in the anatomical analyses and critically discussed the data and revised the manuscript. DT conceived of the study, designed the study, carried out the mathematical model, coordinated the study and helped draft the manuscript. All authors gave final approval for publication and agree to be held accountable for the work performed therein.

2.1 Introduction

Plant stems are exposed to various forces, such as their own weight, but also to additional external loads such as wind, rain, snow or sitting animals. They have evolved to be strong, light and to tolerate damage without catastrophic failure (1). Bending is one of the principal types of environmental loadings experienced by the stems of trees and other above ground plant organs. Therefore, analysis of their mechanical performance should mostly concentrate on the effect of applied bending moments on deformation and failure.

Trees and woody shrubs have stems, which are typically circular in cross-section. Their hierarchical structuring covers 12 orders of magnitude from the chemical composition of the cell wall (size range 10^{-10} m) to the macroscopic stem structure (size range: 10^2 m] (1). Most impact on the mechanical properties in general and the fracture behaviour in particular comes from the biochemistry and ultrastructure of the cell walls, which are made up of cellulose, hemicellulose, pectin and in secondary woody cell walls also lignin (2). The wood cylinder, which governs the mechanical properties of a plant stem consists predominately of longitudinal tube-like elements (tracheids, vessels, wood fibers in angiosperms) which run parallel to the stems longitudinal axis. They function as water conducting (vessels, tracheids) and/or stabilizing elements (tracheids, wood fibers) and form together with the horizontally arranged wood rays a complex 3D-network of hollow micro-tubes with varying wall thickness and central cavity (1). Due to this structuring multifunctional woody plant stems can be considered from a mechanical point of view as porous structures, in which ultrastructure and biochemical set up of the lignified cell walls of tracheids, vessels and wood fibers govern the mechanical properties (1,2).

The present work investigates the failure mechanisms experienced by *Fuchsia magellanica* var. *gracilis* (LINDL.) L.H.BAILEY (later called *F. magellanica*) when subjected to three-point bending.

Despite the stems having a greenish-reddish outer colour they are essentially woody structures. The majority of the cross section is highly lignified with (nearly) no living cells. In line with previous research (1,2) we will assume that the material is homogenous on the macroscopic scale, with the same mechanical properties throughout, though in reality the stems do possess a central parenchymatous pith and a thin outer cortex and bark layer composed of living parenchyma cells which are relatively flexible and soft (3).
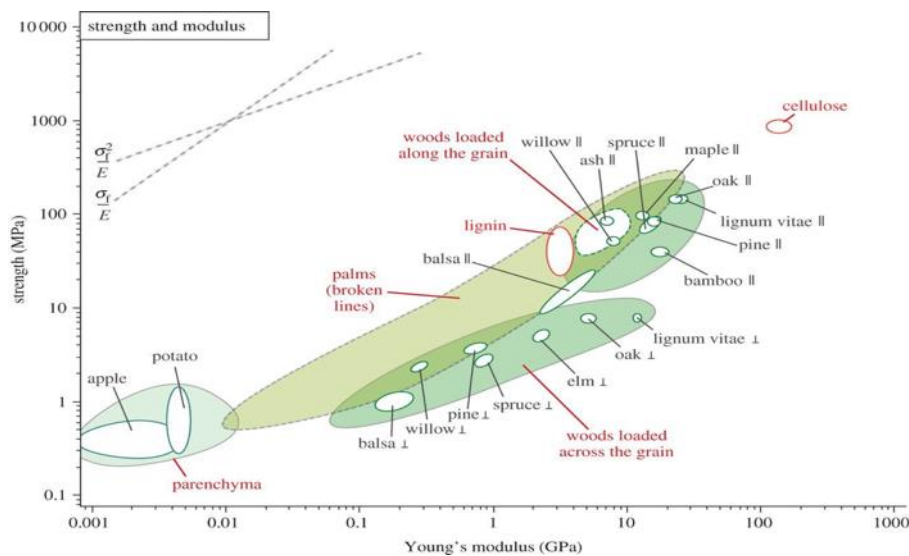
Figure 2.1: Overview of the relation between strength and stiffness (Young's modulus) of plant tissues and related plant groups (2,3).

Woody plants demonstrate a wide range of mechanical properties, as summarised in figure 2.1 which shows a broad overview of their strength and stiffness (Young's modulus). Many properties and some failure mechanisms have been measured and documented previously (e.g (4–11)), though most have concentrated on wood material, which has been dried for commercial use. We chose *F. magellanica* for our work because it was readily available and (as will be shown below) its mechanical properties lie in the mid-range of those shown here, being typical of many shrubs and small trees. *F. magellanica* are traditionally grown for ornamental purposes and therefore there is little information surrounding their mechanical properties. Whereas previous work has examined similar failure mechanisms in trees which have more highly lignified material.

Because of the anatomical heterogeneity, wooden materials display considerable mechanical anisotropy in radial, tangential and longitudinal direction. Strength and stiffness are typically an

order of magnitude greater in the longitudinal direction (parallel to the stem's long axis) than in orthogonal directions (12,13). Though there are some differences between the radial and tangential directions, in what follows we will consider these together as the "transverse" direction, for simplicity. Like many fibrous materials plant stems are relatively strong and brittle when loaded longitudinally in tension, weaker and more plastic in compression (12). These variations in properties depend on the loading direction and sign, creating considerable challenges for the understanding of their mechanical behaviour, especially their strengths and modes of failure.

The work described in the present study was inspired by the study of Ennos & van Casteren (12,13). They developed a theoretical framework to explain the strength and failure mechanisms of woody stems loaded in bending, supporting their predictions with experimental data from the literature. Their work can be described as "semi-quantitative" in that it allowed them to predict general trends in the data from different wood species rather than making detailed predictions for any one species. Two failure mechanisms were observed, which they referred to as "greenstick fracture" and "transverse buckling" (figure 2.2).
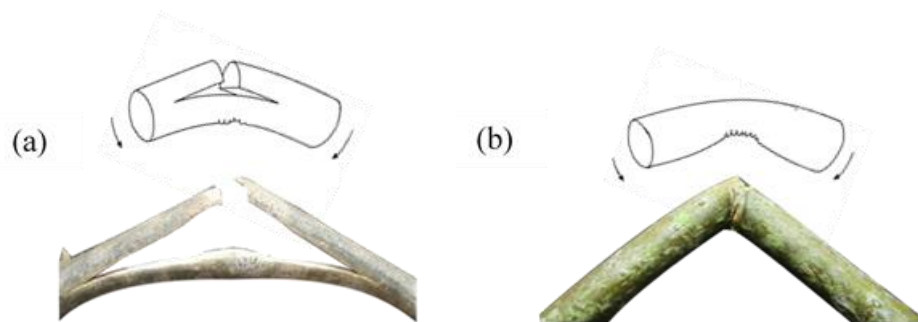
Figure 2.2: (a), Greenstick fracture. (b), Transverse buckling (plastic hinge) (12,13) .

The "transverse buckling" mode occurs when the stem yields through-thickness, allowing extensive plastic deformation to occur. In what follows we will refer to this failure mode as "plastic hinge", because this is the common engineering terminology, frequently applied to consider plastic bending failures in metals and polymers (14). Because, as noted above, wood is weaker in compression than in tension, the stem begins to plastically deform on the concave side where the compressive stress in the longitudinal direction is greatest. Plasticity spreads through the section as a result of wood's low yield strength in the transverse direction, causing the initially-circular cross-section to become compressed into an elliptical shape (known as "ovalisation"). The side under tension load remains intact with no fracture occurring. The stem does not break but simply continues to bend at the hinge (12,13).

Greenstick fracture, which incidentally is also found in fracture of young, soft bones, occurs when a crack initiates in the tensile region on the convex side of the branch. The crack begins to propagate transversally through the stem until it approaches the midpoint of the stem; it then changes direction by 90 degrees and begins travelling parallel to the stems' longitudinal axis. This type of fracture only happens after a certain amount of plastic-hinge behaviour has already occurred (12,13).

Ennos and van Casteren [8], [9] analysed these two failure modes using the elastic mechanics theory of bending beams and drew general conclusions, which they applied to data from the literature [1]. Van Casteren *et al.* tested three angiosperm trees growing in temperate regions: ash (*Fraxinus excelsior*), hazel (*Corylus avellana*) and white willow (*Salix alba*) (13). Willow, with the least dense wood of the three species, failed by forming a plastic hinge. The two other species failed generally by greenstick fracture. They showed that this difference in behaviour is due not so much to the absolute mechanical properties but to their relative values. Higher density wood is able to better resist the transverse compression as a result of a higher ratio of transverse compressive strength to longitudinal tensile strength.

The objective of the present work was to apply and extend the above theory to make detailed predictions of the behaviour of one chosen species: *F. magellanica* var. *gracilis*. The specific aims were to predict the entire stress/strain curve for stems loaded in bending, and to predict the occurrence of plastic hinge and/or greenstick type failure modes. The approach was to conduct a detailed series of mechanical tests to establish relevant material properties and failure modes and to develop a method of prediction, which combined computer simulation and mathematical modelling.

2.2 Materials and Methods

2.2.1 Plant material

Stems of *Fuchsia magellanica var. gracilis* (LINDL.) L.H.BAILEY (later called *F. magellanica*) were collected from Dublin, Ireland in March 2019. The stems were on average two years old. *F. magellanica* is a flowering subshrub, which is widely cultivated in temperate regions.

2.2.2 Mechanical analyses

Straight sections of stems were chosen, having diameters in the range 7-8 mm. The samples were stripped of flowers and leaves and the stem ends coated in Vaseline to minimize drying

effects during transportation to the laboratory. A total of 11 samples were measured. On the same day the stems were then placed in an Instron testing machine (type 3366, Norwood, MA, USA) equipped with a three-point bending apparatus as shown in figure 2.3a and an 8 kN load cell. The span was set to 15 cm, being at least 15 times the diameter of the stems tested, ensuring conformance to standard elastic bending theory. Samples were cut at the most cylindrical sections of branches to eliminate movement and any that displayed movement were instantly discarded. Samples were subjected to a constant displacement rate of 40 mm/min until failure whilst monitoring the load continuously. Displacement and force data were sampled at 20 Hz. The same Instron, load cell and data acquisition rate was used for all mechanical tests.

The same apparatus and specimen type was used to conduct cyclic loading tests. Samples were loaded to a given displacement, which was held for 30 seconds and then unloaded by retracting the loading point at the same rate. The test was paused for another 30 seconds and then the specimen was loaded again. This process was repeated for 6 cycles in total.

Bending stress and strain values were calculated using the standard formulae for elastic loading of beams:

$$\sigma_B = \frac{Mr}{I} = \frac{FL}{\pi r^3} \qquad \text{(Equation 2.1)}$$

$$\epsilon_B = \frac{6D2r}{L^2} \qquad \text{(Equation 2.2)}$$

Where σ_B is the bending stress, ϵ_B is the bending strain, M is the bending moment, F is the applied force, L is the support span, r is the radius of beam, I is the second moment of area (measured using a vernier callipers) and D is the maximum deflection of the centre of the beam. Young's Modulus was then calculated using these values. I was calculated based on measurements taken from the stem using a vernier callipers.

A Brazilian disk test was executed by compressing the stems in the radial direction. The test was performed with the intention of studying failure due to indirect tensile forces that arise in the stem when experiencing compression forces. The maximum tensile stress experienced before cracks begin to propagate across the cross section represents the transverse strength of the interface between the fibres.
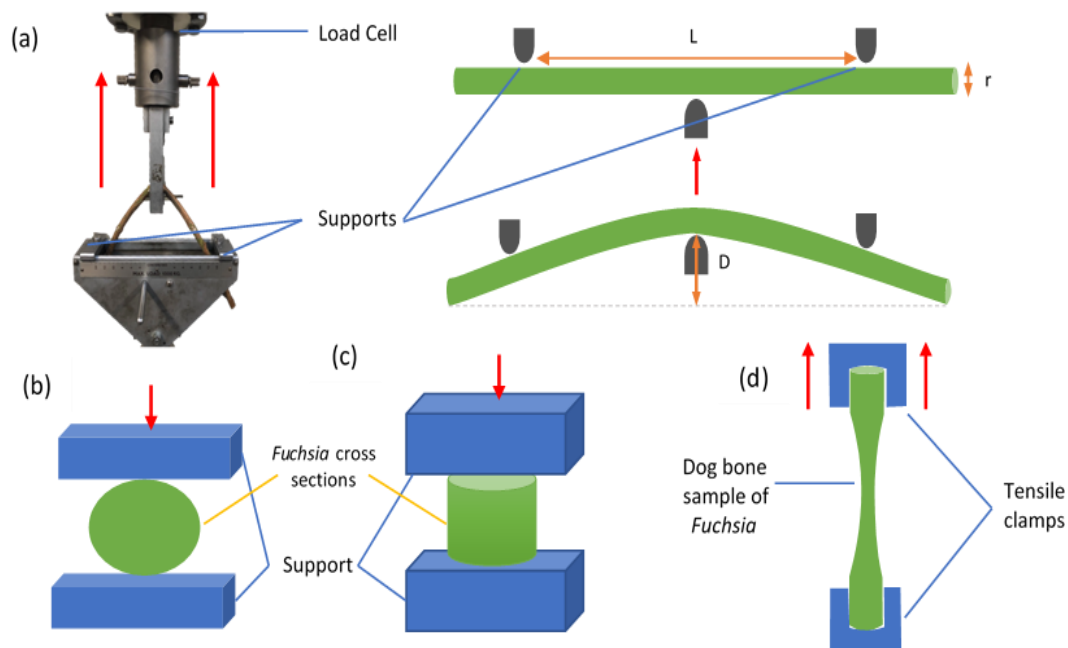
Figure 2.3: (a) Image of three-point bending rig with graphical illustration (supports spaced at 15 cm apart with load cell pulling from centre), (b) Brazilian disk test in radial direction on cross section of Fuchsia, (c) Compression test in longitudinal direction, (d) Tensile test on Fuchsia stem

The formula for calculating the splitting tensile strength σ_t in this test is ((15,16)):

$$\sigma_t = 0.636 \frac{P}{Dt}$$

(Equation 2.3)

Where P is the load (N) at failure, D is the diameter of the specimen and t is the thickness of the test specimen. The test was performed using the same Instron and load cell on samples of *Fuchsia* stems cut to 7 mm in length at a rate of 5 mm/min (figure 2.3b).

Longitudinal compression tests were also performed on specimens that were carefully cut to a length of 10 mm using a precision bandsaw and a miter gauge, which ensured cuts were parallel and at a 90° angle to the longitudinal axis of the stem. Tests were executed at a rate of 5 mm/min (figure 2.3c) and displayed consistent curves, indicating the method was effective.

Longitudinal tensile tests were performed by cutting waisted "dog bone" specimens which had either end embedded in resin for improved grip in the Instron jaws without damaging fibres. The samples were cut using the precision band saw and miter gauge to standard dog bone shape (ISO 527:2012). These were tested at a rate of 20 mm/min (figure 2.3d). Samples suddenly failed consistently with clean fracture through the cross section, within the gauge length, indicating the reliability of the method. Taking the maximum load from this test, the tensile failure stress could be obtained.

2.2.3 Anatomical analyses

Evaluating the stems' cellular composition involved two staining techniques: toluidine blue and phloroglucinol. Samples for toluidine blue stainings were infiltrated and embedded in Technovit (a fast curing cold polymerizing 3-component polymer resin; Technovit 7100, Kulzer Technik, Hanau, Germany) for two weeks. Once cured, sections five microns thick were cut using a rotatory microtome (custom-built, Technical Workshop, Institute of Biology II/III, University of Freiburg, Germany). The sections were then stained using a solution of 0.05% aqueous solution of toluidine blue for three minutes and later rinsed with distilled water. Binding to electrons, it enables the differentiation between tissues with different electron densities. Cytoplasm, RNA and un-lignified cell walls stain red while DNA structures and lignified tissues stain blue or green-blue. Macroscopic images of the stained section were captured using a Stereo microscope (Olympus SZX9, Olympus corporation, Tokyo, Japan) and then photographed with a microscope camera (DP71, Olympus corporation, Tokyo, Japan) by using cell[D] Imaging software (version 2.6, Olympus Soft Imaging solutions GmbH, Münster, Germany).

Phloroglucinol staining can be employed on freshly cut stems. These were cut using a handheld microtome in 25 micron sections and stained using a solution containing 5 g phloroglucinol in 100 ml of 92% EtOH and a few drops of hydrochloric acid (staining time of 30 seconds). Phloroglucinol-staining highlights specifically lignified cell walls in red. The stained slices were photographed and examined using a light microscope (Primo Star, Carl Zeiss Microscopy GmbH, Jena, Germany) with a microscope camera (AxioCam ERc 5s, Carl Zeiss Microscopy GmbH, Jena, Germany).

An Image J (1.8.0) analysis was performed on the images of sections stained with phloroglucinol to measure the contrasting stained areas of lignified tissue and porosity. This involved using a binarization filter (watershed) and the built-in particle analyses.
Micro CT scans were performed on sections that had been deflected during three-point bending to a displacement of 40 mm, giving a bending strain of 0.07-0.09, at which point a plastic hinge had occurred but not a greenstick fracture. The micro CT scanner was a single tube Scanco μCT 40 (Scanco Medical, Brüttisellen, Switzerland) operating at a voltage, current and power of 70 kVp, 114 mA and 8 W, respectively. The scanner was set to take 200 slices from the specimen placed in a field of view 12.3 mm in diameter with a voxel size of 8 μm. The scans were reconstructed and rendered using Dragonfly ORS (Object Research Systems, Quebec, Canada), applying artificial colour to different densities to highlight structural features.

2.2.4 Determination of density

Fresh density was established by taking uniform sections and dividing their weight by volume. The volume was found by taking diameter measurements using a vernier callipers at three equally spaced intervals across the stem and the measurements were averaged. The weight was found using a precision weighing scale.

2.2.5 Finite element analyses
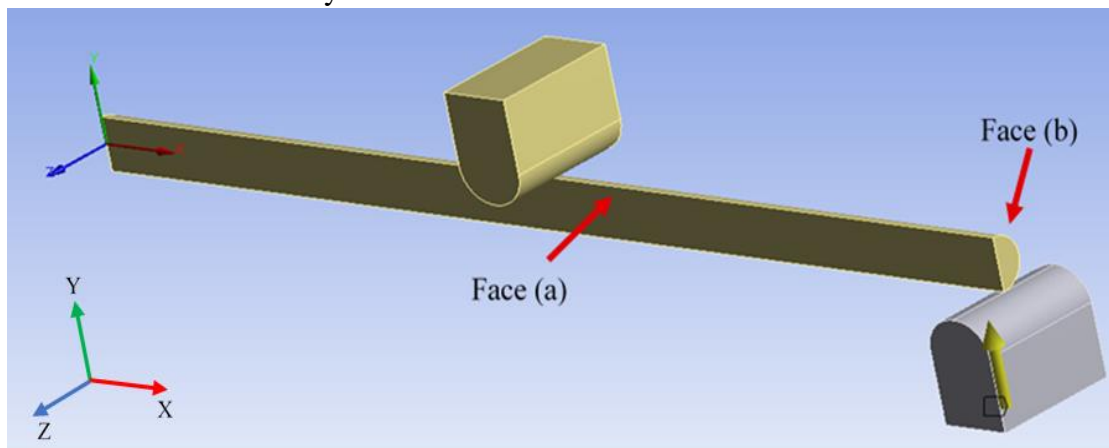
Figure 2.4: Geometry of the FE model. Face (a) is confined to movement in the Y, X planes only and Face (b) is confined to movement in the Z,Y planes. Yellow arrow indicates direction of displacement.

A finite element (FE) model of the stems was developed using Ansys 19.2. A single model was created, representing the geometry and material properties of a typical specimen. A constant circular cross section of diameter 8mm was used. Symmetry in two planes was applied for computational efficiency. As shown in figure 2.4 face (a) is confined to movement in the X and Y planes only and face (b) to the Z and Y planes only. Initial contact points between the stem and loading support (on the symmetry plane) were set to be bonded. All other contact was between the stem and supports were set to be frictional with a coefficient of 0.15. The supports were modelled as rigid bodies. A hexahedral-dominant mesh was applied and refined until mesh independence was achieved. The mesh had a total of 29,142 nodes and 15,385 ten-noded tetrahedral elements of size of 2 mm x 1.15 mm x 0.5 mm. 10 elements were used through the thickness and 130 along the length. Based on our test results (see Results section) the material was assigned a Young's modulus of 2258 MPa and a yield strength of 16.49 MPa. Bilinear elastic/plastic behaviour was assumed with no work hardening. Since we did not measure Poisson's ratio a value of 0.37 was used based on published data for wood (11). The model FEA model was assumed isotropic due to software limitations and then solved statically.

2.2.6 Statistics

Statistical tests were performed using Excel (2019), comparing material properties of the different failure mechanisms. Data were first tested for normality using skewness and kurtosis tests. Since some datasets did not show normal distributions the Mann-Whitney U test was used to test for differences. Significance level is defined at p = 0.05.

2.3 Results

2.3.1 Mechanical analyses

A total of 11 stems of similar diameter were tested in three-point bending, of which, 3 (27%) failed by greenstick fracture whilst the remaining 8 failed with a plastic hinge. Table 2.1 summarises the measured mechanical properties. Figure 2.5 shows two typical stress/strain curves from stems failing with the two different mechanisms.
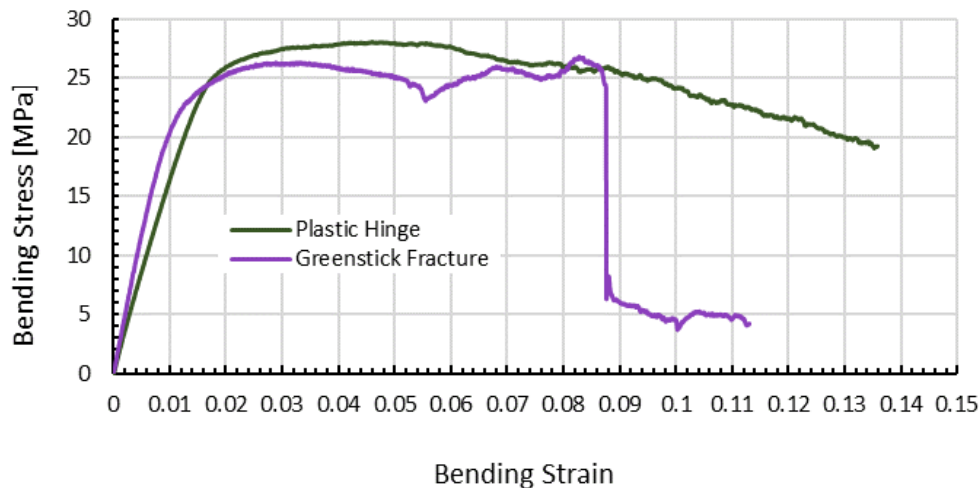
Figure 2.5: Typical stress strain curves for samples failing by greenstick and plastic hinge mechanisms.

Stems that failed by greenstick fracture displayed significantly larger Young's modulus (mean value: 3085.4 ± 623.2 MPa) than those exhibiting a plastic hinge (1948.9 ± 521.4 MPa) only (Mann-Whitney U test; U = 2, p = 0.041). Greenstick failures also exhibited a lower median yield strength and strain relative to plastic hinge failures, 15.5 MPa < 16.7 MPa and 0.00625 < 0.00705 respectively, although the groups were not shown to be significantly different (Mann-Whitney U test; U = 10, p = 0.68 and U = 7, p = 0.3, respectively).

*Table 2.1: Mechanical properties obtained from three-point bending tests, listed for all tests, samples that failed with a plastic hinge and samples that failed with a greenstick fracture. The mean value, the standard deviation and the number of samples (*n*) are given.*

	All specimens	*n*	Plastic hinge	*n*	Greenstick	*n*
Young's Modulus (MPa)	2258.8 ± 741.5	11	1948.9 ± 521.4	8	3085.4 ± 623.2	3
Yield strength (MPa)	16.49 ± 5.92	11	17.26 ± 6.75	8	14.43 ± 2.69	3
Yield strain	0.007 ± 0.003	11	0.007 ± 0.004	8	0.005 ± 0.002	3
Maximum stress (MPa)	30.34 ± 6.78	11	30.19 ± 7.59	8	30.77 ± 5.28	3
Strain at maximum stress	0.049 ± 0.020	11	0.050 ± 0.018	8	0.048 ± 0.024	3
Stress at a strain of 0.12 (MPa)	20.4 ± 9.0	8	20.4 ± 9.0	8	N/A	3
Stress at point of greenstick fracture (MPa)	25.79 ± 1.74	3	N/A	—	25.79 ± 1.74	3
Strain at point of greenstick fracture	0.076 ± 0.03	3	N/A	—	0.076 ± 0.03	3

Figures 2.6a and 2.6b show typical stress/strain curves from the tests conducted in longitudinal compression and tension, respectively. 6 samples were tested in compression where yielding occurred at stress and strain values of 11.38 ± 1.78 MPa and 0.06 ± 0.03, respectively. The stress reached a plateau at 12.55 ± 1.94 MPa and then dropped to a lower plateau at a stress of 7.09 ± 2.03 MPa commencing at a strain of 0.29 ± 0.05.
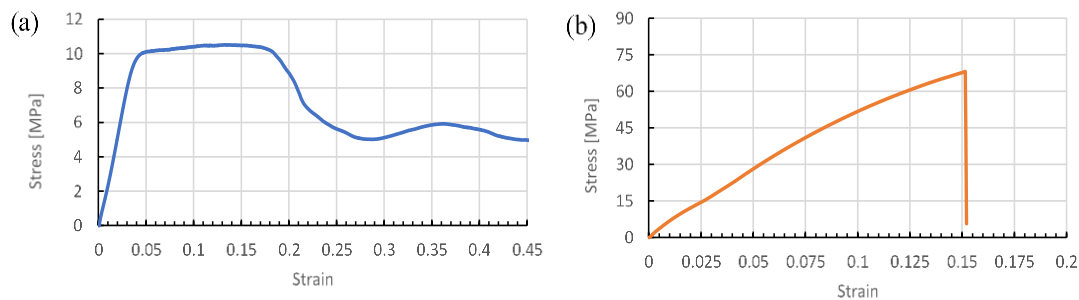
Figure 2.6: (a) Example of a typical compression test epitomising the loading stages experienced by samples with a diameter of 8 mm and a height of 10 mm. (b) Typical tensile test on dog bone samples cut from 8 mm diameter samples.

Accurate tensile tests were difficult to obtain due to the difficulty of clamping the ends of the samples securely without causing damage inflicted by the large clamping force required to grip the moist fibres. Of a large batch of tests performed on dog bone samples, 4 specimens failed within the gauge length. In tension, stems deformed in a linear elastic manner (see figure 2.6b) until sudden failure. An average tensile strength of 54.3 ± 11.20 MPa was obtained, indicating *Fuchsia* is much stronger in tension than compression, as is typical of wood(1), (12,13,17–19).
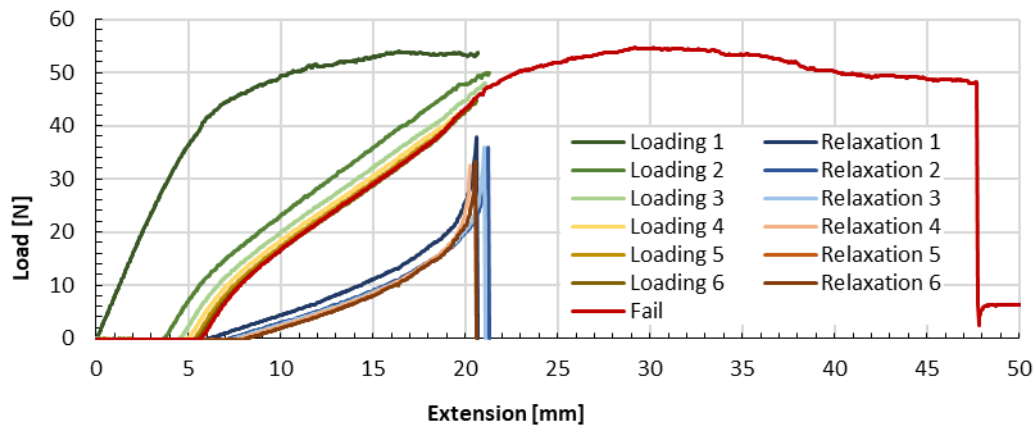
Figure 2.7: Typical cyclic loading test results for stems in three-point bending.

Figure 2.7 shows an example of the results from the cyclic bending tests. Initial loading shows a linear increase up to about 40 to 50 N, followed by a decreasing slope to a maximum force. Unloading begins with a very rapid reduction in force and finishes with an apparently permanent deflection, for the first loop about 4 mm. However, we found that if the test was terminated at this stage, the deflection returned to zero over a period of 10-15 minutes showing typical viscoelastic behaviour. There is considerable hysteresis in every cycle. After 6 cycles the sample was loaded to failure, displaying very similar behaviour to that of the samples in our normal monotonic bending tests.

2.3.2 Anatomical analyses

Micro CT scans captured from pre-bent *Fuchsia* specimens revealed a new failure mode: an internal crack which initiated near the centre and propagated transversally through the stem (figure 2.8). To our knowledge this failure mode has not been observed previously. By loading 6 stems to various amounts we found that this crack initiates at a bending strain of about 0.046. The typical appearance of thin-sections stained using toluidine blue and phloroglucinol is shown in figure 2.8. The toluidine blue shows the parenchyma cells in the pith and the bark and the more dense lignified wood tissue in between. Lignified cell walls are stained red using phloroglucinol staining. Vessel elements reveal as hollow and relatively large cells within the lignified tissue consisting of tracheids and wood fibres with no or much smaller central cavities. Specimens, which failed by greenstick fracture had a significantly lower percentage area of "vascular channels", ie. vessels, than those failing by plastic hinge ($1.87 \pm 0.5\%$ and $4.15 \pm 0.281\%$, respectively: Mann-Whitney U test; $U = 0$, $p = 0.0495$).
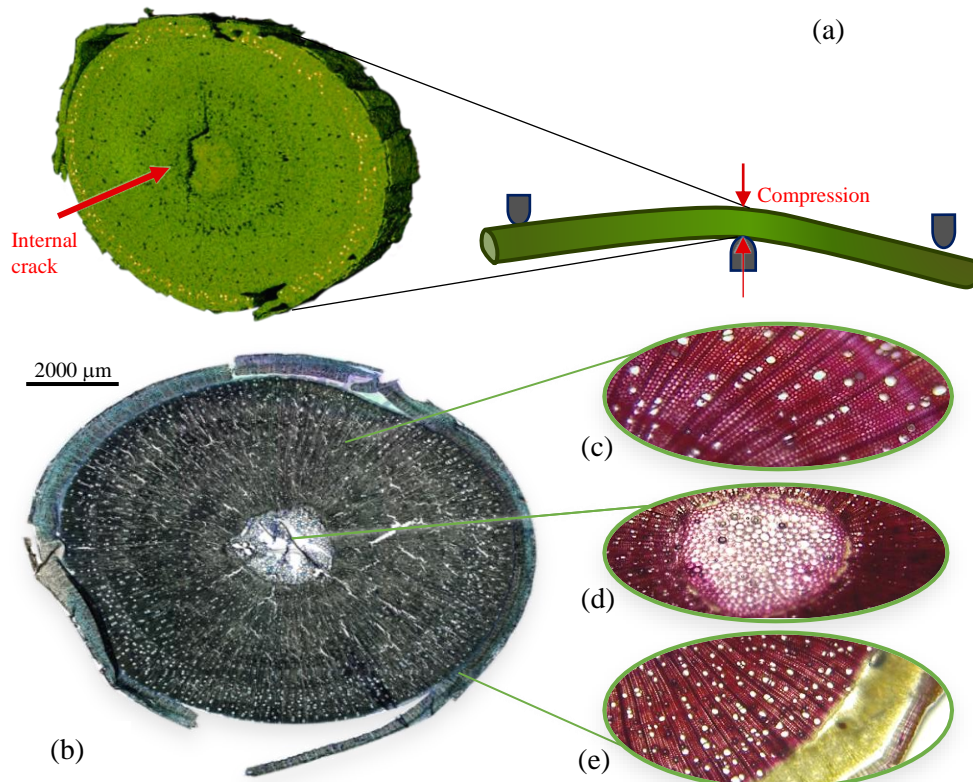
Figure 2.8: Anatomical analyses of stems of F. magellanica. (a) Micro CT scan captured from a stem bent to a strain of 0.05, revealing an internal crack in the centre (arrow). (b-e) Thin-sections of (b) an entire cross section stained with toluidine blue and (c-e) details stained with phloroglucinol (c) xylem with annual growth rings, (d) pith and (e) bark with phloem, cambium and xylem.

Density measurements revealed that specimens failing by greenstick had an average density of 1.181 ± 0.0636 g/cm^3, whereas specimens failing by plastic hinge had a slightly lower average density of 1.128 ± 0.0683 g/cm^3. This difference did not have statistical significance (Mann-Whitney U test; $U = 10$, $p = 0.2$) but it is consistent with the difference in vascular porosity and Young's modulus between these groups.

2.4 Modelling and Simulation

Theoretical modelling included the creation of a finite element model and also a mathematical model, which were then combined to give the final predictions. In both models the material was assumed to display yielding and plastic deformation, with no work hardening. In the mathematical model damage was assumed to occur at a specified strain value, reducing the compressive stress. These assumptions require some justification, as follows.

The geometry for the model was determined by averaging the diameter of the stems taken at regular intervals in different directions using a vernier callipers. Most stems had little to no variation in diameter along the length. The yield strength was taken to be 16.49 MPa, as measured in our bending tests, rather than the lower value measured in axial compression. This difference is commonly seen in composite materials and is usually attributed to differences in stressed volume and restraint. Since we were attempting to simulate bending tests the larger value was more appropriate. The results of the axial compression tests (figure 2.6a) demonstrate no work hardening and, after a certain amount of strain, the stress falls to about half the peak value. We included this reduced loading capacity in our models: the physical interpretation of the experimentally observed decrease is internal damage in the material, such as fibre buckling.

Our interpretation of the cyclic bending results (figure 2.7) is as follows. Whilst the shape of the stress/strain curve in our monotonic bending tests suggests that the material is yielding and undergoing plastic deformation, the cyclic tests show that the dominant feature is viscoelasticity. The apparent yield point and decreasing slope is due to viscous flow, as evidenced by the large hysteresis and sudden drop in force on unloading. The apparent plastic strain is found not to be permanent if sufficient time is allowed for all viscous relaxations. Despite this finding we have assumed yielding and plastic behaviour in our finite element analysis (FEA) and mathematical models. It is much easier to develop the predictions in this way, and we argue that this is valid for predicting the behaviour under monotonic loading, as the stress/strain behaviour of the material will be the same, though we would expect it to change if tested at a different loading rate. We chose a relatively low loading rate to maintain quasi-static conditions.

Figure 2.9 shows the results from the finite element analysis (FEA). A considerable amount of bending deflection occurs, and the stress distribution through-thickness is as expected. In figure 2.9b the bending stress/strain curve from the FEA is plotted along with the typical results from figure 2.5.

As we can see from figure 2.9b the FEA provides results, which are very similar to the experimental data. However, it has some important limitations. It does not model the material's considerable anisotropy, nor does it model the large difference between tensile and compressive behaviour. So it does not allow us to predict phenomena such as greenstick fracture or internal cracking.

(a)

(b)
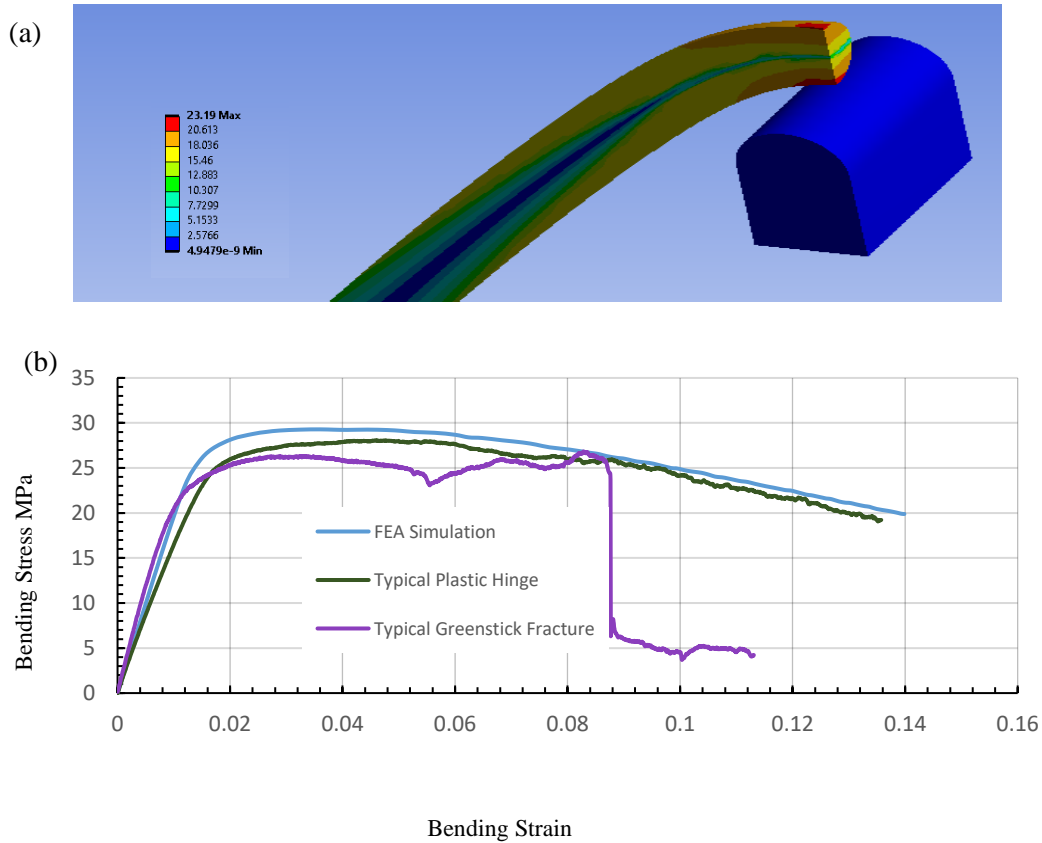
Figure 2.9: (a) Finite element model using symmetry with stress distribution (MPa for applied bending stress of 23.2 MPa), (b) Stress/strain curves, experimental and FEA.

Therefore, a homogenous mathematical model was developed, based on the mechanics of plastic bending. This type of analysis is well understood in engineering design, where it is often applied to metallic materials (e.g. (14)). Normally it is assumed that the material is isotropic and will first yield when the applied bending moment is large enough to exceed the yield strength of the material ($M = M_y$ when $\sigma = \sigma_y$) on the top and bottom surfaces (see figure 2.10). For $M > M_y$ a plastic region spreads inwards from both surfaces: in these regions the maximum stress does not increase beyond the yield stress. The strain however will continue to increase linearly. At $M = M_p$ (the plastic moment) yielding has spread throughout the section and a plastic hinge is formed.
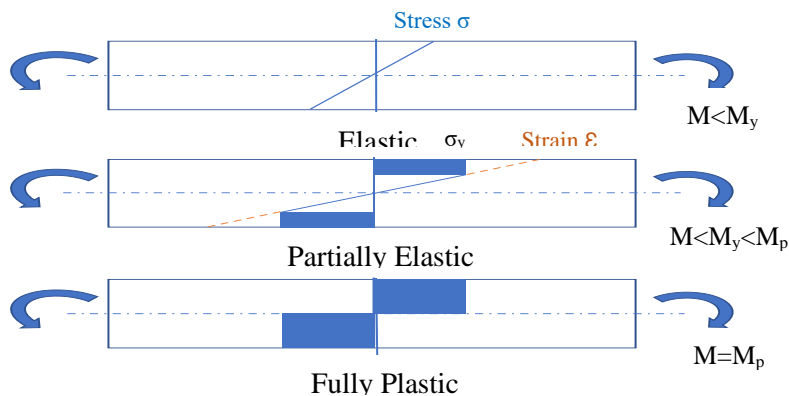
Figure 2.10: Illustration of classic plastic bending theory

Closed form solutions can be derived for simple cross sections such as circular, but here we developed a numerical solution so as to be able to add more complex material behaviour. We define distance x in the vertical direction with x = 0 in the centre of the beam. The neutral axis is located at x_n (equal to 0 if the material has the same yield strength in tension and compression). Yielding occurs at all $x > x_c$ (above and below the neutral axis) where x_c is the limit of the plastic region. In this region the longitudinal stress σ is equal to the longitudinal yield strength $σ_y$.

Outside the plastic region, the stress is elastic, equal to $σ_y$ at x_c and equal to 0 at x_n therefore:

$$\sigma = \sigma_y \frac{(x-x_n)}{(x_c-x_n)}$$
(Equation 2.4)

Assuming that plane sections in the bent stem remain plane (which is necessary to avoid separations in the material) the strain ϵ at all locations is related to the yield strain ϵ_y by:

$$\epsilon = \epsilon_y \frac{(x-x_n)}{(x_c-x_n)}$$
(Equation 2.5)

For a circular beam of radius r the horizontal width W is a function of x:

$$W = 2\sqrt{r^2 - x^2}$$
(Equation 2.6)

The bending moment dM in a small region of height dx is:

$$dM = \sigma W x dx$$
(Equation 2.7)

The total bending moment (sum of all dM) above the neutral axis must be equal to the total M below the neutral axis, to prevent rotation. The nominal bending stress (i.e. the stress on the top and bottom surfaces, assuming elastic behaviour) is given by the standard equation for bending beams (equation 2.1 above); the bending strain is given by equation 2.5 above with x = r.

The above equations were solved iteratively using a numerical procedure. Initially we assumed an isotropic material with the same yield strength in tension and compression. The results are shown in figure 2.12a, plotting the bending stress and strain normalised by their respective yield values. Our predictions agree with previous analytical solutions (6), which predict full plasticity at $M_p = 1.7\ M_y$.

The model was then developed to include the complex behaviour of our material. Figure 2.11a shows the assumed stress/strain behaviour in tension and compression, based on the data from figure 2.6. The region above the neutral axis will remain elastic as it is in tension, failing at a given stress value. The region below the neutral axis will yield as it is in compression. Because yielding occurs only on the compression side, this results in the neutral axis moving towards the upper surface (figure 2.11b) in order to maintain the necessary equality of moments above and below the neutral axis. The prediction is shown in figure 2.12b by the line marked "prediction elastic-plastic". The bending stress does not plateau as it did in the simpler prediction, but rather continues to increase, because the beam never becomes fully plastic. Next, a damage zone was introduced. Based on our test results (figure 2.6a), damage was assumed to occur at a strain of 3 times the yield strain, beyond which the stress decreased to $0.5\sigma_{yc}$. As seen in figure 2.12b (line marked "Prediction adding damage") this caused a large decrease in stress, with a local maximum around 1.93 and a slight upturn at high strain.
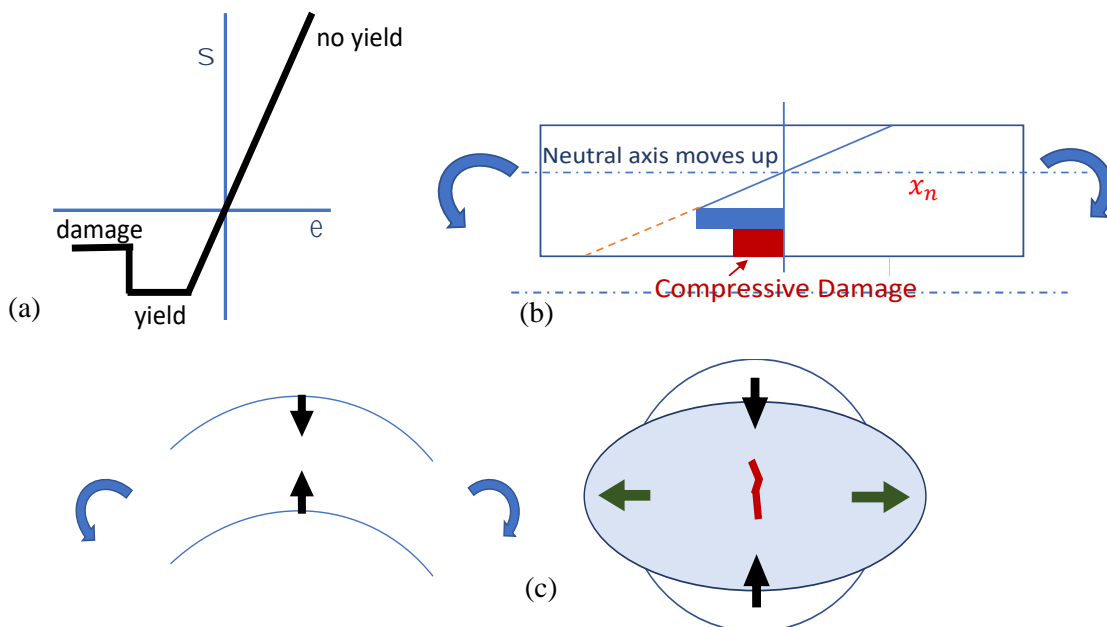
Figure 2.11: Modifications to the theory (a) Material model: yielding and damage in compression, no yielding in tension (b) Plastic and damage regions form on the compressive surface only, so the neutral axis moves up by xn (c) The circular cross section becomes oval, reducing the second moment of area I and creating transverse tensile stress, causing the internal crack to form.

The next phenomenon to be included in the model was ovalisation of the stem. As pointed out by Ennos et al. (12,13), a small transverse force always arises in a bending beam (16), resulting in a reduction in thickness and an increase in width, which is known as ovalisation (figure 2.11c). The force per unit length dF contributed by a small region of height dx is:

$$dF = cw\sigma dx \qquad\qquad (Equation\ 2.8)$$

Here c is the curvature of the beam, which can be found from standard bending theory. The transverse stress experienced by this region is found by integrating dF for all distances x from this region to the surface of the beam (Equation 2.1).

This effect is normally ignored because in isotropic materials it is negligible. But here it is significant due to the material's much lower stiffness and strength in the transverse directions. We did not measure the transverse compressive stiffness or yield strength for our material as it is practically difficult. We assumed (in line with published data on wood (Equation 2.2)) that the Young's modulus and yield strength in transverse direction were 8 times smaller than their longitudinal values. Transverse stress and strain can thus be calculated at all heights x in the beam, allowing for yielding if it occurs. Summing all strains allows the vertical compression of the beam to be predicted, and assuming constant volume then allows the horizontal expansion to be found, thus predicting ovalisation. We found that significant ovalisation only occurred after the material yielded transversely. Ovalisation has the effect of reducing the second moment of area (I) which is given by:

$$I = \int wx^2 dx \qquad\qquad\qquad \textit{(Equation 2.9)}$$

This reduces the moment (and thus the nominal bending stress) required for a given bending strain. This was added to the model: see figure 2.12b, line marked "Prediction adding transverse compression". This caused a significant reduction in stress, but only at high strain: the stress peak at 1.93 remained the same.

The final step in the modelling exercise was to combine this mathematical model with the finite element analysis. Since the FEA assumed an isotropic material with identical properties in tension and compression, it should have given a prediction identical to that of the model in figure 2.12a. The difference is due to the fact that the model assumes pure bending whilst the FEA used three-point bending. This difference is already well known (see for example (14)) and arises due to geometrical effects such as movement of the sample over the loading points. We introduced this into our mathematical model by reducing the bending stress for a given strain by a factor given by the difference between the prediction lines in figure 2.9b and figure 2.12a. This only becomes significant beyond the peak stress, when it causes the predicted stress to further decrease: see figure 2.12b line marked "Prediction adding 3PB correction".

Figure 2.12c shows the experimental results along with the final prediction including all the above factors. This provides a good match to the general shape of the experimental curves and, as Table 2.2 shows, it accurately predicts the stress at the peak and at a higher strain of 0.12. It

tends to underestimate the strain at the peak, though this peak is very broad and flat. It is not significantly better than the simple FE model, however it is much more realistic as we have been able to include several phenomena and demonstrate how they contribute to the shape of the curve.

(a)

(b)

(c)
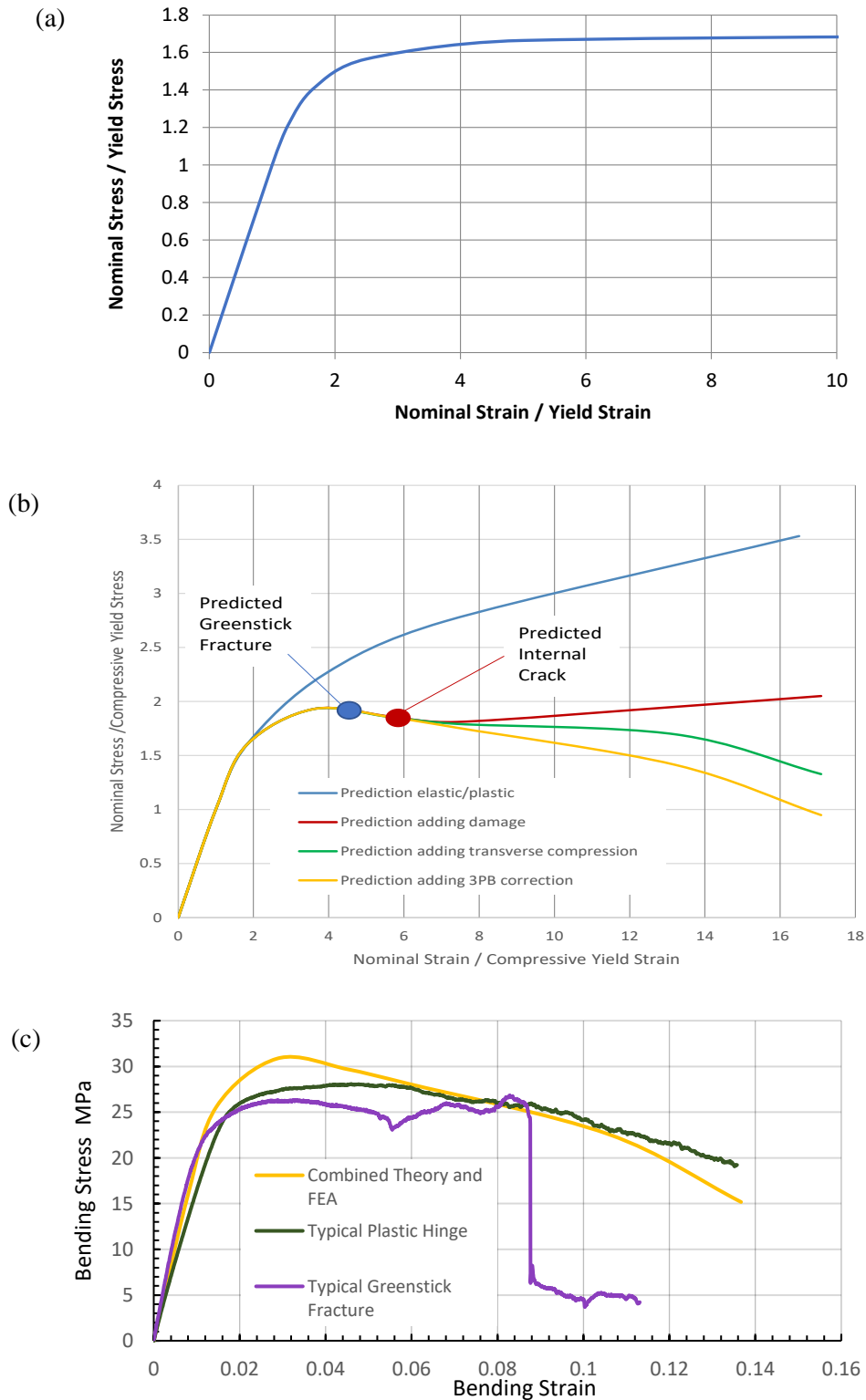
Figure 2.12: (a) Predictions from the mathematical model for a simple isotropic material. (b) Predictions adding various material and geometric effects. (c) Final predictions from the model compared with typical experimental data.

Another advantage of the model is that it is able to make predictions of two other phenomena, which we observed experimentally: greenstick fracture and the generation of an internal crack. Greenstick fracture is predicted to occur when the longitudinal stress on the tensile surface of the beam reaches the longitudinal tensile strength, which we measured to be 54.3 MPa. Figure 2.13a shows the predicted increase in this stress as a function of the nominal bending strain. The predicted failure point is indicated here and also on figure 2.12b. The model predicts the greenstick fracture will occur at a stress and strain of 31.3 MPa and 0.03 respectively. This closely matches the experimental stress (25.79 ± 1.74 MPa) and (as with the peak stress above) underpredicts the experimental strain (0.076 ± 0.03) for the onset of greenstick fracture.
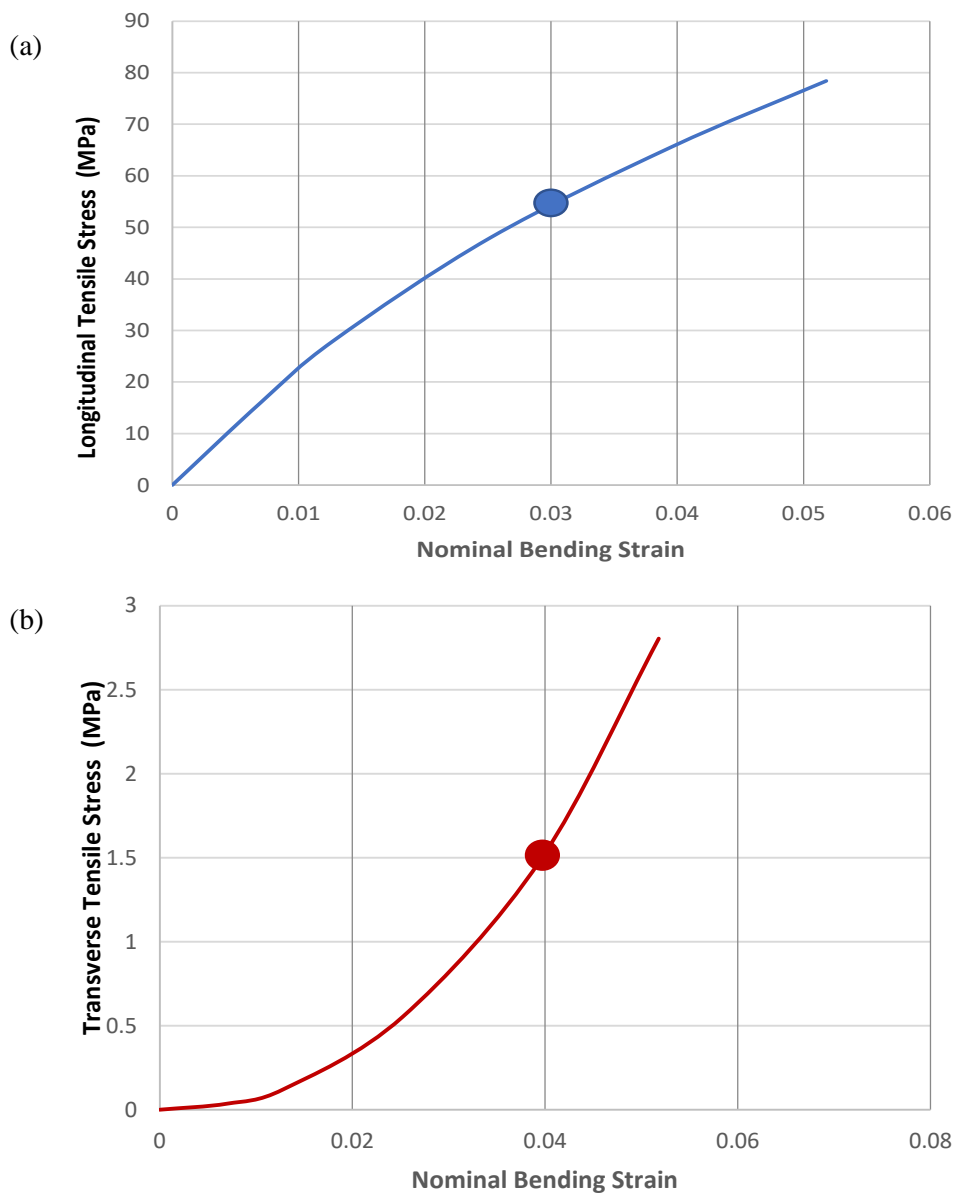
Figure 2.13: (a) Predicted longitudinal tensile stress on the convex surface, as a function of applied bending strain. The point indicates when failure (and thus greenstick fracture) will occur. (b) Predicted transverse tensile stress as a function of applied bending strain. The point indicates when failure will occur, causing the formation of an internal crack.

Ovalisation causes transverse tensile stress in the width direction (figure 2.11c), which can be estimated by noting a similarity to the case of a circular disc loaded in diametral compression, for which the maximum transverse tensile stress was given above in Equation 2.3. As mentioned in the results the measured transverse tensile strength was found to be 1.0-1.5 MPa upon crack initiation. Figure 2.13b shows how this stress is predicted to develop during bending, indicating the failure point here and on figure 2.12b thus predicting that this internal crack will form at a stress of 30.67 MPa and strain of 0.04. The actual value was determined from experimental testing to be 33.4 MPa indicating the model's accuracy.

Table 2.2: Model predictions compared to experimental results. Mean values ± standard deviation and

	Plastic Hinge $n = 8$	Greenstick fracture $n = 3$	Predictions (combined FEA and mathematical model).
Maximum stress (MPa)	30.19 ± 7.59	30.77 ± 5.28	31.8
Strain at maximum stress	0.050 ± 0.018	0.048 ± 0.024	0.029
Stress at a strain of 0.12 (MPa)	20.4 ± 9	N/A	19.5
Stress at greenstick fracture (MPa)	N/A	25.79 ± 1.74	31.3
Strain at greenstick fracture (/)	N/A	0.076 ± 0.03	0.033
Stress at onset of internal cracking (MPa)	33.4 ± 3.3	33.4 ± 3.3	30.67
Strain at onset of internal cracking (/)	0.046 ± 0.009	0.046 ± 0.009	0.040

*number of samples (*n*) are given.*

2.5 Discussion

This work has shown that it is possible to simulate the bending of a woody plant stem, by taking account of various features of the material, notably its strong anisotropy and the large differences found between tensile and compressive behaviour in both longitudinal and transverse directions. Key stages in the process are the development of a plastic zone on the compressive side of the bend, followed by a damage zone, followed by collapse of the material in the transverse direction. We were guided by the important work of Ennos and colleagues [8], [9] who identified the key failure mechanisms and recognised the importance of the often-ignored transverse force in contributing to stem collapse and failure. We have built on their work to provide a precise, quantitative simulation for green stems of *F. magellanica*. Studies of

this kind are relevant because plant stems are primarily loaded in bending, by self-weight and wind forces. They have evolved to adapt to the enormous bending loads, which is also a ubiquitous problem in engineering structures.

Our test species was found to be unusual in that it displayed two possible failure mechanisms in stems of the same age: greenstick fracture and plastic hinge formation. These mechanisms had been identified by earlier workers but not reported in the same species. Ennos and Van Castern [8] argued that greenstick failures occur more often in woods of higher density, owing to the relatively low ratio of longitudinal tensile strength to transverse compressive strength, which allows dangerous tensile stresses to build up before plastic collapse. In our work, greenstick fractures were associated with material of higher density and lower porosity, consistent with this argument. This material also had a higher Young's modulus and yield strength in the longitudinal direction, so it is likely that it was more anisotropic and thus weaker in the transverse directions, though we did not carry out tests to confirm that experimentally. It appears that *F. magellanica* has evolved to achieve an ideal balance between these two failure modes, since they are almost equally likely to occur, implying the best possible strength under the circumstances. This may be typical of shrubs due to the fact their density lies between denser trees that fail with greenstick and less lignified plants that fail with plastic hinge.

We also detected a previously-unknown mode of failure: the formation of an internal crack. The orientation of this crack indicates that it is driven by the transverse tensile stress that arises during ovalisation (figure 2.11c). This builds on observations by Özden et al. where it was indicated that splitting of wood is easier in the transverse/tangential direction (4). The full significance of this crack, and how it might interact with the other failure modes, is yet to be determined. Further work is needed to consider how it might affect transverse collapse by weakening the cross section, and how it might encourage the formation of the crack on the tensile surface, which precipitates the greenstick fracture.

Our theoretical model, since it has incorporated the physical mechanisms of deformation in this material, was also able to make predictions of the onset of greenstick fracture and of internal cracking. A further question, which arises is, why doesn't the greenstick fracture always occur eventually, since as the bending strain increases, the tension on the convex surface also continues to rise? The reason is probably that the amount of material, which experiences this very high stress becomes smaller and smaller, and other local deformation modes not included here act to eliminate it.

Working with biological materials often comes with limitations in terms of the consistency of data and the variability of results from sample to sample. All samples tested were included in the results presented here, except for a small number of cases in which outliers could be attributed to flaws in the sample or errors in the execution of the test. Data were analysed appropriately to determine statistical significance.

The nonlinear (viscoelastic) behaviour of the stems mean that the results will be dependent on the speed of loading, a factor which was not explored in this work, for which all tests were carried out at load rates which were relatively fast and of the same order of magnitude for all the experiments. Their orthotropic composition and complex geometrical structures make modelling complicated. The FEA and mathematical models assumed the material to be homogenous and did not include the effects of crack initiation and propagation. The end point for predicting greenstick fracture was the predicted initiation of a transverse crack on the tensile surface: the subsequent propagation of this crack was not modelled. The growth of the internal crack would be expected to increase the amount of ovalisation but this effect was not explicitly modelled.

The significance of this work is twofold. Firstly, it provides insights into how this natural material has evolved to resist its principal mechanical threat: failure due to bending. Secondly, it provides inspiration for the creation of strong, lightweight engineering structures made from anisotropic materials such as fibre composites.

2.6 Conclusions

The stress/strain relationship for *F. magellanica* stems loaded in three-point bending and failing by plastic hinge formation can be quantitatively predicted, using a combination of FEA and a mathematical (plastic bending) analysis. The FEA accounts for complicating factors during three-point bending. However, it does not account for the non-isotropic properties and different strengths in compression and tension, which were incorporated using the mathematical model.

The combined model can also indicate the stage at which greenstick fracture may occur due to high longitudinal tension. Experimentally we found that it is related to high Young's modulus caused by greater density, reduced porosity and higher lignification in some samples.

The behaviour, which previous workers referred to as "plastic", and which is a crucial precursor to both of these failure modes, is in fact not primarily plastic yielding behaviour but rather transient viscoelastic deformation. However, we showed that this could be modelled as

plasticity and accurate predictions achieved, provided all data are obtained at similar strain rates.

During loading an internal crack forms: this failure mode has not been previously reported. The formation of this crack could be included in our predictive mode as the point where the transverse tensile strength of the material was exceeded, due to ovalisation.

These findings may provide inspiration for novel engineering structures where it would be desirable for a structure to flex and deform dramatically without catastrophic failure. As we have seen from our specimens, the density of these natural structures has an impact on the failure mechanisms. Manipulation of this concept could be effective when designing structures for materials with low fracture toughness, where preventing crack formation is crucial.

2.7 References

1. Speck T, Burgert I. Plant Stems: Functional Design and Mechanics. Annu Rev Mater Res [Internet]. 2011 Aug 4 [cited 2020 Oct 1];41(1):169–93. Available from: http://www.annualreviews.org/doi/10.1146/annurev-matsci-062910-100425

2. Gibson LJ. The hierarchical structure and mechanics of plant materials. Vol. 9, Journal of the Royal Society Interface. Royal Society; 2012. p. 2749–66.

3. Gibson L, Ashby M, Harley B. Cellular materials in nature and medicine [Internet]. 2010 [cited 2020 Jan 14]. Available from: https://books.google.com/books?hl=en&lr=&id=AKxiS4AKpyEC&oi=fnd&pg=PR9&ots=JlXUXADdvW&sig=oX4e5jm-P1EsVFWhqrqTXPMxzRc

4. Özden S, Ennos AR, Cattaneo MEGV. Transverse fracture properties of green wood and the anatomy of six temperate tree species. Forestry [Internet]. 2017 Jan 1 [cited 2020 Oct 2];90(1):58–69. Available from: https://academic.oup.com/forestry/article/90/1/58/2605844

5. Mattheck C, Breloer H. The body language of trees: a handbook for failure analysis. body Lang trees a Handb Fail Anal. 1994;

6. Hesse L, Bunk K, Leupold J, Speck T, Masselter T. Structural and functional imaging of large and opaque plant specimens [Internet]. Vol. 70, Journal of Experimental Botany. Oxford University Press; 2019 [cited 2020 Oct 1]. p. 3659–78. Available from: https://academic.oup.com/jxb/article/70/14/3659/5477825

7. Beismann H. Brittleness of twig bases in the genus Salix: fracture mechanics and ecological relevance. J Exp Bot. 2000;51(344):617–33.

8. Jeremy Roberts PA, Black by M, Bewley J, Marshall B, Roberts J, Black D, et al. Wood Quality and its Biological Basis [Internet]. 2003 [cited 2020 Jun 10]. Available from: www.blackwellpublishing.com

9. Desch HE, Dinwoodie JM. Strength, Elasticity and Toughness of Wood. In: Timber Structure, Properties, Conversion and Use. Macmillan Education UK; 1996. p. 102–28.

10. Forest Service U, Products Laboratory F. Wood Handbook, Wood as an Engineering Material [Internet]. 2010 [cited 2020 Aug 10]. Available from: www.fpl.fs.fed.us.

11. Green DW, Winandy JE, Kretschmann DE. Mechanical Properties of Wood.

12. Ennos AR, Van Casteren A. Transverse stresses and modes of failure in tree branches and other beams. Proc R Soc B Biol Sci. 2010;277(1685):1253–8.

13. van Casteren A, Sellers WI, Thorpe SKS, Coward S, Crompton RH, Ennos AR. Why don't branches snap? The mechanics of bending failure in three temperate angiosperm trees. Trees - Struct Funct. 2012;26(3):789–97.

14. Milligan R V. Moment - Strain Relationships in Elastic-Plastic Bending of Beams.

watervliet; 1981.

15. Conshohocken W, Conshohocken W. Splitting Tensile Strength of Intact Rock Core Specimens 1. Current. 2001;(Reapproved):1–3.

16. Li D, Wong LNY. The brazilian disc test for rock mechanics applications: Review and new insights. Rock Mech Rock Eng. 2013;46(2):269–87.

17. Ennos R. Trees: A Complete Guide to Their Biology and Structure | NHBS Good Reads [Internet]. London Natural History Museum. London Natural History Museum; 2001 [cited 2020 Jun 28]. Available from: https://www.nhbs.com/trees-a-complete-guide-to-their-biology-and-structure-book

18. Reiterer A, Burgert I, Sinn G, Tschegg S. The radial reinforcement of the wood structure and its implication on mechanical and fracture mechanical properties - A comparison between two tree species. J Mater Sci. 2002;37(5):935–40.

19. Panshin AJ, De Zeeuw C. Textbook of Wood Technology (Vol. I) by Panshin, A.J., Carl De Zeeuw, and H.P. Brown: Good+ Hardcover Second Edition | Beautiful Tomes [Internet]. Vol. 1. New York, NY: McGraw-Hill; 1980 [cited 2020 Jun 28]. Available from: https://www.abebooks.co.uk/Textbook-Wood-Technology-Vol-Panshin-A.J/21053483571/bd

Chapter 3 Fracture and Repair in a Bio-Inspired Self-Healing Structure

Timothy Hone, Sarah Kelehan and David Taylor

Department of Mechanical, Manufacturing and Biomedical Engineering

Trinity College Dublin, the University of Dublin

Dublin, Ireland

Abstract

Many self-healing materials have been developed, but very few self-healing structures. We designed a structure in the form of a cylinder required to resist bending. Taking inspiration from plant stems, it has a cellular structure including longitudinal vascular channels for the delivery of healing agents. The structure was found to be capable of absorbing energy effectively, by deformation and fracture of cell walls. The introduction of healing agents (a two-part liquid adhesive) into the vascular channels allowed fractured cell walls to be repaired. The resulting structure was capable of near-perfect self-healing, restoring its original mechanical properties even after significant damage. A computer simulation (finite element analysis) successfully predicted the early-stage deformation and the initiation of damage. We advocate this structure-level approach as a more appropriate way to introduce self-repair into engineering systems.

Author Contributions

TH conceived the study. SK and TH carried out the experiments and computer simulations. DT supervised the project and wrote the paper.

Keywords

Self-healing; self-repair; structure; damage; failure; bending; ovalisation; biomimetic

3.1 Introduction

Materials with the capacity for self-healing (also called self-repair) have been developed and researched for several decades, but as yet they have not found significant commercial applications. In the search for improved self-healing materials, researchers have looked to nature for inspiration because it is well known that many organisms and body parts are capable of repairing damage, thus improving their durability and resilience. In the present work we consider the development of a self-healing *structure*: a concept which is distinctly different from that of the self-healing material. We begin by defining some terminology that will be used throughout this paper:

Material: A material is homogenous on the macroscopic scale; a piece of material can be sampled and found to have the same properties independent of the sampling location or the size of the sample. It may however consist of various discreet phases on the microscopic scale. It can be produced in different sizes and shapes. Examples of materials are steel, concrete and composite laminate materials such as carbon fibre/epoxy. Materials can contain pores, and can be produced with open cell structures to reduce their density.

Structure: A structure is characterized by having a specific size and shape. It is made from one or more materials. It is intended to be exposed to known forces and restraints. Examples of structures are a crankshaft in an engine, a girder in a building and the arm of a robot. If more than one material is used in the structure, then these materials are joined in a fixed way, for example a coating of zinc applied to a component made from steel, or metal reinforcing bars placed in a beam of concrete.

System: A system is made up of two or more structures. Examples of systems are a bridge, an artificial hip joint and a robot. Individual structures (often referred to as components) are connected together using joints which may be either rigid or mobile.

At the design stage, a system is envisaged consisting of various structures. Analysis at the system level determines the boundary conditions (i.e. forces and restraints) experienced by each structure within the system. Individual structures are then designed to withstand these applied conditions by giving them appropriate shapes and choosing appropriate materials.

The success of a structure depends on the interaction between geometrical shape and material properties. Within a structure, stress varies from place to place. For example a girder in a building will experience bending loads, giving rise to regions of tensile, compressive and shear

stress. Stress concentration features such as holes and corners create locally high stresses. Design activities focus on identifying areas of high stress since it is from these locations that failure will initiate. Many failure processes accelerate because the greater the damage (e.g. the longer the crack), the faster it will grow, so it is important to identify the early-stage damage modes in order to be able to detect and repair them.

The following quotation from Vincent (1) recognises the distinction between materials and structures in the case of plants:

"It seems very probable that a large part of the mechanical design of plants is concerned with structural stability and the plant's ability to suffer local damage without incurring structural failure. In a plant, with its hierarchical design (cellulose, cell-wall, cell-tissue, organ, plant), it is not always easy to know whether one should consider a particular stability/strength problem as one in materials or structures. In general, behaviour under a tensile load will depend only on material properties whereas a compressive or shear load will depend on structural properties as well."

To this we would add that bending, as well as compression and shear, is also a structural problem.

In contrast to a structure, the design criteria for a material are relatively simple because there are a limited number of mechanical properties required to describe the material's monotonic behaviour and its long term failure characteristics.

The separation between material and structure is not a perfect one. Though it is generally true in engineering products, one exception is the use of functionally graded materials which gradually change their structure and properties over larger length scales, typically of the order of millimetres. Similar graded materials are found in biological structures, such as cartilage in orthopaedic joints, and in plant stems where bending may be resisted by using a stiff outer shell grading into a softer core. Despite this complication we believe that the distinction made in this paper between material and structure is a useful one.

We now briefly review the literature on self-healing in materials, structures and systems, noting aspects of biomimetics.

3.1.1 Self-Healing Materials

There has been considerable effort to develop materials capable of repairing themselves. Normally the aim is to repair small defects that arise due to fatigue, surface damage or overload which would otherwise compromise the structural integrity of the material, leading to eventual failure. Some self-healing materials have a very long history: for example cracks in concrete tend to fill up thanks to a reaction with water and CO_2 in the environment which generates more cement material (2). The greatest advances in self-healing materials have been made with polymers and polymer composites. Figure 3.1a shows an early example (3) of a type of system which has since been extensively investigated. It consists of a polymer containing a healing agent and a catalyst which together form an adhesive. At least one of these (here the healing agent) is a liquid, contained in microcapsules. A crack brings the two components into contact and their reaction creates new polymer material which fills the crack. Since that time, considerable advances have been made and a large body of work has built up. For example, the literature on self-healing epoxies has recently been reviewed (4). Polymer-based self-healing materials have been shown to be capable of restoring the strength of a material to a value close to that of its original, undamaged state (3,5). There is, however, a compromise involved, because the introduction of the reactive agents means that the initial strength of the material will be lower than it would otherwise have been. The real benefit comes in increased durability, especially the endurable number of cycles before fatigue failure occurs. But even here there is a significant drawback: this repair process can only operate once in a particular location, after which the reactive agents have been used up. If a second fatigue crack appears in the same location then no self-healing will occur. This is very likely to happen in practice, since, as noted above, structures tend to fail from specific regions of high local stress.

Some self-healing materials have been developed which are specifically inspired by repair strategies found in nature (7). In particular the vascular channels found in animals and plants for transporting fluids have been reproduced in the form of hollow channels containing healing agents in a variety of materials, including polymers, composites and ceramics (6,8,9). Figure 3.1b shows an example of such a material: a fibre reinforced polymer which was capable of returning to about 97% of its original strength after damage. The existence of vascular channels may allow for the continuous supply of reactive agents into the material, giving the capacity for repeated repair in the same area.
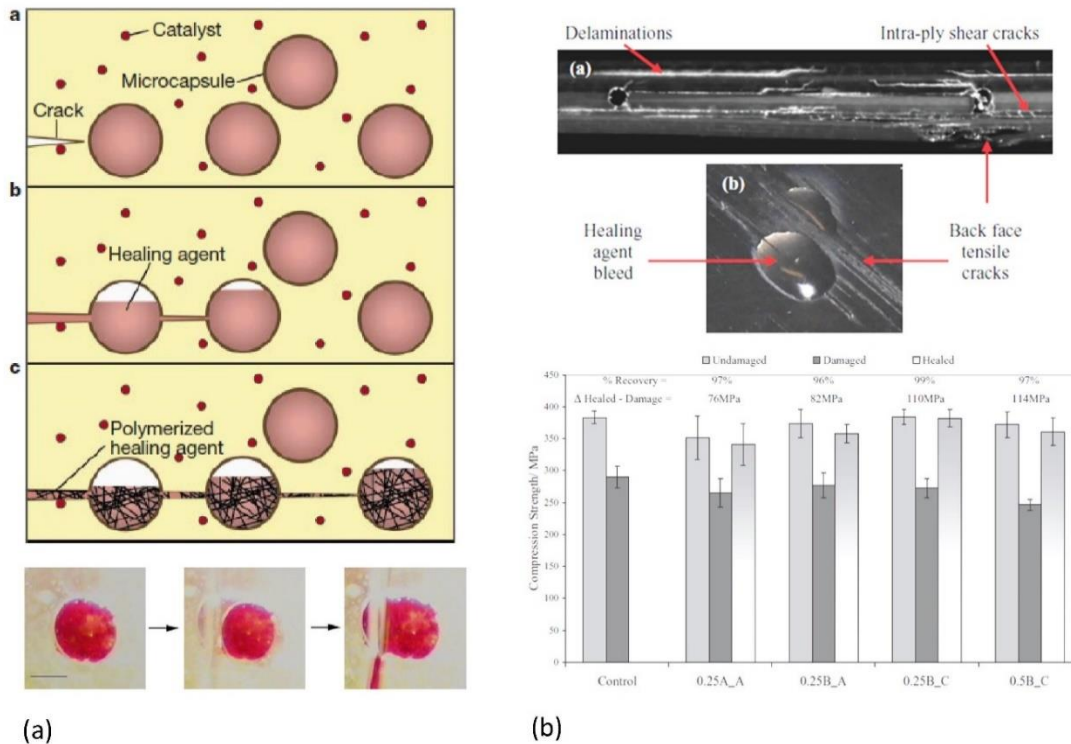
Figure 3.1: (a) An example of a self-healing polymer (3): schematic showing the principle of operation, and images showing rupture of a micro-capsule (scale bar = 0.25mm). (b) An example of a bio-inspired self-healing fibre composite (6).

Toohey *et al.* investigated suitable two-part adhesives for use in self-healing materials with vascular systems (10). Several characteristics are important for these adhesives. They should be two-liquid systems designed to react in a one-to-one ratio as they will encounter each other in approximately equal volumes. They should have low viscosity, allowing the liquids to flow along the microscopic channels and to mix with each other rapidly. They should react quickly at ambient temperature, and should have a long-shelf-life under ambient conditions so that they can remain within the material for a long time and still react effectively when needed. Finally they should be compatible with the host material in order to form a strong bond across the damaged area.

3.1.2 Self-Healing Structures

In contrast to self-healing materials, relatively few self-healing structures have been developed. One example is an inflatable structure which was designed with an outer skin and an internal membrane. When the skin was punctured, the membrane moved to fill the gap, preventing catastrophic collapse of the structure (11). This was inspired by the deformation of plant parenchyma cells to fill wounds. It was defined by the authors as *self-sealing* rather than self-healing, because the repaired area is relatively weak. It is an example of a first-response stage

seen in many natural healing systems, other examples being latex secretion in plants and blood clotting in mammals. The different stages in a natural repair process, and their uptake in biomimetic technology, have been usefully reviewed (12).

This work (11) illustrates a distinct change in thinking from the material level to the structure level. Rather than using a self-healing material for the skin, the designers chose to make use of a different material, below the surface. Another type of structure for which self-healing strategies have been developed is the sandwich panel, consisting of two thin sheets made from relatively rigid material, separated by a softer core. Such panels provide resistance to bending with relatively low weight. Frequently they suffer from impact damage which can reduce their flexural strength. Williams *et al.* introduced self-healing capability into a sandwich structure with a polymer foam core and glass fibre/epoxy skins, using a biomimetic vascular system (13). Other workers have considered sandwich structures, for example Chen *et* al. introduced self-healing at the sheet/core interface which is often the source of initial damage (14). John and Li introduced self-healing in a grid-stiffened sandwich structure (15). But such examples are rare, despite the huge amount of literature on self-healing composite materials, and they generally focus on damage caused by impact loading.

3.1.3 Self-Healing Systems

Self-repair at the system level has been implemented in several inventions in which systems are designed with inbuilt redundancy or with the ability to reconfigure themselves after some of their structures have become damaged. Some of these have taken inspiration from nature. For example a walking robot capable of adapting to the loss of one or more limbs was inspired by the ability of the starfish to adjust the positions of its arms when some are lost (16).

It can be seen from the above examples that the approaches involved in developing self-healing capability will be significantly different depending on whether they are considered at the level of the material, the structure or the system. In the case of the material, the aim is usually to extend fatigue life, whilst almost inevitably sacrificing some initial strength. For a structure or system, specific failure mechanisms must first be identified, such as puncturing or limb loss, and a solution sought which addresses each specific type of failure. Making the entire structure, or system, from self-healing materials is unlikely to be the optimum solution because most parts will never become damaged and so will not need self-healing capacity. This may be one reason why so few self-healing materials have been used in commercial products. They are relatively expensive and so only make commercial sense if they are used in a targeted manner.

Motivated by the above considerations, we embarked on a project to create a self-healing structure inspired by a biological organism. The aims were as follows:

- To identify a suitable natural structure, this being one which is subject in nature to a known type of mechanical loading, and which becomes damaged and fractures in a known manner.
- To design a corresponding engineering structure which fails in a similar manner.
- To introduce self-healing capability located specifically in the region(s) where early-stage damage initiates.
- To compare the mechanical performance of the structure with and without self-healing capability.
- To develop a computer simulation (finite element analysis) of the structure for comparison with the experimental results.

3.2 Materials and Methods

3.2.1 Choice of Natural Structure

For our natural structure we chose plant stems. The main type of loading to which all plant stems are subjected is bending, principally due to wind loading. This was a useful choice for a biomimetic development because bending is also very common in engineering structures. Examples are structural beams in buildings, bicycle frames and antennae.

Previously (17) we investigated the failure modes in stems of the shrub *fuchsia magellanica*, which are partially woody, having a relatively stiff outer cortex containing dead, lignified cells and a softer inner core containing living cells. Vascular channels run longitudinally. We found that when stems were loaded in bending, small cracks formed internally in the core region. Figure 3.2 shows examples. We discovered that these cracks occurred due to tensile stresses generated by the process of ovalisation, whereby the initially-circular stem becomes flattened into an oval shape during bending. This cracking, which we identified for the first time, constitutes the first stage of damage in this structure.
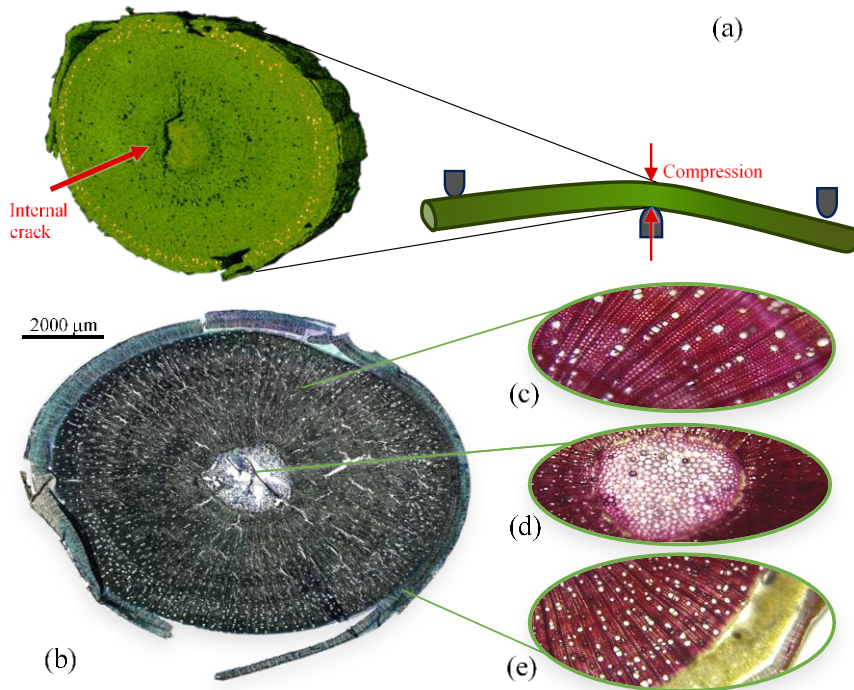
Figure 3.2: Results from previous work on bending of plant stems (17). (a) CT scan image showing an internal crack, which is the first damage event in the structure. (b)-(e) stained sections showing cells and vascular channels (white circles).

Ovalisation, i.e. changes in the cross section of a beam during bending, is a phenomenon which occurs to some degree in all beams, but it can generally be ignored in engineering structures made from isotropic materials such as steel because the deformations and stresses that arise are negligibly small. It becomes important, however, in anisotropic materials which have much greater stiffness and strength in the longitudinal direction compared to the transverse direction. In that case, much larger amounts of ovalisation occur, and the stresses generated, though still small, may be large relative to transverse strength. This phenomenon has been studied theoretically and experimentally in various natural materials, such as bamboo (18,19), other plant stems (20) and insect legs (21). Anisotropy is common in nature, and it is very useful because it allows resources to be more effectively employed, creating high stiffness and strength in directions parallel to the principal stresses. Some engineering materials are anisotropic, for example certain fibre composites, but as yet relatively little advantage has been taken of their potential in this regard.

3.2.2 Design and Manufacture

We created a structure in the form of a beam of circular cross section. This can be described as a generic type of structure. It is not intended for any specific purpose: rather, it represents a type of structure which is commonly found in many engineering systems. Taking inspiration from plant stems we designed the structure to have two features: (i) a hard, continuous outer shell to resist the high longitudinal stresses that arise near the surface during bending, and; (ii) a flexible inner core created by using a cellular structure, incorporating vascular channels for the introduction of self-healing constituents.

The structure was manufactured with a 3D printer using stereolithography (Form 2 SLA printer, Formlabs Inc, Somerville, USA). The material used was a clear polymer resin supplied with the printer. Structures were built up in horizontal layers, with the axis of the cylinder oriented vertically. To determine the mechanical properties of the resin we manufactured solid samples with a standard "dogbone" shape with a thickness of 2mm, for tensile testing according to BS EN ISO 527. After printing the samples were washed in IPA (Isopropyl alcohol) for 20 minutes and cured at a temperature of 60ºC for 30 minutes as specified by the printer manufacturer.

Figure 3.3 shows the structure as designed and manufactured. It has an outer diameter of 25mm and a length of 25mm. It contains 57 vascular channels of diameter 2.3mm. For comparison we also designed and tested a hollow cylinder made from the same polymer, with the same outer diameter and an inner diameter of 17.36mm, giving it the same cross sectional area, and therefore the same weight, as our structure. This is also shown in figure 3.3.

Self-healing was achieved using a two-part adhesive. In choosing a suitable adhesive we were guided by previous research, notably that of Toohey *et al.* mentioned above (10). Several different adhesives were trialled, the final choice being made on the basis of efficacy and convenience of supply. The first part consisted of EPON Resin 828 mixed in equal amounts with a diluent DER 732 to achieve sufficiently low viscosity (Henkel Dublin, Ireland). The second part was EPIKURE 3072 curing agent (Hexion, Columbus, USA). This adhesive system is stoichiometric, requiring equal amounts of the two agents to produce the optimal effect. Using a syringe, alternate rings of vascular channels were filled with the first or second parts, so that if rupture occurred in any cell wall linking channels in the radial direction, the two agents would mix and react, creating new polymer to repair the rupture. End caps (figure 3.3f) were fabricated using a soft, flexible resin and sealed to the structure using tape, to prevent loss of the liquid agents. Preliminary tests demonstrated that these end caps did not affect the mechanical performance of the structure.
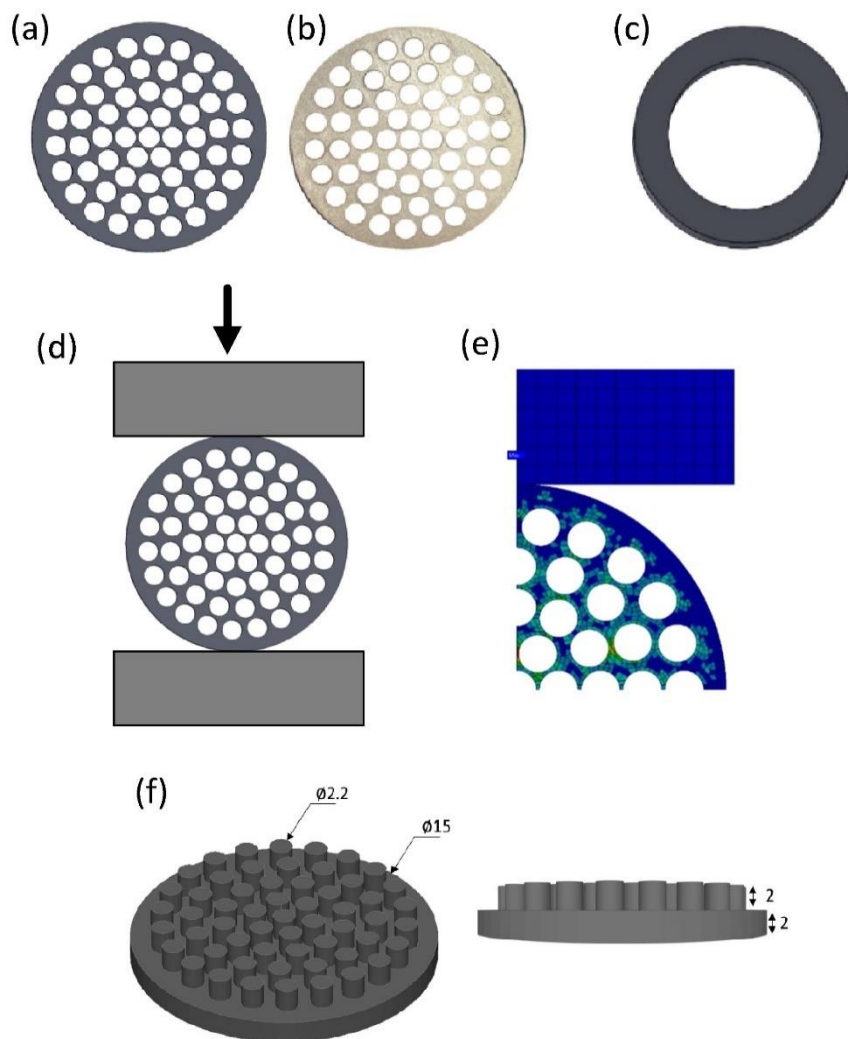
Figure 3.3: Cross sections of the structure: (a) CAD drawing; (b) 3D-printed resin specimen; (c) hollow cylinder with the same weight as the test structure; (d) method of testing by compression across the diameter; (e) the finite element model; (f) design of the end caps (dimensions in mm).

It is envisaged that, ultimately, this structure will be made in the form of a much longer cylinder, suitable for incorporation into a system where it will be subjected to bending such as cantilever bending or three-point bending. However, we were limited in the length of our specimens by the 3D printing equipment available to us and by the method we used to incorporate the healing agents. So this initial phase of the work was carried out using short cylinders of length 25mm.

3.2.3 Testing and Modelling

Since we had already identified that the initial damage will be internal cracking due to ovalisation [17], we simulated this by creating ovalisation in a simple way, applying compression across the diameter, as shown in figure 3.3. The similarity between ovalisation caused by bending and ovalisation due to diametral compression has been recognised and used in previous work 18,22.

Samples were placed with the axis of the cylinder lying horizontally and loaded between flat, horizontal steel platens in an Instron testing machine (see figure 3.3). Compression was applied at a rate of 2mm/min and load was recorded continuously. Failure modes were observed visually during testing and subsequently using optical and scanning-electron microscopy. Tests were conducted using two loading cycles to determine the effect of healing after first-cycle damage. Samples were first loaded to a displacement of 3mm, unloaded and reloaded, the reloading phase being continued until failure occurred. Initial trials showed that the first loading cycle created sufficient damage to significantly reduce the strength of the structure. A period of 2 days was allowed between the first and second loading cycles to give time for curing of the adhesive system.

A finite element model of the structure was created using ANSYS software. Figure 3.3e shows the model, which was reduced in size by taking advantage of symmetry. The model had a hexahedral-dominated mesh which was refined until mesh independence was achieved, giving a constant maximum stress to within 4%. It had 138,516 nodes and 28,074 elements. Based on our test results the material was assigned a Young's modulus of 717MPa and a yield strength of 57.9MPa. Bilinear elastic/plastic behaviour was assumed with no work hardening. The presence of the liquid healing agents was not included in the model.

The statistical significance of the differences found in the experimental results was tested using Student's T-test, with a critical p value of 0.05.

3.3 Results

Three tensile tests were carried out on samples of the polymer resin, giving a Young's modulus of 717MPa (standard deviation 149MPa) and a tensile strength of 57.9MPa (standard deviation 5.1MPa).

Figure 3.4a shows the results of tests conducted on five samples of the control (i.e. non-self-healing) structure, plotting load against applied displacement during compression. A line representing the averaged values is also shown.
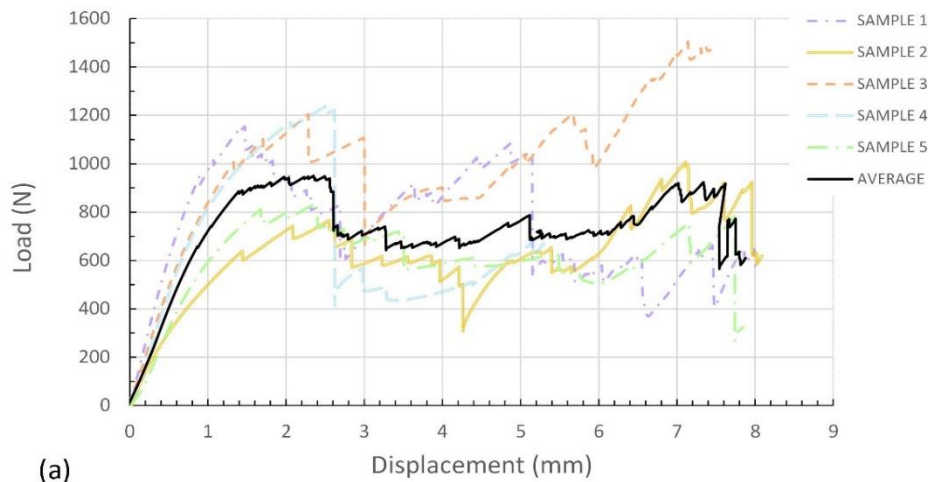
(a)
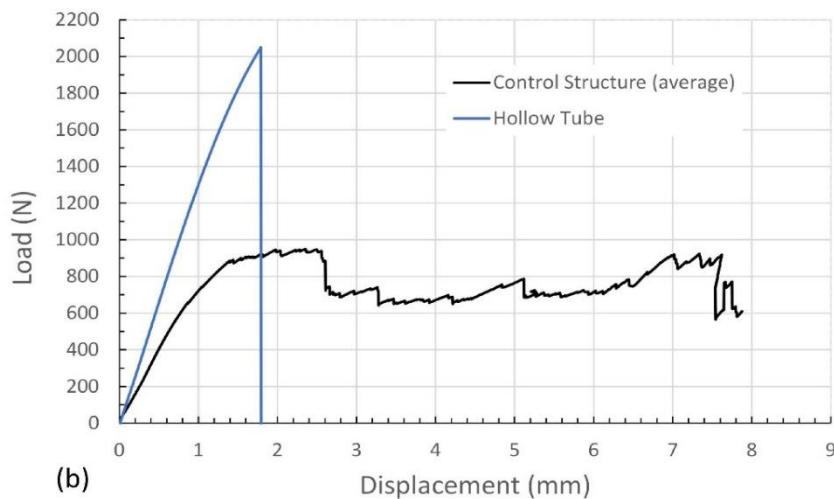
(b)

Figure 3.4: (a) Load/displacement results for five control (i.e. non-self-healing) samples. Also shown is a line drawn using the average load for each displacement. (b) Comparison of results for the hollow tube specimen and the control structure.

The main features of the load/displacement plot are:

- An initial steep rise in load. The line here is approximately straight, implying elastic behaviour, but with some decrease in slope with increasing deformation which is likely due to viscoelasticity in the polymer.
- A peak in load followed by a sudden, relatively large drop in load, or several smaller drops. This coincided with the appearance of damage in the form of internal cracks created by brittle fractures of the cell walls between the vascular channels.
- A plateau region in which load remained relatively constant with increasing compression, with further small drops in load associated with further damage events.

- The specimen was deemed to have failed when a crack penetrated the outer cortex: at this point the test was concluded. Before this point, some samples show signs of an increasing force which may be the start of densification by compression and closing of the channels.

Figure 3.5 shows typical damage, which took the form of fractures in cell walls. The initial load drop coincided with cracks forming in just one or two cell walls. By the end of the test, damage was extensive across many cell walls.
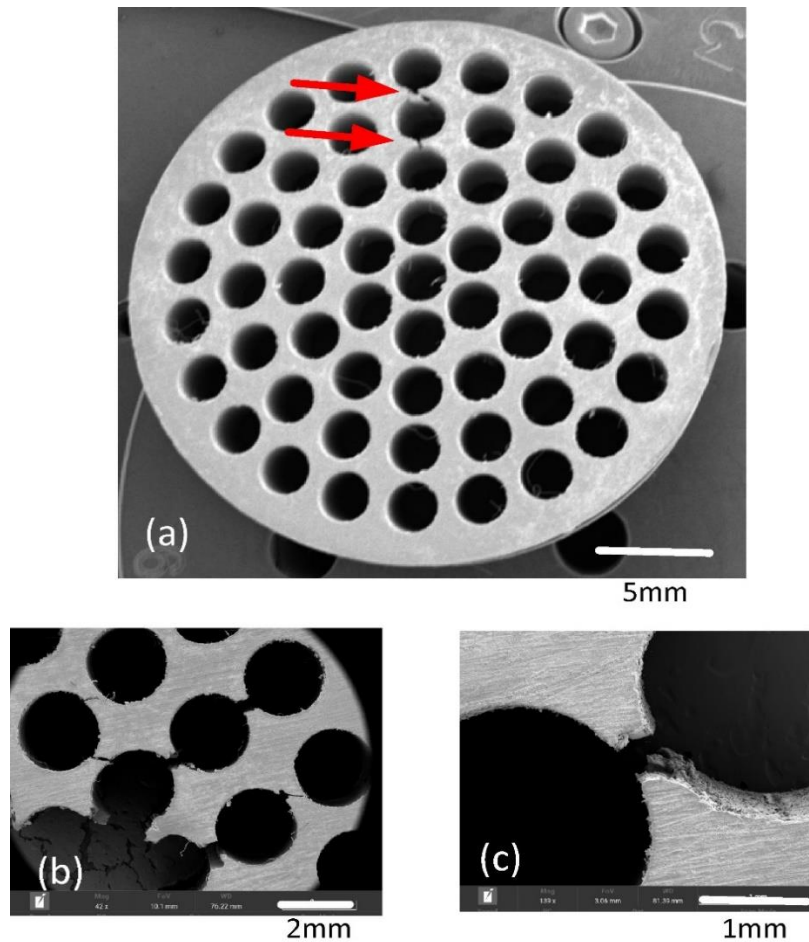
Figure 3.5: SEM images of damaged structures. (a) Initial damage after a displacement of 3mm (fractures in two cell walls, arrowed); (b) More extensive damage at the end of a test (8mm displacement); (c) A close-up view of a fractured cell wall.

For these control specimens the energy absorbed up to final failure, given by the area under the entire curve, was on average 5.29J, with a standard deviation (SD) of 1.38J. The average load when damage commenced was 980N (SD 242N). This occurred at displacements varying from 1.5mm to 3mm. At a displacement of 3mm the average load had dropped to 672N (SD 216N). So at this stage in the test the samples were on average 31.4% weaker, having sustained significant damage. Therefore this was the displacement to which we chose to load the self-healing samples in the two-cycle tests.

Figure 3.4b shows a comparison with a hollow tube having the same cross sectional area, which had a considerably higher failure load of 2048N but much less absorbed energy (1.99J).

Figure 3.6a shows first and second loading cycles for typical control and self-healing samples. Both the control and the self-healing sample peaked at about 1350N on the first loading cycle, followed by a load drop to about 900N. On the second cycle the control sample returned to the previous load of 900N and showed a further load drop shortly after. It failed at a relatively small displacement of 3mm, having been significantly damaged on the first cycle. By contrast the self-healing sample showed second-cycle loading behaviour which was very similar to its first-cycle behaviour up to 3mm, and then displayed a generally increasing load until failure at 6.3mm.
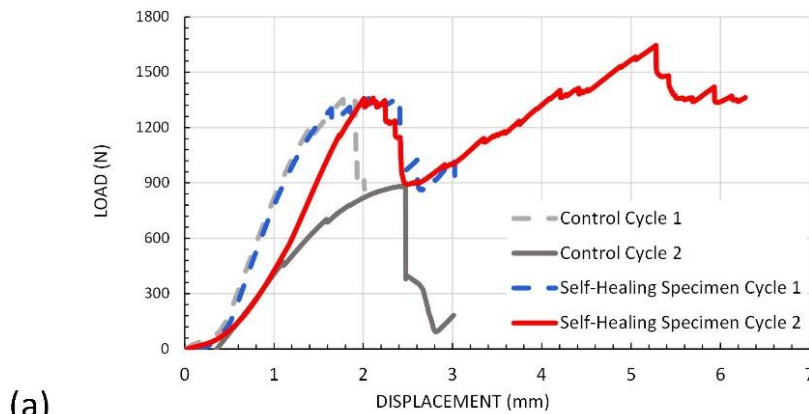
(a)
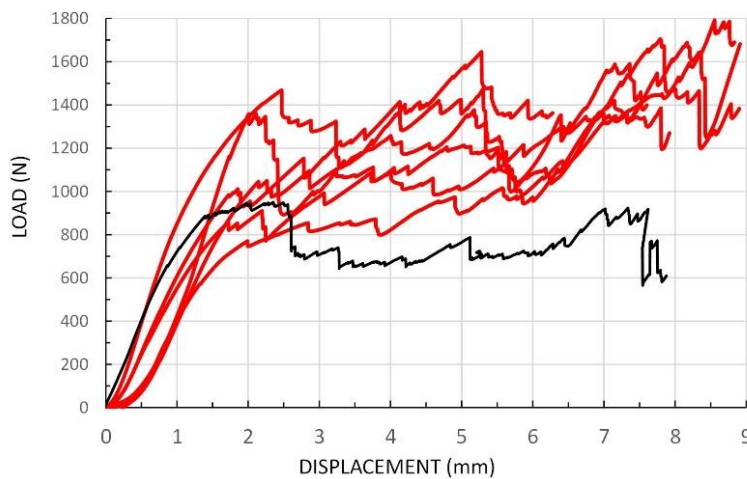
(b)

Figure 3.6: (a) Examples showing typical behaviour of control and self-healing samples subjected to two loading cycles. (b) Behaviour of self-healing specimens on their second cycle, after a first cycle to 3mm displacement. For comparison, the average behaviour of control specimens (single loading cycle) is included, from figure 3.4.

Figure 3.6b shows second-cycle results for all six self-healing samples tested, along with the average first-cycle behaviour of the control samples for comparison. The behaviour of the healed samples was very similar to that of the controls at low displacements up to 3mm. The crack initiation load was 1085N (SD 275N), which is on average slightly higher than that for the controls, but the difference was not statistically significant (p=0.52).

At higher displacements the healed samples performed better than the controls. Regarding total energy to failure, the self-healing samples had an average value of 8.36J (SD 1.24J), which was significantly greater than the controls (5.29J) by 58%. This was largely due to a continued rise in the force/displacement curves for the self-healing samples at displacements greater than 3mm, which was not seen in most of the control samples (see figure 3.4).

The average initiation load for the self-healing samples on their first cycle of loading was 1230N (SD 199N), which was higher than that of the controls (980N), however this difference was not significant (p=0.10). On their second cycle, after healing had been carried out, the self-healing samples had a slightly lower crack initiation load 1085N (SD 275N) on the second cycle, implying an average healing efficiency of 87%. However this load was not significantly different from the first-cycle load (p=0.32) nor was it different from the first cycle load for the controls (p= 0.52).

The energy for loading up to 3mm also showed similar characteristics. It was 2.34J (SD 0.24J) for self-healing samples on the first cycle and slightly lower at 2.10J (SD 0.45J) on the second cycle, giving an average healing efficiency of 89%. But again this difference was not statistically significant (p = 0.29). Table 3.1 gives a summary of some key results from this study.

Table 3.1: Key Results: Load to Initial Damage and Total Energy to Failure
Average ± standard deviation

	Control structure (non-healing)	Hollow Tube	Self-healing structure (first cycle)	Self-healing structure (second cycle)
Load to initiate damage	980N ±242N	2048N	1230N ±199N	1085N ±275N
Total energy to failure	5.29J ±1.38J	1.99J	Not applicable	8.36J ±1.24J

Figure 3.7 shows an example of the observed healing process. A crack has formed between two vascular channels. The adhesive agents in the two channels have reacted, leading to a loss of liquid in the channels. Cured adhesive material can be seen filling the gap. The channels have remained open, not blocked by cured adhesive.
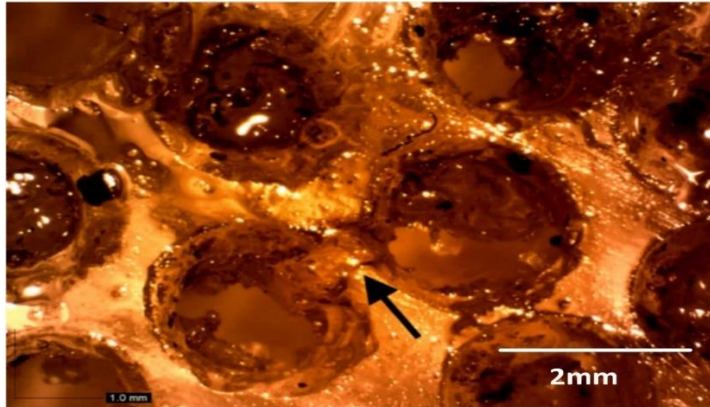
Figure 3.7: Image showing the healing of a broken cell wall (arrowed).

Figure 3.8 shows results from the finite element model: contours of Von Mises stress for an applied load of 900N. Also shown is a load/displacement plot with the experimental results included for comparison, and a plot showing how the maximum stress in the model changed with applied load.
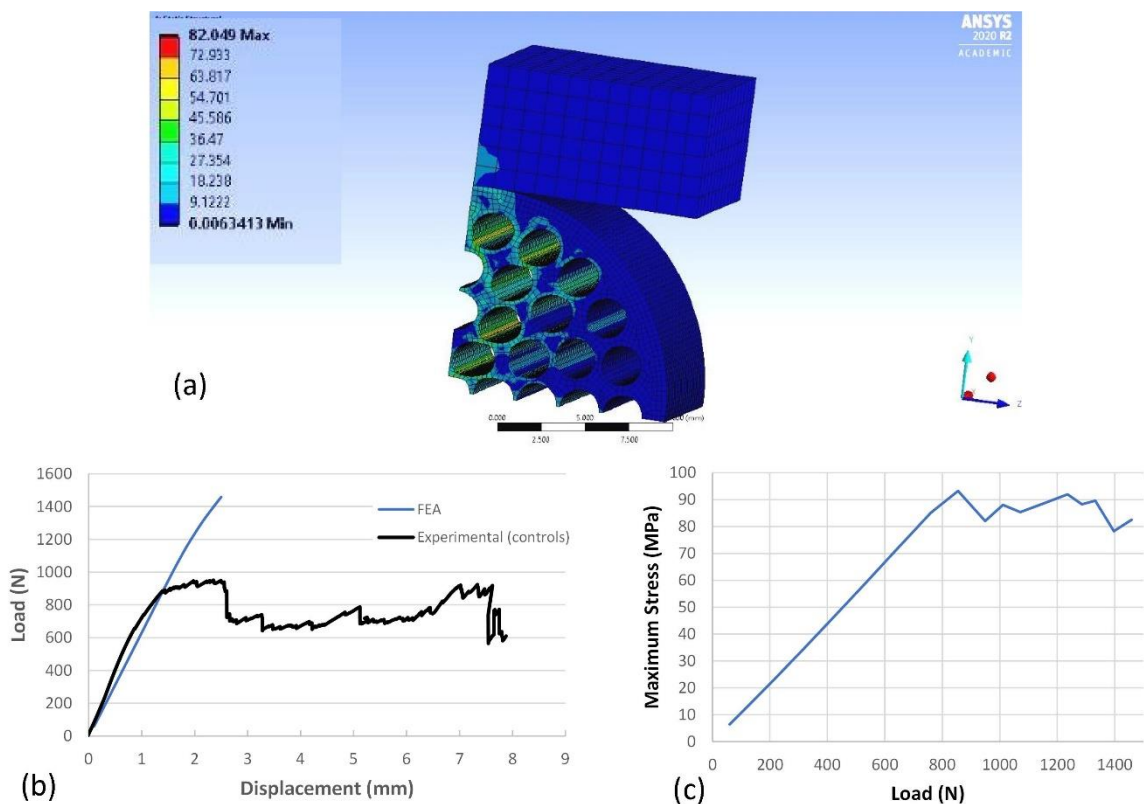
Figure 3.8: FEA predictions. (a) Contour plot (Von Mises stress) for an applied load of 900N; (b) Load/displacement plot, comparing FEA to experimental results (average of the non-healing controls); (c) Maximum stress in the FE model as a function of load.

3.4 Discussion and Conclusions

This paper introduces the concept of self-healing at the structure level, as opposed to the material or system levels. We believe that the idea of creating self-healing structures has not received sufficient attention and that it could greatly improve the uptake of self-healing technology in commercial products.

Our example in this work was a cylindrical structure suitable for use in an application where it would be exposed to bending moments. An example of such a structure would be part of the frame of a bicycle. We tested this in the form of a cylinder of short length loaded in diametral compression, to simulate early-stage failure by ovalisation. Thus, and quite incidentally, we found that it functions well when loaded in compression in this direction, absorbing large amounts of energy. So our structure might also find application in resisting compressive impact, for example as the bumper of a car.

Even before introducing self-healing properties, we found that the use of a hard outer shell and softer, cellular core produced a structure which was capable of greater energy absorption (though less peak strength) than a hollow cylinder of the same weight. This is due to the more gradual failure mode, involving large deformations and progressive fracture of the cell walls. There are many similar structures to be found in nature, not only in plants but also, for example, mammalian bones and bird beaks. The advantages of arranging material in this way have also previously been recognized by engineering designers, not necessarily inspired by nature. An example is honeycomb sandwich panels used in aircraft.

The improved energy absorption of such structures comes at a price: internal damage which weakens the structure and may render it unusable. So this kind of structure is an ideal candidate for self-healing, which, if successful, would allow it to be used repeatedly whilst maintaining its strength and energy-absorption capabilities.

The structure which we created is highly anisotropic. Though we did not measure its load/deflection characteristics in the longitudinal direction, they can easily be calculated based on our measurements of the material itself, and knowing that the structure has a constant cross section. The results are as follows: if loaded in the longitudinal (i.e. axial) direction, the cylinder will deform by 0.13mm for an applied load of 1.0kN. It will fail at a load of 15.5kN. Comparing to the load/deflection behaviour in the diametral direction (figure 3.4) the structure can be seen to be 9 times stiffer and 16 times stronger in the longitudinal direction. This degree of anisotropy is of the same order as that found in wood and plant stems (20).

The ability of our structure to heal itself was evident in the behaviour of samples which had been subjected to significant damage by loading to 3mm deflection, which reduced the strength by 31.4%. After being allowed to self-heal for 2 days their strength (crack initiation load) was the same as that for the original intact samples and the same as measured in separate control samples with no self-healing present. The energy absorbed up to final failure was, remarkably, 58% greater than that of the controls. The reason for this increase is not clear. This may have been due to the presence of the fluid adhesive agents, filling the vascular cells and preventing them from collapsing, especially at large applied displacements. This is not a factor, however, at low displacements, as can be seen by comparing the control and self-healing samples in their first cycle (figure 3.6). It may also have been partly due to the healing processes occurring during the test, as more and more cell walls ruptured, causing adhesive agents to react. This should be investigated in future work. However it is not very important in the present context: our aim was to prevent early-stage damage and if this aim is realized then the progression to final failure will not occur anyway.

Results showed a large amount of variability. For example for the control samples the total energy to final failure varied across the five samples from 3.58J to 7.28J. This would not be surprising in a natural structure but was somewhat unexpected in these manufactured samples. One possible explanation is the stochastic nature of the failure process. Several different cell walls are highly stressed so failure may occur in a different sequence, causing different load drops at different stages during the test. Specimen-to-specimen variability in the manufacturing process (e.g. variation in cell wall thickness) may also have an effect, though from our observations this would seem to be low.

The finite element model was able to predict the initial part of the load/displacement curve but not the later part, which is to be expected because we did not model the fracture process. The maximum Von Mises stress in the model increased linearly up to a value of 93MPa (figure 3.8c) after which it plateaued. The material in the FE model was given a yield strength of 57.9MPa and no work hardening, so the existence of stresses around 80-90MPa suggests local conditions close to pure shear (which would give rise to a Von Mises stress of 100.3MPa). The plateau commenced at a load of 850N, which is close to the experimental value at which fracture first occurred (980N). As figure 3.8a shows, the highest stresses occurred in cell walls. Thus the model appears to be capable of predicting the point at which cell wall fracture will begin. Further work could be carried out to include damage events in the model specifically, as well as their repair by self-healing. However the main purpose of the model was to predict the point of initial damage, since this dictates the disposition of the self-healing agents.

This work had some limitations, notably the fact that we were not able to create long cylinders suitable for full-scale bending tests. We plan to do so in the future, and also to incorporate these structures into systems. A practical problem for the full-scale structure will be how to ensure continued supply of healing agents, flowing along the vascular channels to replace those which have reacted. The long-term stability of the healing agents was not investigated here. Despite these limitations we feel that this preliminary work has been useful in establishing a novel approach to self-healing and realizing this concept in a specific example structure. Future work could consider other different structures, such as those containing stress concentration features, to identify appropriate self-repair strategies.

Conflict of Interest and Ethics

The authors have no conflicts or ethical issues to declare.

3.5 References

1. Vincent JFV. Fracture Properties of Plants. In. *Advances in Botanical Research.* Vol 171990:235-287.

2. deRooij M, Van Tittleboom M, De Belie N, Schlangen E. *Self-Healing Phenomena in Cement-Based Materials.* Springer; 2013.

3. White SR, Sottos NR, Geubelle PH, et al. Autonomic healing of polymer composites. *Nature.* 2001;409(6822):794-797.

4. Zhang F, Zhang L, Yaseen M, Huang K. A review on the self-healing ability of epoxy polymers. *Journal of Applied Polymer Science.* 2021;138(16).

5. Cho SH, White SR, Braun PV. Room-temperature polydimethylsiloxane-based self-healing polymers. *Chemistry of Materials.* 2012;24(21):4209-4214.

6. Norris CJ, Meadway GJ, O'Sullivan MJ, Bond IP, Trask RS. Self-healing fibre reinforced composites via a bioinspired vasculature. *Advanced Functional Materials.* 2011;21(19):3624-3633.

7. Cremaldi JC, Bhushan B. Bioinspired self-healing materials: Lessons from nature. *Beilstein Journal of Nanotechnology.* 2018;9(1):907-935.

8.   Lee MW, Sett S, Yoon SS, Yarin AL. Fatigue of Self-Healing Nanofiber-based Composites: Static Test and Subcritical Crack Propagation. *ACS Applied Materials and Interfaces.* 2016;8(28):18462-18470.

9.   Shields Y, De Belie N, Jefferson A, Van Tittelboom K. A review of vascular networks for self-healing applications. *Smart Materials and Structures.* 2021;30(6).

10.   Toohey KS, Hansen CJ, Lewis JA, White SR, Sottos NR. Delivery of two-part self-healing chemistry via microvascular networks. *Advanced Functional Materials.* 2009;19(9):1399-1405.

11.   Rampf M, Speck O, Speck T, Luchsinger RH. Investigation of a fast mechanical self-repair mechanism for inflatable structures. *International Journal of Engineering Science.* 2013;63:61-70.

12.   Speck O, Speck T. Self-repair in nature and technology: Seal, heal, repair. *Biologie in Unserer Zeit.* 2015;45(1):44-51.

13.   Williams HR, Trask RS, Bond IP. Self-healing composite sandwich structures. *Smart Materials and Structures.* 2007;16(4):1198-1207.

14.   Chen C, Peters K, Li Y. Self-healing sandwich structures incorporating an interfacial layer with vascular network. *Smart Materials and Structures.* 2013;22(2).

15.   John M, Li G. Self-healing of sandwich structures with a grid stiffened shape memory polymer syntactic foam core. *Smart Materials and Structures.* 2010;19(7).

16.   Bongard J, Zykov V, Lipson H. Resilient machines through continuous self-modeling. *Science.* 2006;314(5802):1118-1121.

17.   Hone T, Mylo M, Speck O, Speck T, Taylor D. Failure mechanisms and bending strength of Fuchsia magellanica var. gracilis stems. *Journal of the Royal Society Interface.* 2021;18(175).

18.   Wegst UGK, Ashby MF. The structural efficiency of orthotropic stalks, stems and tubes. *Journal of Materials Science.* 2007;42:9005-9014.

19.   Taylor D, Kinane B, Sweeney C, Sweetnam D, Reilly P, Duan K. The biomechanics of bamboo: investigating the role of the nodes. *Wood Science and Technology.* 2014;49(2):345-357.

20.   Ennos AR, Van Casteren A. Transverse stresses and modes of failure in tree branches and other beams. *Proceedings of the Royal Society B: Biological Sciences.* 2010;277(1685):1253-1258.

21.   Parle E, Herbaj S, Sheils F, Larmon H, Taylor D. Buckling failures in insect exoskeletons. *Bioinspiration and Biomimetics.* 2015;11(1).

22.   Keogh L, O'Hanlon P, O'Reilly P, Taylor D. Fatigue in bamboo. *International Journal of Fatugue.* 2015;75:51-56.

Chapter 4 Investigating Defect Tolerance and Failure Mechanisms of Three Plant Stems with Different Cross-sectional Tissue Patterns

Timothy Hone[1,], Max Mylo[2,3], Olga Speck[2,3] and David Taylor[1]*

[1]Trinity Centre for Biomedical Engineering, Department of Mechanical, Manufacturing and Biomedical Engineering, Trinity College Dublin, The University of Dublin, Ireland

[2]Plant Biomechanics Group, Botanic Garden, Faculty of Biology, University of Freiburg, Germany

[3]Cluster of Excellence *liv*MatS @ FIT—Freiburg Center for Interactive Materials and Bioinspired Technologies, University of Freiburg, Germany

Abstract:

Plant stems have evolved to resist mechanical forces and to survive events which cause damage. This study investigates their ability to resist the impacts of external damage on their mechanical integrity. This resistance is defined in engineering by a property known as defect tolerance. We developed a new approach for quantifying defect tolerance as a structural attribute, based on relative changes to various mechanical properties. Stems from three species (fuchsia, elder and ash) were tested in three point bending: results were compared with those from two idealised engineering materials obtained from finite element analysis. Testing revealed that the defect tolerance of plant stems is remarkably good, in many cases exceeding the expected maximum behaviour derived from the ideal materials. This was attributed to a number of factors: material anisotropy; differences between tensile and compressive behaviour, and inbuilt residual stress. Imaging techniques (microscopy and microCT scanning) contributed to our understanding of how both structural and material properties determine performance. This work advances our understanding of how plants have developed superior defect tolerance and may assist in the development of future engineering structures and materials.

4.1 Introduction

In nature plants are continuously exposed to damage by external forces, in particular wind, wildlife and human interference [1]. They have evolved to be defect tolerant in that they can continue to survive after being damaged without catastrophic failure occurring. To illustrate the concept of defect tolerance, we can consider two materials, which demonstrate very different properties: glass and steel. If a small crack is induced in a sample of glass, its mechanical strength will be dramatically reduced relative to when it was defect free. On the other hand, if a small crack occurs in a steel sample, it's strength will be much less affected [2].

The concept of defect tolerance is very import in industry as it plays a crucial role in determining factors of safety in designing engineering structures. Metals such as steel usually have very high defect tolerance, which is related to their fracture toughness (i.e. resistance to crack propagation) which comes about due to their plasticity. Other engineering materials have poor defect tolerance but strategies exist for improving it. For example, concrete on its own has poor defect tolerance, especially in tension. However with the addition of steel reinforcing bars the defect tolerance can be greatly improved [3]. Likewise the introduction of carbon fibres into a polymer to make a fibre reinforced composite greatly improves its defect tolerance [4]. Despite the extensive use of the term defect tolerance to describe engineering materials and structures, it's exact meaning is not precisely defined. This will be discussed in more detail below in the Theory section.
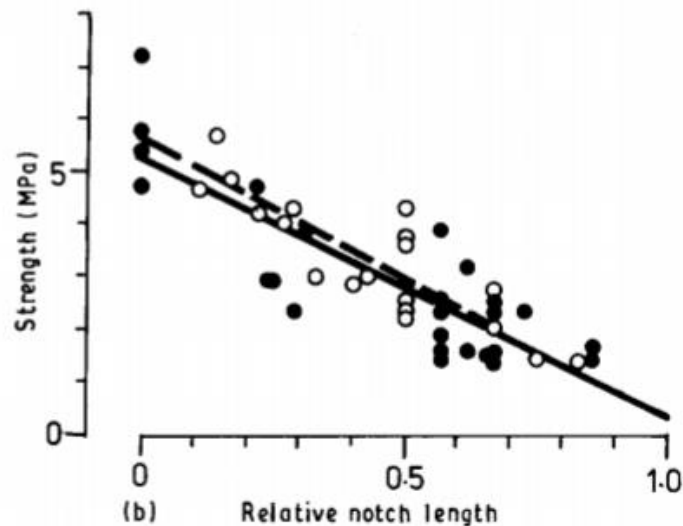
Figure 4.1: Notch sensitivity of leaves of Dactylis glomerata). (●, -) Edge notches, (○ --) centre notch [5]. Straight lines passing through zero strength at 1.0 relative notch length indicate perfect defect tolerance.

Vincent et al. [5] investigated defect tolerance in leaves by measuring the effect of introduced notches on strength (nominal stress to failure). Figure 4.1 shows an example of their data, in which strength is plotted as a function of relative notch length, i.e. the notch length divided by the sample width. The best possible defect tolerance is expected to occur if the only effect of the notches is to reduce the width, and therefore the area of the cross section. In that case data would be expected to lie on a straight line as shown on the graph. These workers found that this optimal defect tolerance often occurred, though not in all cases investigated. They concluded that the laterally separated fibres play an important role in toughening a leaf and thus reducing its sensitivity to damage. Vincent has also researched the defect tolerance of soft (un-lignified) stems [1]. The study contains several insights into how plants withstand the mechanical effects of wind, water and gravity without negatively impacting their integral parts. Plant stems usually contain several bundles of fibres arranged around the periphery of the stem and it appears these "dictate the tensile and bending strength of the stem". These arrangements of fibres will either deflect cracks or resist the development of stress concentrations. Water content also plays an important role as with " simple parenchyma and leaves, wilting increases toughness by increasing strain to failure". The final factor affecting plants resistance to damage is the ability to change its Young's modulus (i.e. material stiffness) and also its second moment of area, I, a structural property which describes resistance to bending.

Gaining a better knowledge of why plants are defect tolerant involves considering in detail the nature and behaviour of plant structures. The mechanical properties of plants are determined by the biochemistry and ultrastructure of the cell walls. These are primarily composed of cellulose

hemicellulose, pectin and in secondary woody cell walls, lignin. The lignin tubes have the greatest impact on the material's strength and consist predominantly of longitudinal tube-like elements (tracheids, vessels, wood fibres in angiosperms) which run parallel to the stem's longitudinal axis. These tubes primarily function as water conducting vessels/tracheids and/or stabilizing elements tracheids/wood fibres and combine with wood rays to form a complex 3D-network of hollow micro-tubes with varying wall thickness and a central cavity [6]. This complex 3D-network likely determines the stem's defect tolerance.

In a previous study [7] we examined how plant stems resist failure. We subjected stems of *Fuchsia magellanica* var. *gracilis*, to three-point bending and noted two different failure mechanisms, a plastic hinge and greenstick fracture. In the present work this approach was extended to consider the effect of an introduced notch and also broadened to include stems from two other species: *Sambucus nigra* and *Fraxinus excelsior*.

The aims of this study were:
- To develop a tool for precisely making artificial cracks (i.e. sharp notches) in the plant stems.
- To record and analyse data from three-point bend tests to compare notched and unnotched (i.e. plain) stems.
- To compare these results with those expected theoretically for idealised engineering materials having high and low defect tolerance.
- To interpret the results in terms of the internal structure and failure mechanisms in the plant stems.

4.2. Materials and Methods

4.2.1 Plant material

Stems from the following three species were investigated: *Fuchsia magellanica* var. *gracilis*, (referred to as fuchsia), *Sambucus nigra* cultivated in temperate regions (referred to as elder) and *Fraxinus excelsior* cultivated in temperate regions (referred to as ash). A total of 13 fuchsia, 9 elder and 13 ash stems were used for testing. The stems were collected from Dublin, Ireland in March 2020.

4.2.2 Mechanical analyses

Straight stems with few or no nodes were chosen, with diameters ranging from 7-12mm and a length of 30cm. Samples were stripped of anything that could interfere with the bend tests, such as leaves, flowers and nodes. The ends and any exposed sections were coated in Vaseline to minimise water loss during transportation to the laboratory. Stems were tested on the same day as being collected, in an Instron testing machine (type 3366, Norwood, MA, USA). The Instron was equipped with a three-point bending rig with an 8kN load cell (figure 4.2). The span was set to 15 cm, being at least 15 times the diameter of the stems tested, ensuring conformance to standard elastic bending theory. Samples were subjected to a constant displacement of 40 mm/min until failure whilst force and displacement were recorded simultaneously at 20 Hz.
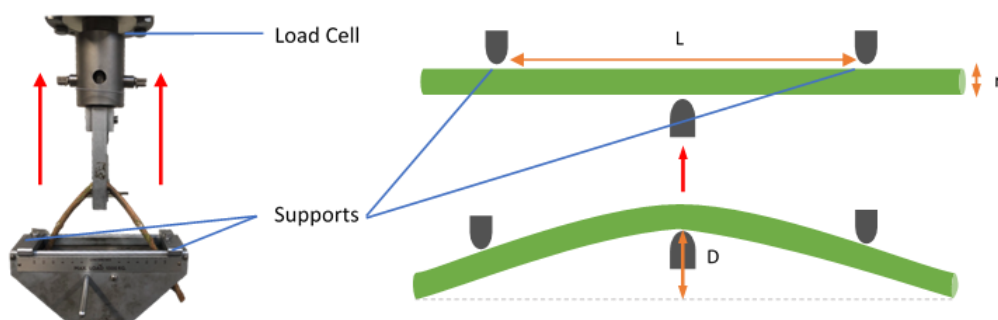
Figure 4.2: Image of three-point bending rig with graphical illustration (supports spaced at 15 cm apart with load cell pulling from centre)

Approximately half of the stems were tested with no introduced notch: these will be referred to as "plain" specimens. In the other specimens we introduced a sharp notch using a specially developed apparatus (Figure 4.3).
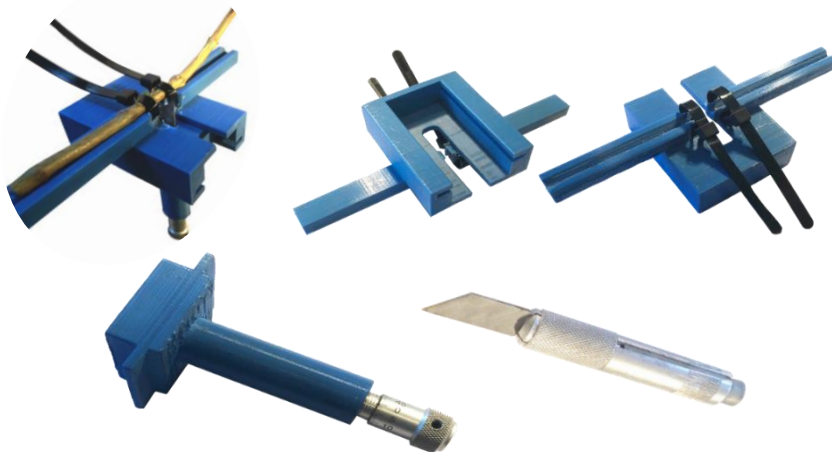
Figure 4.3: (a) overview of apparatus developed for inserting precise cuts in plant stems, (b) Slide where stems are attached (c) slider with micrometre attached, (d) scalpel to be inserted into slide.

The body of the apparatus was designed on Solid Works (a Computer Aided Design programme) and then 3D printed. It consisted of a slide and slider. A thread was cut into the top of the cylinder (c) in the slider. The micrometre was then screwed into the thread thus keeping the body of the micrometre rigid but still allowing the depth gauge to move up and down. The

scalpel was then machined down with slots cut at 180 degrees to each other so that it could slide in the cylinder without rotating. A magnet was used to attach the scalpel to the micrometre. This allows the micrometre to rotate without rotating the scalpel. It also facilitates changing the scalpel blades.

The apparatus was adjusted so that, for each individual stem, the notch penetrated to a depth equal to half the stem diameter. This is a limitation of the study: other notch depths were not used. It was chosen so that the notch would penetrate all the different structural layers from outside to inside.

When testing the notched specimens the notch was placed opposite the central loading point, on the tensile (i.e. convex) side of the bend. The raw data was manipulated to correct for differences in diameter from specimen to specimen, using a method described below (section 4.2.4).

4.2.3 Fracture Toughness

The standard formula for fracture toughness is:

$$K_c = Y\sigma_f\sqrt{\pi a} \qquad\qquad \textit{(Equation 4.1)}$$

Where Kc is the fracture toughness, Y is the geometrical factor, σ_f is the applied stress and a is the crack length. The value of Y for the present case (a circular beam in bending with a crack length equal to half the beam diameter) is 1.2 [8]. This applies to the case of a crack which propagates through the beam in the transverse direction, which happened in some cases. However in other cases the stem failed due to a greenstick fracture, meaning the crack turned 90 degrees and propagation occurred longitudinally.

We were unable to find a solution in the literature for this crack geometry in bending. However, there is a solution for this crack in tension [9]. For a straight crack in tension in an infinite body Y = 1. For a crack containing a 90-degree bend giving a small extension parallel to the tensile load, two stress intensity factors can be defined: Y(I) = 0.289 for tension and Y(II) = 0.327 for in-plane shear. Conventionally the total K value is obtained by finding the square root of the sum of the squares of each K value. As a result, the appropriate value for Y for greenstick fractures is 0.436, so this was used to obtain K_c in those cases.

4.2.4 Morphological and anatomical analyses

Morphological analysis was done using microtomographic (microCT) scans performed using a Bruker Skyscan 1272 (Kontich, Belgium). A 10 to 15 mm long sample was cut from each of the three species. All recordings were performed as 360° scans with a rotatory step size of 0.6 and a spatial resolution of 5 µm. NRecon software (Version 1.6.10.1, Skyscan, Kontich, Belgium) was used for data reconstruction, including ring artefact reduction and beam hardening correction. The data was visualized using CTVox software (Bruker, Kontich, Belgium) and analysed using Image J software.

Anatomical analysis of the stems' cellular composition involved using a phloroglucinol staining technique. A handheld microtome (MT.5503, Euromex Microscopen, Arnhem, Netherlands) was used to cut transverse sections of fresh plant stems with a thickness between 15 and 25 µm. The sections were stained using a solution of Phloroglucinol (5 g in 100 ml of 92% EtOH and a few drops of hydrochloric acid; colouring the lignified cell walls in red) for 30 seconds and photographed using a light microscope (Primo Star, Carl Zeiss Microscopy GmbH, Jena, Germany) equipped with a camera (AxioCam ERc 5s, Carl Zeiss Microscopy GmbH, Jena, Germany).

4.2.5 Finite element analyses

Finite element models were made of idealised materials subject to three-point bending to compare and contrast against our plant stems. Models were developed on Ansys 2021 R2. The model was developed from that used in our previous work [7]. The geometry for the stems was chosen to be a 15cm long cylinder with a constant cross-sectional diameter of 8mm. Symmetry was applied in two planes for computational efficiency. A fixed support and loading support were modelled as rigid bodies and added to the model to replicate the supports found on the Instron testing machine. Displacement was applied to the loading support and a frictional coefficient of 0.15 was applied. Notches were modelled with a perfectly sharp tip increasing to a width of 0.5mm at the tensile surface. Two material models were used, the rationale for which is explained below in the Theory section. For the "plastic, tough" material we used Ansys's built in properties for steel which included a Young's modulus of 200GPa, a bilinear stress/strain curve with a yield strength of 250MPa (assuming no work hardening) and a Poisson's ratio of 0.3. The "elastic, brittle" material used built in properties for glass, with a Young's modulus of 70GPa, a tensile strength of 32.56MPa and a Poisson's Ratio of 0.21. For both notched and plain specimens a hexahedral-dominant mesh was applied and refined until

mesh independence was achieved. The mesh had a total of 27473 nodes with 5874 elements. Elements were primarily 20 node hexahedrons (Hex20) 1mm in size. Hollow models were made by removing a 5.4mm diameter cylindrical section from the stem. Mesh independence required more elements due to the thin wall of the stems. The model had a total of 49010 nodes and 9490 elements. The elements were primarily Hex20 with a size of 0.5mm.

The FEA model was also used, with no introduced notch, to determine correction factors in order to normalise plant stems of different diameters. Models were created based on the initial plastic, tough model with diameters ranging from 7mm to 12mm. From the results was determined a correction factor that could be applied to the experimental force values to normalise all test results to a stem diameter of 8mm, allowing direct comparison of all data. The model used the same properties as the plastic, tough idealised material.

4.2.6 Statistics
Statistics were performed using Excel (2019), comparing parameters from each species as well as from notched and plain specimens. T-tests were performed at a significance level defined at $p = 0.05$.

4.3. Theory

4.3.1 Defining Defect Tolerance

The term "defect tolerance" is used extensively in engineering to define the resistance of materials and structures to the presence of cracks and other defects which cause local stress concentrations. However, there is no strict definition of the term. Conventionally, in the fracture mechanics literature, defect tolerance is defined using the fracture toughness, in its linear elastic form K_c or, if appropriate, its elastic/plastic form J_c. As such it is a material property, defining the tendency of the material's strength to be reduced as a result of the presence of a crack of a given length. However, in engineering structures defect tolerance will depend not only on material properties but also on the geometry of the component in question as well as the manner in which it is loaded.

Here we propose a new definition of defect tolerance, in terms of a factor DT, defined as the ratio between the failure force for a structure containing no defects to the same structure containing a given defect. For convenience, we refer to the defect-free structure as "plain" and

the defect-containing structure as "notched". Defining F_p and F_n as the failure force for the plain and notched cases respectively, then:

$$DT = F_n/F_p \qquad\qquad\qquad\qquad \text{(Equation 4.2)}$$

The failure force in this context could refer to, for example, the force to cause yielding (i.e. the onset of plasticity), the maximum force that the structure can bear, or the force to cause fracture. The concept of a DT factor can be extended to cover other mechanical parameters of a structure which may define its performance, such as elastic stiffness, deflection at failure and absorbed energy at failure. The most appropriate parameter will depend on the circumstances and applications of the structure.

Defined in this way, DT will take a value of 1.0 if the structure is perfectly defect tolerant, i.e. if the defect in question has no effect. Values between 1.0 and 0.0 indicate some degree of defect tolerance, allowing quantitative comparisons between different materials and designs.

We chose the following mechanical parameters from which to calculate DT values:

- Slope of the initial, force/displacement line. This determines how much the beam deflects elastically under load.
- Force at which yield occurs F_y, and the displacement at this force.
- Maximum force F_{max} (or the force at which fracture occurs if this happens before the maximum force) and the displacement at this force.
- The force required to reach a given large value of displacement.
- Energy parameters, calculated as the area under a given segment of the force/displacement curve. Three parameters can be defined: the energy up to the yield point, the energy up to the maximum force (or fracture force) and the energy for a given large deflection.

It is useful to consider what values of DT will occur in certain cases of well-known engineering materials. This will provide baseline values against which to compare our experimental results. Therefore, we define the following two idealised materials:

"Plastic, tough". This material yields and is capable of significant plastic deformation before failure. It has a high fracture toughness so it does not fail by propagation of a crack from the notch. Rather, it undergoes complete yielding through the remaining cross section and thus

develops a plastic hinge. An example of such a material is low-carbon structural steel. This material will display very high defect tolerance and so we propose it as a baseline against which to compare other materials. We hypothesise that any experimental tests will reveal DT values which are equal to, or less than, the ones derived for this material.

"Elastic, brittle" (e.g., glass). This material has a low fracture toughness and relatively high yield strength and Young's modulus. In bending tests it does not yield. Plain samples will fail from small manufacturing defects at an ultimate stress σ_u which depends on the manufacturing conditions. In practice σ_u will vary somewhat from specimen to specimen but can be defined by an average value. The notched bar fails when the elastic fracture toughness K_c is reached (treating the notch as a crack). An example of such a material is glass. This material is expected to have low DT values for most specified parameters. We hypothesise that experimental results from our plant stems will show DT values which are greater than or equal to those derived for this material.

Though it would be possible to carry out experimental tests on steel and glass to obtain DT values, in the present work we obtained them using FEA, as described above, since the aim was to obtain extreme values of DT for comparison with our tests on plant stems. In the present work we confined ourselves to one particular type of loading: three point bending. We considered two different geometries: a solid beam of diameter 8mm and a hollow beam of outer diameter 8mm and inner diameter 5.4mm, to reflect the cross sections of our plant stems (see Results below). These two beams were chosen to reflect the geometries found in our test specimens, which will be described below. In both cases we considered the effect of a sharp notch of depth 4mm.

4.4. Results
4.4.1 FEA Results

Figure 4.4a shows results from FEA for the plastic, tough material, for the four geometries considered. Initially the force/displacement lines are straight and steep, indicating elastic deformation, following by a reduction in slope as yielding occurs. The force rises to a maximum as the plastic hinge forms and subsequently decreases due to ovalisation and other factors. For a detailed description of the behaviour of plain stems see our previous paper [7]. Behaviour is similar for the hollow stem except for a reduction in force due to the reduced I value of the cross section. Behaviour is similar for notched beams but, even though no crack propagation occurs from the notch, the force for a given displacement is still reduced due to the reduced load-bearing cross section.
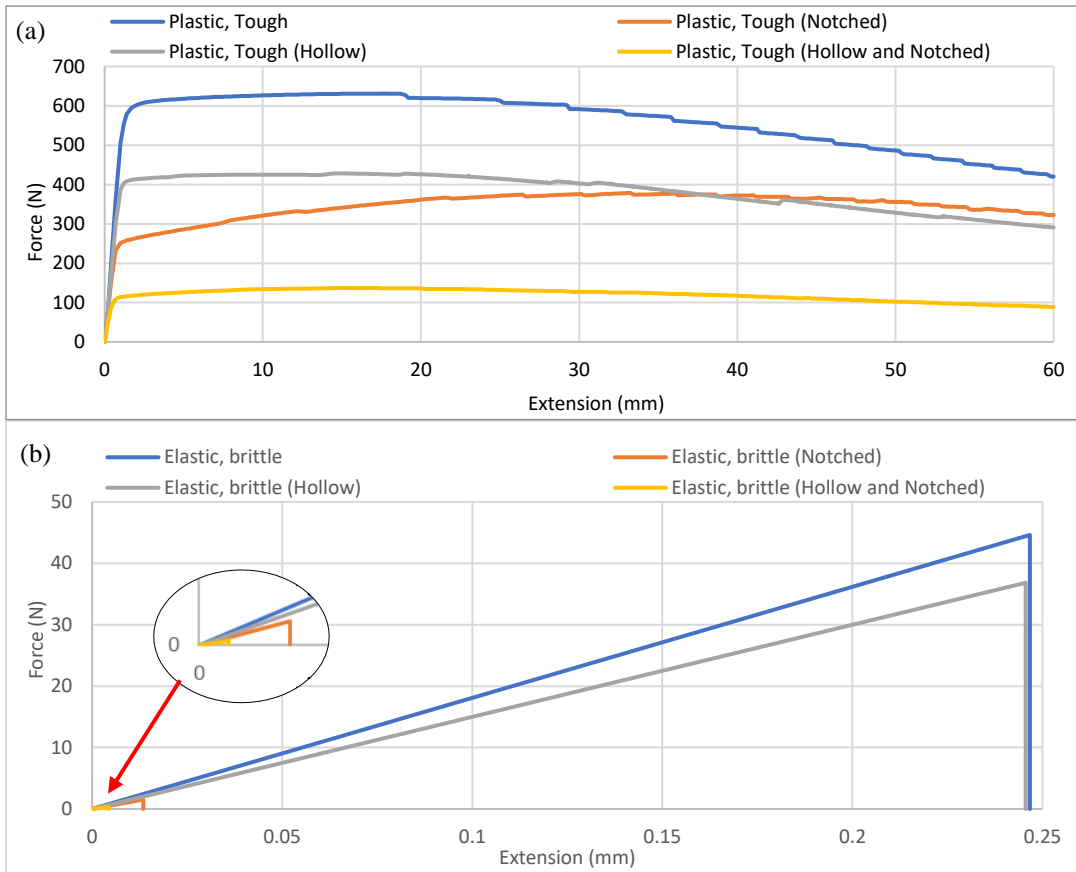
Figure 4.4: (a) Plastic tough comparison of three-point bending curves for notched, hollow and plain specimens. (b) Elastic, brittle comparison of three-point bending curves for notched, hollow and plain specimens.

Figure 4.4b shows results for the elastic, brittle material. Linear, elastic behaviour is maintained up to failure. Notched specimens fail by crack propagation when K_c is reached. Here the effect of the notch can be seen to greatly reduce the structural integrity of the specimens.

Table 4.1 compares the defect tolerance values obtained from the results shown in figure 4.4. The DT of slope of the elastic region is the only parameter that is essentially the same for both the plastic tough and elastic brittle materials. The slight difference is likely due to the two materials having different Poisson's ratios. For all other parameters the DT for the elastic, brittle material is, as expected, much lower than that of the plastic, tough material. Most DT parameters for the plastic, tough material are significantly less than 1.0, due to the effect of the reduced load-bearing cross section at the notch. Exceptionally, the DT values for extension and energy at maximum force are greater than 1.0, implying a benefit to the presence of the notch. This is because the notched specimens displace more for given force. This can be regarded as advantageous for plant stems, as they will be able to deflect more without breaking. For engineering components, it may or may not be an advantage, depending on the circumstances.

Table 4.1: DT parameters from FEA for plain and hollow plastic, tough and elastic, brittle materials.

Specimen	Slope of Elastic Region	Yield force	Yield extension	Max force	Extension at max force	Energy to 30mm	Energy to yield	Energy to max force
Plastic, Tough	0.66	0.46	0.70	0.60	1.88	0.54	0.35	1.04
Elastic, Brittle	0.63	N/A	N/A	0.03	0.05	N/A	N/A	0.0019
Plastic, Tough (Hollow)	0.49	0.28	0.58	0.32	1.05	0.08	0.17	0.07
Elastic, Brittle (Hollow)	0.48	N/A	N/A	0.01	0.02	N/A	N/A	0.0002

4.4.2 Experimental Results
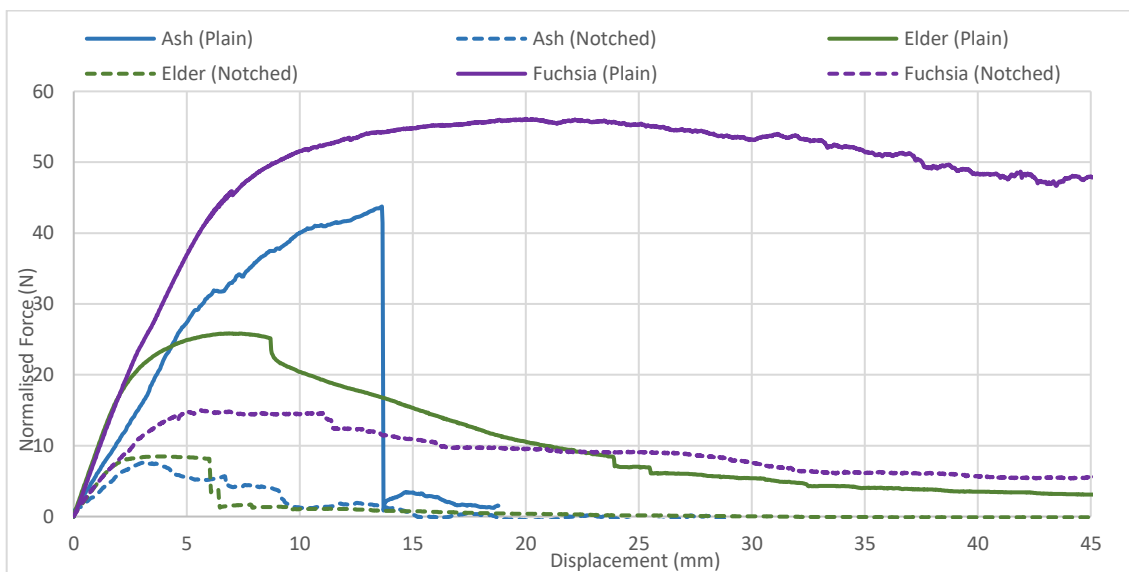
Figure 4.5: Typical three-point bending curves of ash, elder and fuchsia for notched and plain specimens. Force values have been normalised to represent stems of the same diameter (8mm).

Figure 4.5 shows typical force/displacement results for plain and notched specimens from each species. The force values were normalised to a stem with a diameter of 8mm (as explained above) to allow comparison. As expected, notched specimens perform considerably worse than their plain counterparts. Table 4.2 shows results for all mechanical properties measured.

	Slope of elastic region (N/mm)	Yield force (N)	Yield extension (mm)	Max force (N)	Extension at max force (mm)	Energy to yield (mJ)	Energy to max force (mJ)	Energy up to 30mm (mJ)
Fuchsia (P)	8.01 ± 4.4	21.5 ± 5.61	4.09 ± 2.13	42.18 ± 9.99	28.28 ± 8.27	35 ± 23.1	572.4 ± 281.1	868.1 ± 316.9
Fuchsia (N)	4.69 ± 1.73	13.79 ± 5.21	4.27 ± 2.65	17.77 ± 8.69	11.53 ± 9.9	28.5 ± 24.9	143.1 ± 187.2	410.9 ± 230.1
Ash (P)	4.05 ± 1.14	18.69 ± 6.06	3.4 ± 1.13	31.57 ± 8.52	13.59 ± 5.96	49.1 ± 26.1	403.3 ± 155.8	551.5 ± 164.2
Ash (N)	3.63 ± 1.67	10.79 ± 3.77	1.89 ± 0.98	12.21 ± 3.65	2.98 ± 1.53	21.7 ± 10.6	40.97 ± 17.8	155.46 ± 78.4
Elder (P)	8.11 ± 2.84	24.67 ± 9.19	1.75 ± 0.26	26.77 ± 11.88	3.78 ± 1.35	45 ± 30.4	112.5 ± 53.9	422.7 ± 201.6
Elder (N)	5.46 ± 2.35	8.06 ± 1.53	0.62 ± 0.1	10.26 ± 2.66	2.16 ± 1.39	7 ± 1.4	39.7 ± 18.1	65.2 ± 23.1

(a)

(b)

Figure 4.6:(a) Progression of greenstick failure in fuchsia. (b) Plastic hinge failure mechanism in fuchsia.

Fuchsia was the strongest and has the largest area under the curve in both notched and plain specimens. In the plain state once the yield point has been exceeded it has little impact on the mechanical integrity of the stem as it has the ability to continuously plastically deform near the maximum stress. For the example shown in figure 4.6, no crack was formed from the notch: rather, the specimen failed by forming a plastic hinge in the same manner as our ideal "plastic, tough" material. In our previous work [7] we found that fuchsia will primarily fail with a plastic hinge (figure 4.6b) however in a minority of cases it fails by crack propagation, always in the form of a greenstick fracture (figure 4.6a). Of the seven tests on plain specimens five failed with plastic hinge and two with greenstick. In the notched tests all six samples failed with a greenstick fracture. This phenomenon was also observed by other workers [7], [10], [11]. In plain specimens a greenstick occurs when a crack forms on the surface at the tensile side and rapidly propagates through the cross section until reaching a point where it changes direction and propagates longitudinally.
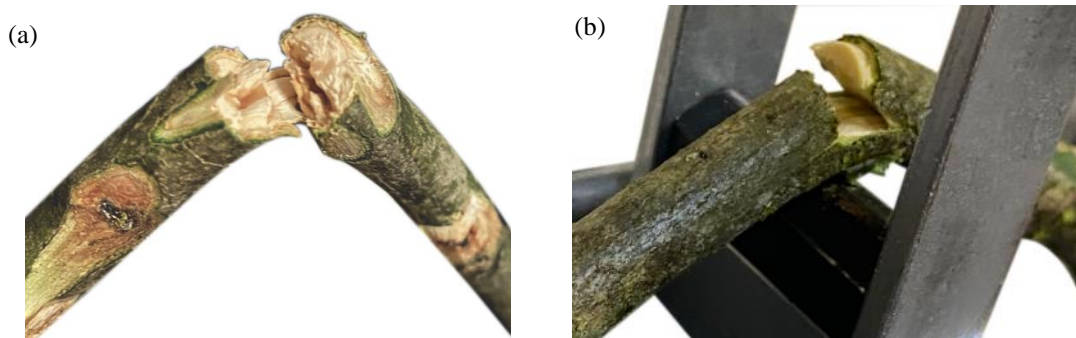
Figure 4.7:(a) Tensile diffuse fracture in plain specimen ash (b) Greenstick failure in plain ash.

Interestingly, the presence of the notch had virtually no effect on the elastic slope. All other measured parameters except the yield extension decreased significantly.

Ash was found to be somewhat weaker than fuchsia. A major difference is that ash can fail suddenly once the maximum force is reached. This is a result of in some cases a tensile diffuse fracture (previously observed by other workers [10], [12]). In plain specimens, tensile fracture initiated on the tensile side of the stem and propagated through the cross section, leaving a rough, jagged fracture surface characterised by short longitudinal splits (figure 4.7a). In the plain specimens four failed with a greenstick (figure 4.7b) and two with tensile diffuse fracture. In the greenstick fractures that occurred, the longitudinal crack tended to divert diagonally through the cross section of the stem until it almost reached the other side. Both of these failure mechanisms are undesirable as they do not preserve the mechanical integrity in the same way a plastic hinge or longitudinal greenstick fracture will. All seven notched ash specimens failed

with a form of tensile crack propagation. As Table 4.2 shows, all measured properties decreased when a notch was introduced.

(a)   (b)
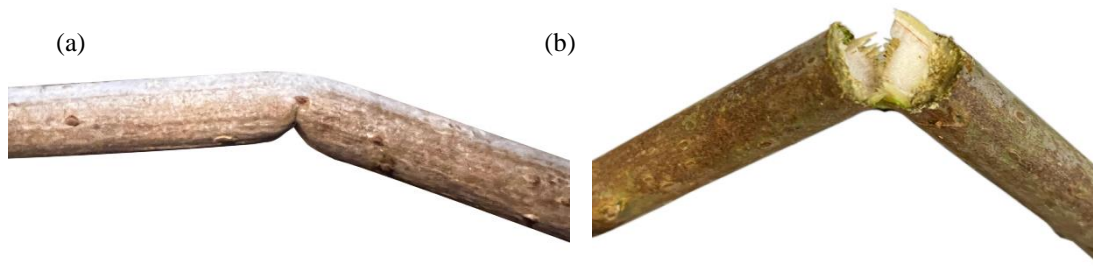
Figure 4.8: (a) Buckling failure in plain specimen elder. (b) Tensile fracture in notched elder.

The stems of elder were found to have a large central pith (see results below) making the cross section more like that of a hollow tube. Plain specimens failed by buckling (figure 4.8a). Despite buckling, no external crack is formed, and the specimen therefore gradually fails while continuing to absorb energy. All six of the plain specimens failed by buckling. Once a notch was introduced into elder, specimens failed with a tensile fracture by transverse crack propagation (figure 4.8b). As Table 4.2 shows, the introduction of a notch reduced all measured properties.

Table 4.3 shows results of T-tests to identify statistically significant differences. Considering the differences between plain and notched samples of the same species, there is no significant change in elastic slope in any species. Most of the other parameters show significant changes, especially if one includes those cases for elder where the p value is only slightly above 0.05. Exceptionally, fuchsia shows non-significant changes for yield extension and yield energy and elder is non-significant for extension at maximum force.

Comparing one species to another, it is notable that whilst there are many significant differences, some quite larger differences are non-significant, owing to the relatively large amount of scatter in some measured properties.

Table 4.3: T-Tests comparing notched and plain specimens of fuchsia, elder and ash (p < 0.05, P=Plain, N=notched).

T Tests	Slope of Elastic Region	Yield Force	Yield Extension	Max Force	Extension at Max Force	Energy to yield	Energy to max force	Energy up to 30mm
Fuchsia (P/N)	0.11	0.027	0.898	0.0007	0.007	0.634	0.009	0.014
Elder (P/N)	0.209	0.020	0.0002	0.055	0.136	0.075	0.063	0.021
Ash (P/N)	0.617	0.015	0.025	0.0002	0.0008	0.027	0.00007	0.0001
Fuchsia/Elder (P)	0.366	0	0.002	0	0	0.517	0.002	0.013
Fuchsia/Elder (N)	0.590	0.0002	0.0187	0.001	0.055	0.191	0.387	0.040
Elder/Ash (P)	0.009	0	0	0	0.00004	0.806	0.002	0.253
Elder/Ash (N)	0.193	0.00004	0.003	0.00001	0.001	0.050	0.920	0.094
Fuchsia/ Ash (P)	0.838	0.403	0.982	0.066	0.004	0.326	0.218	0.050
Fuchsia/ Ash (N)	0.286	0.254	0.049	0.150	0.044	0.519	0.176	0.018

Table 4.4 shows the measured fracture toughness properties of our three plant species, including for comparison the value used for our idealised elastic brittle material. Fracture toughness was calculated because, as noted above, it is often used as a measure of defect tolerance. All three species showed toughness values of the same order of magnitude. The only species that failed by longitudinal (i.e. greenstick) fracture from the notch was fuchsia, giving it the lowest fracture toughness.

Table 4.4: Fracture toughness properties of specimens.

Material	K (MPam^0.5)
Fuchsia Greenstick	0.97 ± 0.36
Elder	1.66 ± 0.5
Ash	2.02 ± 0.6
Elastic, Brittle	0.70

4.4.3 Microscopy and Micro CT

Figure 4.9 shows cross sections through stems obtained using microCT, revealing
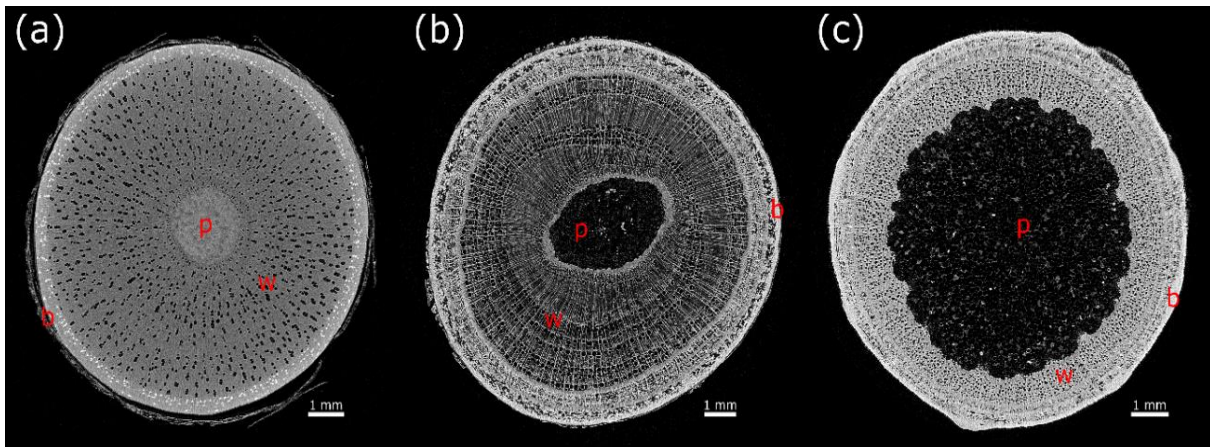
different patterns in each species.All three have a pith in the centre composed of

Figure 4.9: Micro CT scans of (a) fuchsia, (b) ash and (c) elder. p indicates the pith,w, indicates the woody tissue and b the Bark.

parenchyma cells, which are known to have very little mechanical strength. Fuchsia has the smallest pith taking up 4.2% of the cross section (figure 4.9a), and the pith in fuchia is denser than in the other two species. Ash has a pith taking up 7.6% of the cross section (figure 4.9b). Elder has the largest pith, taking up 46.2% of the cross-sectional area (figure 4.9c). As a result of these observations, hollow tubes reflecting the cross section of elder were created in FE models (see above). The other two species were treated as having solid cross sections.

Staining with Phloroglucinol provides a more detailed breakdown of the different cell types within the cross-section (figure 4.10). The dark red areas are the xylem, composed of dense, lignified cells: this area provides the main load-bearing capacity. The central pith can generally be identified as a region of larger cells with lower density. The pith dominates the cross section of elder: the dark staining of the xylem payer in elder indicates that though relatively small, it is highly lignified. However, it can be noted that elder consists of a more densely packed wooden ring. Ash has the most lignified cross section, that includes a lignified pith, which is not present in fuchsia or elder.

(a) Ash
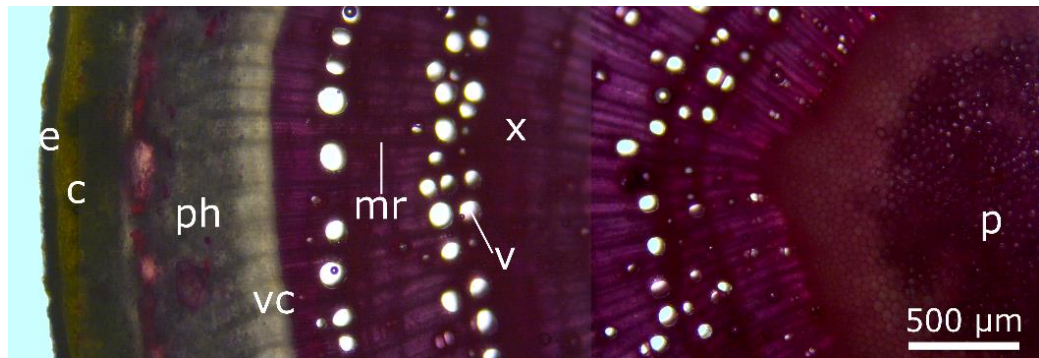
(b) Fuchsia
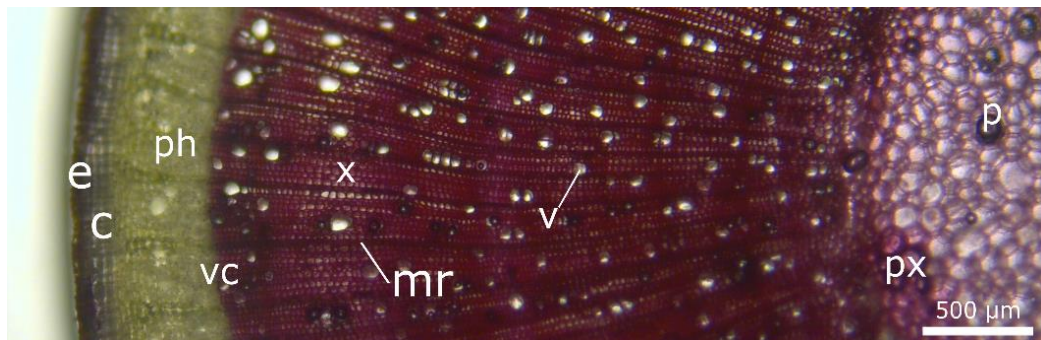
(c) Elder
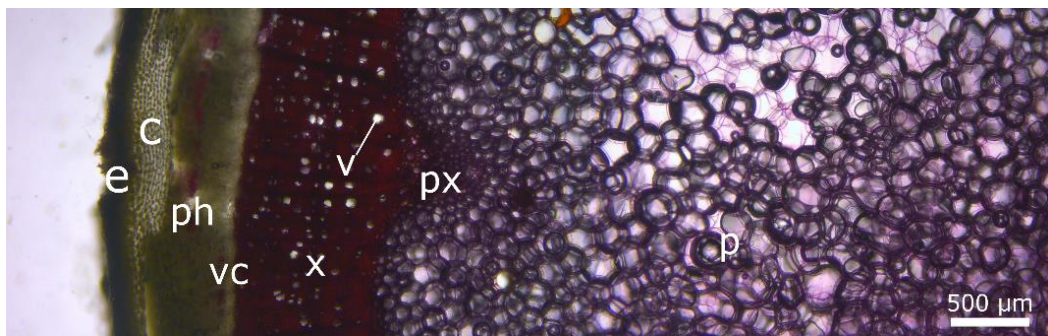
Figure 4.10: Phloroglucinol stained sections of (a) ash, (b) fuchsia and (c) elder, going from the outer surface on the left to the centre on the right. e = epidermis, c = cortex, ph = phloem, vc = vascular cambium, x = xylem, p = protoxylem, p = pith.

4.5. Discussion

The experimental results have revealed considerable differences between the three plant species, not only in their force/displacement curves but also in their mechanisms of deformation and failure and in their response to the introduction of a defect in the form of a notch.

Table 4.5: DT values for normalised fuchsia, ash and elder compared to FEA models of a "plastic, tough" and "elastic, brittle" homogenous materials.

	Slope of elastic region	Yield force	Yield extension	Max force	Extension at max force	Energy to yield	Energy to max force	Energy up to 30mm
Fuchsia	0.59	0.64	1.04	0.42	0.41	0.81	0.25	0.47
Elder	0.67	0.33	0.35	0.38	0.57	0.16	0.35	0.15
Ash	0.90	0.58	0.56	0.39	0.22	0.44	0.10	0.28
Plastic, Tough	0.66	0.46	0.70	0.60	1.88	0.35	1.04	0.54
Plastic, Tough (Hollow)	0.49	0.28	0.58	0.32	1.05	0.17	0.07	0.08
Elastic, Brittle	0.6257	0.0341	0.0545	0.034	0.0545	0.0019	0.0019	N/A
Elastic, Brittle (Hollow)	0.4758	0.0085	0.0179	0.009	0.0179	0.0002	0.0002	N/A

Table 4.5 and Figure 4.10 show the defect tolerance (DT) values calculated for the various mechanical properties measured. These are shown for the experimentally measured values and also for those of our two idealised materials (calculated for both solid and hollow cross-sections). Those DT values based on stiffness, force or energy are invariably less than 1.0, indicating a significant effect of the presence of the notch. DT values based on extension can be greater than 1.0 in some cases, reflecting the increased deflection of notched samples, which could be interpreted as favourable or unfavourable, depending on the circumstances. For a plant stem, the ability to deflect a large amount under wind loading without breaking is a useful attribute, but it may be unsuitable for an engineering component.

Fuchsia on average has the best DT properties compared to the other species (and compared to the idealised materials) for the yield force, and area to yield (figure 4.11). The idealised plastic, tough material outperforms the stem materials for maximum force, energy to 30mm and energy to the maximum force. This suggests that fuchsia is highly defect tolerant in the initial stages of loading, especially up until the yield point. Whereas our idealised material is able to continue to be defect tolerant at larger deflections.
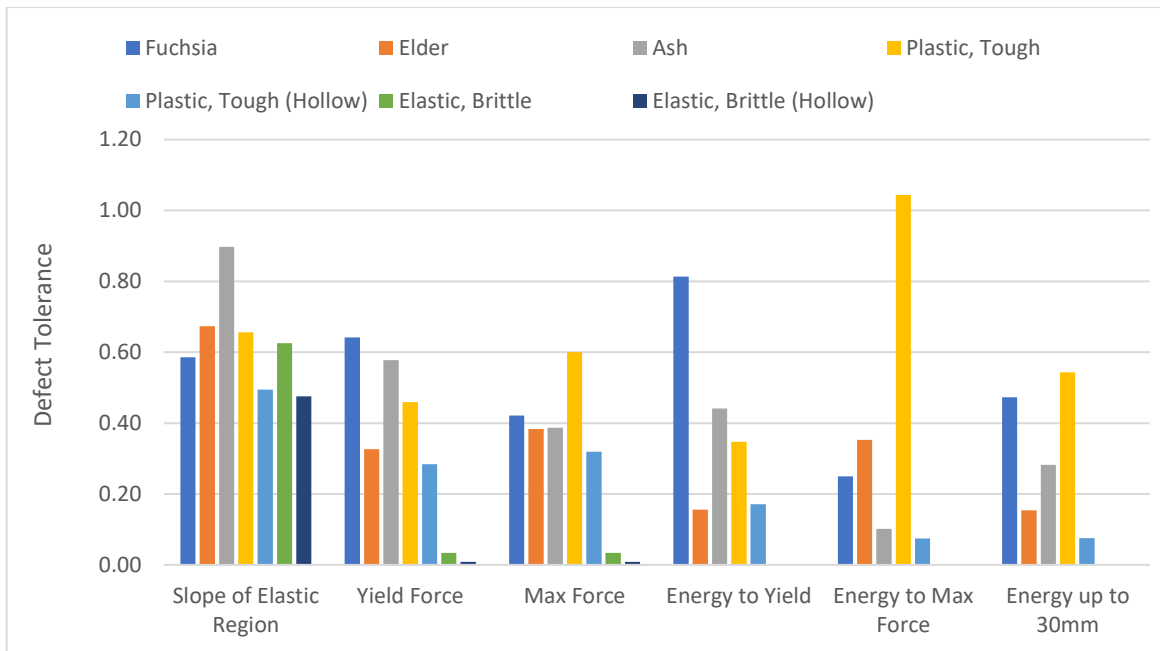
Figure 4.11: Defect tolerance comparison of all specimens.

A possible explanation for these results is the fact that the stem material (along with all woody materials) has a much higher strength in tension than in compression. In previous work [7] we showed that fuchsia stems loaded in tension failed at a stress of 54.3MPa, showing no yielding behaviour, whilst in compression they yielded at a stress of 11.4MPa. Thus, when a stem is loaded in bending, all the yielding occurs on the compression side. Introducing a notch, though it has some effect by reducing the cross section, has less effect that in a conventional engineering material because yielding does not occur at the notch tip. In the plastic, tough material, by contrast, the yield point will be characterised by a plastic zone spreading from the notch. Another possible explanation for this lies in the presence of residual stress. Plants grow with a tensile and compressive residual stress throughout their cross sections [13]. The outer fibres are in tension and the inner fibres are in compression. By putting a notch in the specimen we have moved the location of maximum applied tension from a region of residual tension (the outer surface) to one of residual compression (the core). The presence of the notch will also cause some local stress redistribution, but nevertheless the remaining residual stress will tend to oppose the applied bending stresses.

After yielding, the structure appears to be more compromised than the plastic, tough material. This is most likely due to the accumulation of damage in the material. In our previous work we noted two types of damage: compressive damage which reduced the load-bearing capacity of the material by approximately half for applied strains greater than 0.29, and cracking near the

centre of the stem due to ovalisation [7]. Fuchsia appears to be the most balanced of all three species as it can fail with either a plastic hinge or a greenstick fracture; this coincides with high DT for the yield load. Its ability to absorb energy when damaged is likely due to its ability to plastically deform without breaking. As a greenstick fracture occurs after yielding, properties such as slope of elastic region, yield strength and yield extension are unaffected by the change in failure mechanism. We found that once the notch was introduced the specimen always failed by crack propagation, with the crack travelling exclusively longitudinally from the notch tip. This leaves half the stem intact, thus preserving some of its mechanical strength.

Elder differs from fuchsia in having a soft central core, thus approximating to a hollow tube. Plain and notched elder specimens exhibit two very different failure mechanisms. The buckling in the plain specimens occurs after yielding, presumably as a consequence of collapse at the compression surface; it preserves a large proportion of the mechanical integrity until very large displacements are reached. However, in notched specimens a tensile fracture occurs by crack growth from the notch, causing a sudden load drop and a much reduced area under the curve in comparison to the fuchsia samples, especially those failing by plastic hinge formation. Its relatively low DT values are thus seen as a consequence of its low fracture toughness and its inability to deflect the crack to cause a greenstick fracture.

Elder had a relatively high DT value for elastic slope, though the effect is less dramatic than for ash, perhaps due to a smaller effect of compressive residual stress owing to the core material having a lower Young's modulus. For all DT values except energy to yield, elder was found to be higher than the hollow version of our plastic, tough material but lower than the solid version. This may simply reflect the role of the soft core, which provides some limited support to the structure. Karam and Gibson analysed the effect of a low-stiffness core in the bucking of tubes loaded in bending [14], showing that core stiffness has a strong effect.

While reasonable DT values are achieved for the force applied, those for the area under the curve are very poor meaning a notched specimen is unable to absorb much energy during loading. This is because the tensile fracture propagates right through the cross section leaving no material to resist the bending. As seen from the phloroglucinol staining, aside from the pith, elder has a stiff outer core. This allows the crack to travel straight through the cross section as if it was a brittle material. However, being fibrous it does not perform nearly as poorly as the elastic, brittle FEA model would predict. The energy to maximum force is considerably higher than for fuchsia or elder. This is likely due to elder reaching its maximum force relatively quickly in plain specimens relative to the other species.

Ash is a material commonly used for making sports implements such as baseball bats and hockey sticks. This is because it is a well-balanced wood in that its more flexible than a dense wood such as maple, but still demonstrates enough hardness not to deform on impact. Ash has the largest DT for the slope of elastic region and a high yield force and maximum force. However, it is not able to absorb as much energy, which is most likely due to the wood being stiffer and unable to displace as much under large deflections and failing with a catastrophic failure mechanism. The plastic, tough material is far superior at large displacements compared to ash. This is most likely due to the fibres being lignified in the pith and not deforming once a crack is introduced during bending. From figure 4.10a it can be seen that ash has the darkest overall cross section, indicating a large amount of lignification which gives rise to it demonstrating tensile and greenstick failure mechanisms.

 Having a slightly larger pith than fuchsia likely has a negative impact on ash's mechanical strength when notched. This is because the tensile forces are acting on a smaller area than that in the case of fuchsia.

In this work we have proposed a novel approach to the concept of defect tolerance. Our definition of DT values for a number of different mechanical parameters has enabled us to extract a large amount of information which allows different materials and structures to be compared in a more complete and nuanced way. It is clear that defect tolerance is not a single-valued quantity but rather a multi-factor property. Which of the several DT values is most important will depend on the circumstances. It is interesting to note that the well-recognised defect tolerance parameter K_c fails to capture the relative behaviour of these plant stems. In fact fuchsia, which had the lowest K_c value of the three species tested, proved to be the most defect tolerant according to our DT parameters. This is due in part to fuchsia's ability to deflect the crack into the longitudinal direction (a feature of its high anisotropy) and therefore prevent total failure.

Our results have revealed that plant stems possess remarkably high defect tolerance, in some cases greater even than an idealised material which we originally chose in order to establish an upper bound to possible DT values. These very high DTs appear to result partly from structural properties in the stem (e.g. residual stress, hollow tube with soft core) and partly from special material properties such as differences in compressive and tensile strength, allowing sharp notches to be tolerated effectively. On the other hand, the plastic, tough material was found to out-perform the stem materials in those properties related to high levels of deformation. This illustrates the advantages of those engineering materials (mostly metals) which are capable of undergoing large plastic strains.

This work had some limitations. We considered only one type of loading (three-point bending) and only one type of defect: a sharp notch with a depth equal to the radius of the stem. Future work is needed to build up a more complete picture including notches of different depth and sharpness. The results may prove useful in understanding the mechanical integrity of plant stems, giving insights which in future may help to create better, more defect tolerant engineering structures.

4.6. Conclusions

This study investigated a new approach for calculating defect tolerant properties of natural structures, and applied the approach to three different plant stems. The approach involved analysis of force/displacement curves recorded during three-point bend tests on each species. Due to their complex fibrous compositions with integrated residual stresses the three species performed exceptionally well compared to their idealised material counterparts. Fuchsia performed the best out of the three species for our given set of tests. We believe this is due to its ability to fail with both plastic hinge and greenstick failure mechanisms. Imaging techniques revealed that each stem had different cross-sectional area and composition of tissues. This aided in explaining why some structures are more advantageous than others. Defect tolerant values indicate that plants can outperform many conventional engineering materials.

It is clear from the results of this work that plant structures have developed complex processes to resist damage by external forces. In-depth studies of the behaviour of plants in terms of their defect tolerance and ability to withstand bending forces should lead to inspire the development of man-made materials with further improvements in these characteristics. By optimising the geometry and structure of modern engineering materials in a similar way to plants in nature, we could potentially unlock new and as yet unseen defect tolerant properties. These properties could have a magnitude of uses where crack propagation must be avoided to maintain the integrity of a structure.

Acknowledgements:

4.7 References:

[1]   J. F. V. Vincent, "Fracture Properties of Plants," *Adv. Bot. Res.*, vol. 17, no. C, pp. 235–287, Jan. 1990, doi: 10.1016/S0065-2296(08)60135-4.

[2]   N. Kosteski, J. A. Packer, and R. S. Puthli, "Notch Toughness of Internationally Produced Hollow Structural Sections," *J. Struct. Eng.*, vol. 131, no. 2, pp. 279–286, Feb. 2005, doi: 10.1061/(asce)0733-9445(2005)131:2(279).

[3]   R. P. Johnson, "COMPOSITE STRUCTURES OF STEEL AND CONCRETE VOLUME 1 BEAMS, SLABS, COLUMNS, AND FRAMES FOR BUILDINGS SECOND EDITION."

[4]   X. Huang and S. Zhao, "Damage tolerance characterization of carbon fiber composites at a component level: A thermoset carbon fiber composite," *J. Compos. Mater.*, vol. 52, no. 1, pp. 37–46, Jan. 2018, doi: 10.1177/0021998317702435.

[5]   J. F. V. Vincent, "Strength and fracture of grasses," *J. Mater. Sci.*, vol. 26, no. 7, pp. 1947–1950, Jan. 1991, doi: 10.1007/BF00543628.

[6]   T. Speck and I. Burgert, "Plant Stems: Functional Design and Mechanics," *Annu. Rev. Mater. Res.*, vol. 41, no. 1, pp. 169–193, Aug. 2011, doi: 10.1146/annurev-matsci-062910-100425.

[7]   T. Hone, M. Mylo, O. Speck, T. Speck, and D. Taylor, "Failure mechanisms and bending strength of *Fuchsia magellanica* var. *gracilis* stems," *J. R. Soc. Interface*, vol. 18, no. 175, p. 20201023, Feb. 2021, doi: 10.1098/rsif.2020.1023.

[8]   A. E. Ismail, A. K. Ariffin, S. Abdullah, M. J. Ghazali, M. Abdulrazzaq, and R. Daud, "Stress intensity factors under combined bending and torsion moments," *J. Zhejiang Univ. Sci. A*, vol. 13, no. 1, pp. 1–8, 2012, doi: 10.1631/jzus.A1100040.

[9]   Y. Murakami, *Stress intensity factors handbook*. Oxford: Elsevier, 1987.

[10]   A. R. Ennos and A. Van Casteren, "Transverse stresses and modes of failure in tree branches and other beams," *Proc. R. Soc. B Biol. Sci.*, vol. 277, no. 1685, pp. 1253–1258, 2010, doi: 10.1098/rspb.2009.2093.

[11]   S. Özden, A. R. Ennos, and M. E. G. V. Cattaneo, "Transverse fracture properties of green wood and the anatomy of six temperate tree species," *Forestry*, vol. 90, no. 1, pp. 58–69, Jan. 2017, doi: 10.1093/forestry/cpw023.

[12]   A. van Casteren, W. I. Sellers, S. K. S. Thorpe, S. Coward, R. H. Crompton, and A. R. Ennos, "Why don't branches snap? The mechanics of bending failure in three temperate angiosperm trees," *Trees - Struct. Funct.*, vol. 26, no. 3, pp. 789–797, 2012, doi: 10.1007/s00468-011-0650-y.

[13]   R. Vandiver and A. Goriely, "Differential Growth and Residual Stress in Cylindrical Elastic Structures," *Source Philos. Trans. Math. Phys. Eng. Sci.*, vol. 367, pp. 3607–3630, 1902.

[14]   G. N. Karam and L. J. Gibson, "Elastic buckling of cylindrical shells with elastic cores—I. Analysis," *Int. J. Solids Struct.*, vol. 32, no. 8–9, pp. 1259–1283, Apr. 1995, doi: 10.1016/0020-7683(94)00147-O.

Chapter 5 Self-Repair of Fuchsia Magellanica Stems

Timothy Hone[1,], Max Mylo[2,3], Olga Speck[2,3] and David Taylor[1]*

[1]Trinity Centre for Biomedical Engineering, Department of Mechanical, Manufacturing and Biomedical Engineering, Trinity College Dublin, The University of Dublin, Ireland

[2]Plant Biomechanics Group, Botanic Garden, Faculty of Biology, University of Freiburg, Germany

[3]Cluster of Excellence *liv*MatS @ FIT—Freiburg Center for Interactive Materials and Bioinspired Technologies, University of Freiburg, Germany

Abstract:

The design and development of new engineering materials and structures are often inspired by what can be found in nature, especially in plants. Self-healing is an exciting new concept but is still in its infancy in that little technology has found its way to market. Plants have evolved to endure the unpredictable forces of nature. A mechanism that plays a key role in this survival is the ability to self-heal and repair damage to their stems. The damage inflicted is often as a result of the bending forces that arise from gusts of wind. This study draws on the strengths of both biological and engineering disciplines by discussion of a novel experiment where damage is inflicted on a live stem using three-point bending to emulate wind rather than a conventional methods of cutting. A portable three-point bending rig was developed and plant stems were tested and observed over a period of four and eight weeks in their natural habitat. An average increase in diameter at the damaged site was found to be 0.65 ± 0.33mm and 2.4 ± 0.54mm for the samples left for four and eight weeks to repair respectively. Mechanical repair was also evident for several parameters, including stiffness and maximum load. Numerous tests demonstrated the healing coefficient for the maximum load in the repaired samples was higher than that of the initial test. A combination of binocular images, stained microscopy and MicroCT scans assisted in understanding the responses and mechanisms plants experience during repair. The findings have relevance for the development and use of man-made materials which could mimic the behaviour of plant materials, as well as leading to a better understanding

of the biological processes involved. This is a pilot study, to develop the experimental method, and as such is useful even though more results are needed to confirm the findings.

Keywords: Bending, cracking, self-healing, self-sealing, plant stems, repair.

Authors' contributions:

Timothy Hone carried out the mechanical tests, developed the FEA models, designed and built the portable bending rig and wrote the manuscript. Max Mylo carried out the morphological and anatomical analysis of the specimens. David Taylor supervised the work and assisted in editing the manuscript.

5.1 Introduction

Our previous work (1) led to new information surrounding how plant stems initially respond to the forces that arise during three-point bending, emulating the effect of wind. Two failure mechanisms were observed, a greenstick fracture and plastic hinge. These failure mechanisms were unique and complex but also provided inspiration for a new self-healing structure (2) that made use of the discovery of an internal crack. We are optimistic that further investigating the response of fuchsia to damage over time will provide inspiration for future self-healing structures.

Plants are constantly battling the forces of nature and while they have impressive mechanical properties and unusual failure mechanisms (1) that optimise their chance of survival, they also have the ability to repair damage over time. Previous studies from biological disciplines have investigated repair in plants which primarily involved inflicting damage by means of cutting the stems (3–5). Studies have also investigated repair due to damage from internal growth stress (6) and twisting of vines (7). This study takes a novel approach by inflicting damage on stems using three-point bending. This is similar to previous work performed in our department on insect legs (8). Understanding the response mechanism of the plant could yield inspiration for engineering structures where bending forces could result in catastrophic failure.

A comprehensive review of the current literature on self-repair for bioinspired and biomimetic technology was documented by Speck and Speck (9). Quantifying self-repair is a primary focus of this paper. They reviewed that in previous literature (10–12) the healing efficiency (η) of

mechanical properties is calculated as a percentage of the property of the pristine material by using one of the following equations:

$$\eta\ (\%) =\ 100 \left[\frac{healed\ property}{pristine\ property}\right] \qquad \text{Equation 5.1}$$

There are two main mechanisms found in multicellular organisms when exposed to damage; self-sealing and self-healing (9). Generally, self-sealing comes first and then self-healing follows. So- called rapid self-sealing is carried out to close the wound and seal it off from the outside world. It will usually result in an injury remaining sub-surface such as a fissure where the functionality is restored to a point where is can still perform its previous functionality but all mechanical properties such as strength and stiffness are not completely restored. However, in the subsequent self-healing phase the injury is repaired and mechanical properties can be partially restored (9).
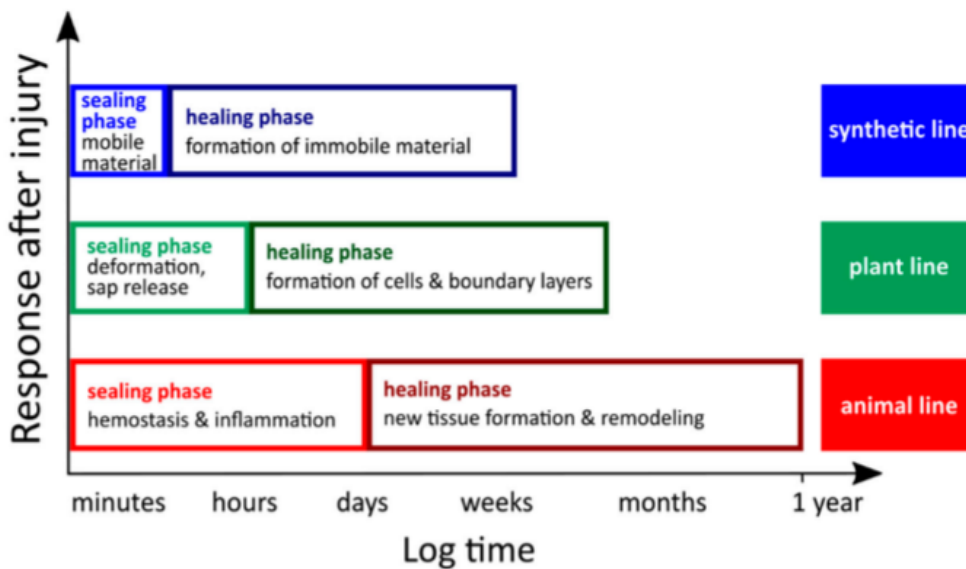
Figure 5.1: "Comparative depiction of self-repairing phases in plants, animals and technical materials. Although the phases may vary in duration and the underlying mechanisms are different, they all have in common that the initial sealing phase guarantees wound or damage closure and the healing phase leads to a (partial) restoration to the uninjured state" (9).

Plants being typically sessile cannot escape unfavourable environmental conditions and as a result have evolved a variety of morphological, anatomical and biochemical adaptations to survive (9). In plants such as latex, self-sealing can occur in minutes as a result of the discharge of plant saps that seal the crack or fissure. This helps to prevent infection and provides some mechanical support to the wounded site. Self-sealing is primarily based on physical reactions

whereas self-healing is based on chemical reactions and biological responses leading to a structural repair of these fissures so that they are no longer present. Self-healing is predominantly related to the formation of a "(ligno-) suberized boundary layer to the development of a wound periderm that induces cell division lasting from several days to weeks" (9,11).

The objective of this study is to develop a novel experiment to quantify and understand the healing mechanisms of fuchsia stems that have been overloaded in a manner similar to that which would occur naturally. The specific aims were to discover whether healing would occur and, if so, to calculate a healing coefficient for fuchsia. The addition of microscopy and Micro CT assist in understanding the mechanism of repair and change in load/displacement curves.

5.2 Materials and Methods

5.2.1 Plant material
Stems of Fuchsia magellanica var. gracilis (LINDL.) L.H.BAILEY (fuchsia) were tested in springtime in Dublin, Ireland in March 2020. F. magellanica is a flowering subshrub, which is widely cultivated in temperate regions. The stems on average were three years old.

5.2.2 Mechanical analyses
Performing three-point bending on live specimens required a portable three-point bending rig that could be used in the plant's natural habitat. The rig shown in Figure 5.2 was specifically designed and developed to perform these tests.
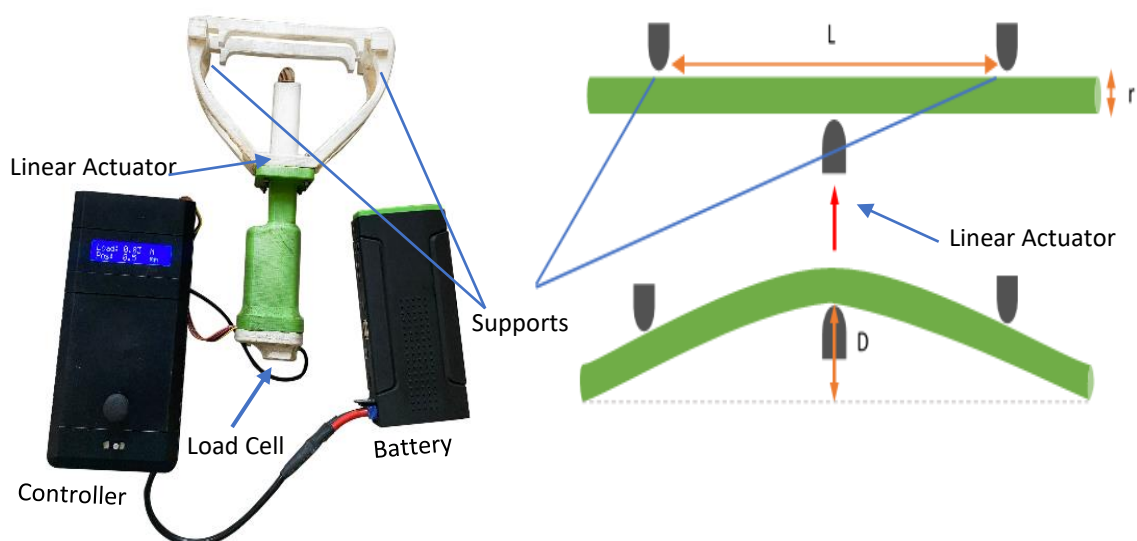
Figure 5.2: Image of three-point bending rig developed for performing tests on live plants with graphical illustration (supports 15cm apart)

Figure 5.3: Portable three-point bending rig used in the field.

This handheld three-point bending rig was constructed using 3D printing. The housing has adjustable mounts to set the span for three-point bending. For the following experiments the span was set to 15cm. The control was built around an Arduino Uno R3 microcontroller board with standard LCD display indicating measured load and extension. Joystick proportional-action for position/speed control is via a Parallax 2-axis joystick. The 3D printed housing contained a Sparkfun HX11 I2C load cell which permits 0.01N load measurement resolution. This is coupled to the end of a PWM (Pulse width modulation) bidirectional linear actuator controlled via a Cytron MD10 driver board. The linear actuator could extend to a maximum displacement of 150mm. As the linear actuator extends and loads the specimen, the load cell at the base reads the force simultaneously. The actuator feeds back an analogue voltage proportional to the displacement providing a 1mm displacement resolution. The maximum load that could be applied was 300N.The portable bending rig was then calibrated midrange by placing deadweight loads on the loadcell. The measured span limits of the actuator were checked against a scientific ruler.

Loading was performed on straight sections of fuchsia stems of diameters in the range 7-9mm. A cyclic loading test was performed first so that we could identify the viscoelastic response of the stem over a short period of time. For the cyclic loading, the sample was loaded at 1mm/min until the set displacement, the displacement was then held for 30 seconds and then, unloaded by retracting the linear actuator at the same rate. The specimen was then loaded again after 30 seconds, and the cycle repeated. This process was repeated 4 times.

Following the cyclic tests, a sample was loaded in three-point bending and then unloaded rapidly and left for 10 minutes to recover. It was further subjected to another three-point loading test to determine the response of the stem given more time to recover.

For the repair tests, a total of 14 samples were tested. The initial diameter was measured at the location where maximum bending stress was applied. The repaired diameter was measured at the same site but after the repair time had elapsed. The section of stem below the wound was measured after repair. This provides us with a useful comparison to differentiate between a repair response and general growth of the stem. Nine samples were tested for a period of four weeks, and five samples for a period of eight weeks. Samples were initially loaded at a constant displacement of 1mm/min until a displacement between 50mm and 60mm. Stems were rapidly unloaded for these tests. The same target was set for the second test but often could not reach it due to limitations such as other obstructing stems. Samples were loaded in the same orientation before and after healing.

5.2.3 Anatomical analysis

Macroscopic overview images of stem cross-sections were captured on fresh plant material using a stereomicroscope (Olympus SZX9) equipped with a camera (ColorView II, both Olympus Corporation, Tokyo, Japan) and Cell^D imaging software (Version 2.6, Olympus Soft Imaging Solutions GmbH, Münster, Germany).

Samples for anatomical analyses were embedded in Technovit (a fast-curing cold polymerizing resin) following a protocol according to manufacturer instructions (Technovit 7100, Kulzer Technik, Hanau, Germany). After curing, 5 μm thick cross sections were cut using a rotary microtome (CUT 5062, SLEE medical GmbH, Nieder-Olm, Germany) and stained with a 0.05% aqueous solution of toluidine blue for about 3 min, then rinsed with distilled water. Binding to electrons, it stains Cytoplasm, RNA and un-lignified cell walls red while DNA structures and lignified tissues are stained blue or green-blue. The stained sections were analysed and captured under a light microscope (Olympus BX61, Olympus Corporation, Tokyo, Japan) equipped with a camera (DP71, Olympus Corporation, Tokyo, Japan) using Cell^P imaging software (Version 2.6, Olympus Soft Imaging Solutions GmbH, Münster, Germany).

Microtomographic analysis of the samples was conducted using a high-resolution 3D X-ray scanner (Bruker Skyscan 1272, Kontich, Belgium). 360° scans with a rotatory step size of 0.3° and a spatial resolution of 5-6μm were performed and NRecon software (Version 1.6.10.1, Skyscan, Kontich, Belgium) was used for data reconstruction (applying ring artefact reduction

and beam hardening correction). CTVox software (Bruker, Kontich, Belgium) was used for data visualization.

5.2.4 Finite element analyses

To account for the growth that occurs alongside repair, correction factors were determined. These correction factors would account for the effects of an increased diameter on three-point bending so that the effective diameter was the same for the initial test and the repair test. To quantify the effects of varying diameters on three-point bending and to calculate these correction factors, a finite element model was developed using Ansys 2021 R2. The base geometry for the stem was set to be 8mm in diameter with a span of 15cm. The model used the same loading, supports and applied symmetry as in previous work (1). The model made use of material that performs in a similar way to fuchsia under loading in that it forms a plastic hinge under large deformation. This included a Young's Modulus of 200GPa, a Bilinear Yield Strength of 250MPa (assuming no work hardening) and a Poisson's ratio of 0.3. Simulations were performed while varying the diameter at regular intervals (1mm and 0.5mm where needed) from 7mm to 12mm. The simulation provided a force reaction at the moving support similar to that on the portable three-point bending rig. The force reaction recorded over the entire three-point bend test was averaged and compared to that of a plain theoretical stem, which had a new diameter, accounting for the effects of normal growth. This was performed to find the correction factor that we could use to multiply the experimental data by to get the normalised data.

FEA was also used to determine how much damage had occurred in the cyclic loaded and rested specimens. This was done by applying mechanical properties to the model described so that the force displacement curve equated that of the specimen in its initial loading phase. These mechanical properties were then reduced until the second loading curve was emulated, providing an indication of how much damage had occurred.

5.2.5 Statistics
Statistical analysis was performed using Excel (2019), and involved comparing parameters from four and eight week periods of repair. T-tests were performed at a significance level defined at p = 0.05.

5.3 Results and Discussion:

It is important to differentiate between viscoelastic behaviour and repair when studying a material's response to loading. The viscoelastic behaviour and damage were approximately determined by performing cyclic loading tests on live fuchsia stems (Figure 5.4) which demonstrated how live plant stems respond to loading and relaxation cycles.
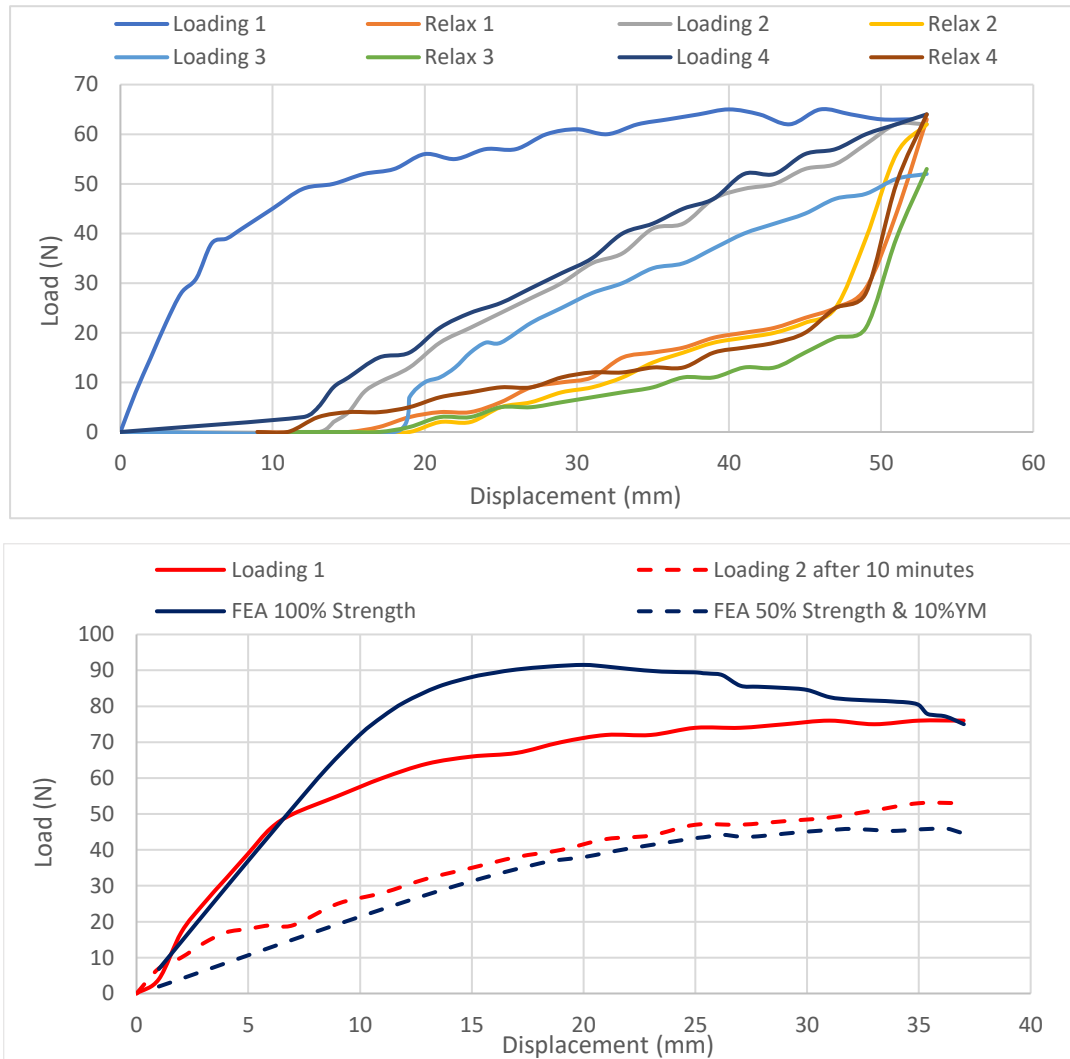
Figure 5.4: (a) Cyclic loading test on live fuchsia subject to three-point bending. (b) Three-point bend tests on stem with 10-minute interval compared to FEA model of 100% strength and 50% strength with 10% Young's Modulus.

The initial loading phase (labelled "loading 1") begins with a settling-in period (up to load of 10N) during which the stem makes full contact with the loading rig. Subsequent load/displacement behaviour has been studied in detail in our previous work (1): it begins with an initial steep rise in the curve characterised by elastic behaviour, with some viscoelasticity causing the slope to gradually decrease. As displacement increases the load levels off to a maximum value, at which stage the stem has experienced yielding and damage on its

compressive side (i.e. close to the central loading point) whilst the rest of the stem remains undamaged. Further increases in the displacement (not shown here) cause the load to decrease as damage spreads across the stem. Since the aim of the present work was to induce a controlled amount of damage the loading was stopped at a displacement of 50-60mm. The subsequent unloading and reloading shows considerable hysteresis typical of viscoelastic behaviour. The slope of the reloading line ("loading 2") is much lower than that of the initial line, indicating that damage has occurred. However, this line reaches the same load at a displacement of 52mm, demonstrating the load-bearing capacity of the remaining undamaged section of the stem. Further cycles of unloading and reloading show relatively little change, with a hysteresis cycle indicating viscoelastic behaviour, though by the third load cycle there is a small decrease in load, indicating some further damage has occurred.
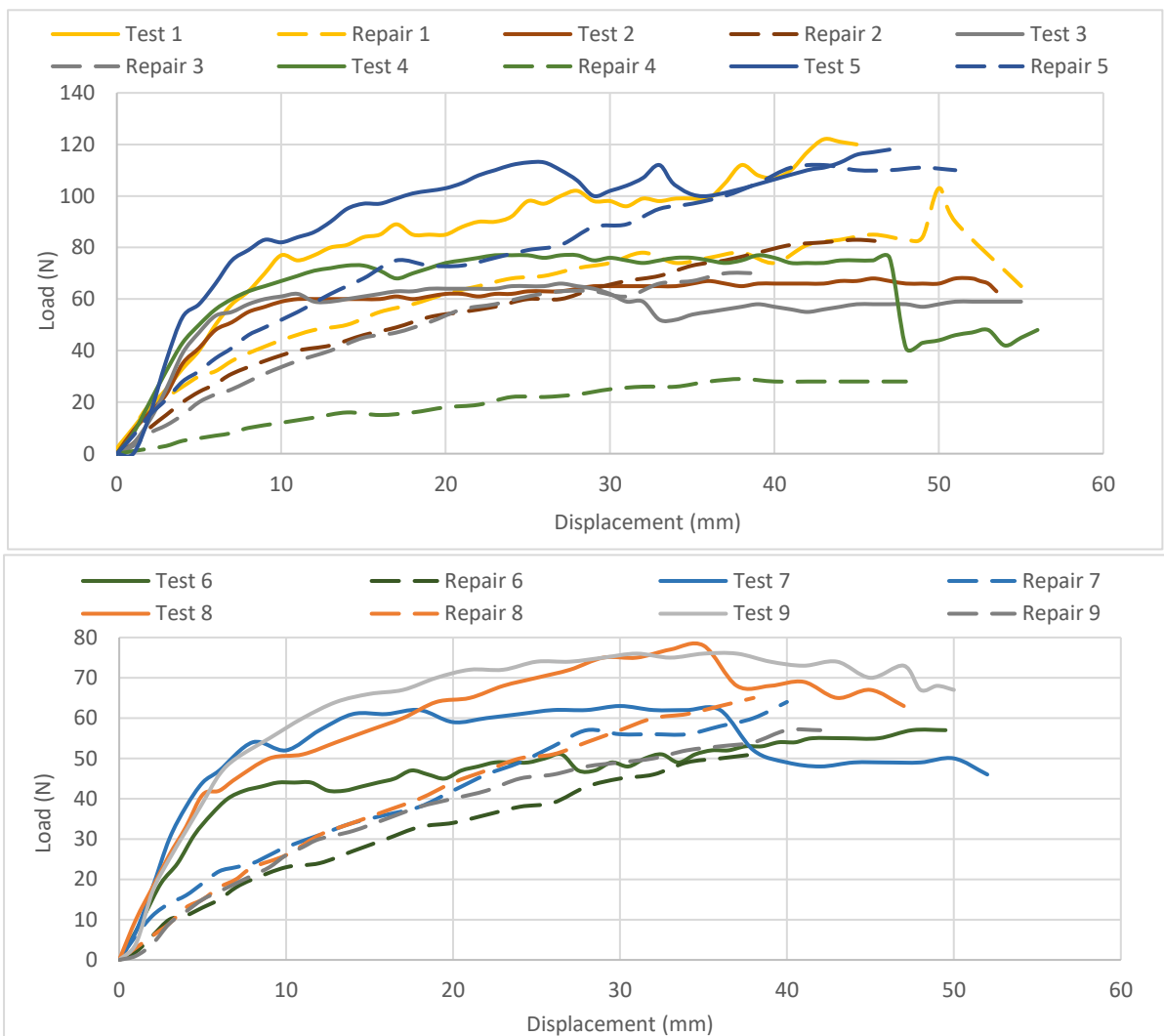
Figure 5.5: Load/extension curves of 9 fuchsia stems subject to damage by three-point bending, left for four weeks to repair and then re-tested. In each case the initial loading line is marked "Test" and the loading line for the same stem after four weeks is marked "Repair".

Figure 5.5 shows the results of the experiments in which living stems were loaded, unloaded, left for a four week period and then reloaded. It is clear that the degree of repair differs from sample to sample. Some specimens were significantly compromised after repair in that they could not withstand the load they could previously. Two repaired samples were able to withstand a greater load than in the original test. This is an indication that mechanical repair could be occurring in periods as short as 4 weeks. It can also be noted that Test specimens 1, 2 and 7 were of stems with leaves that were optimally exposed to sunlight. Samples 3, 8, and 9 had leaves with very poor access to sunlight. This may have some implication on repair results.
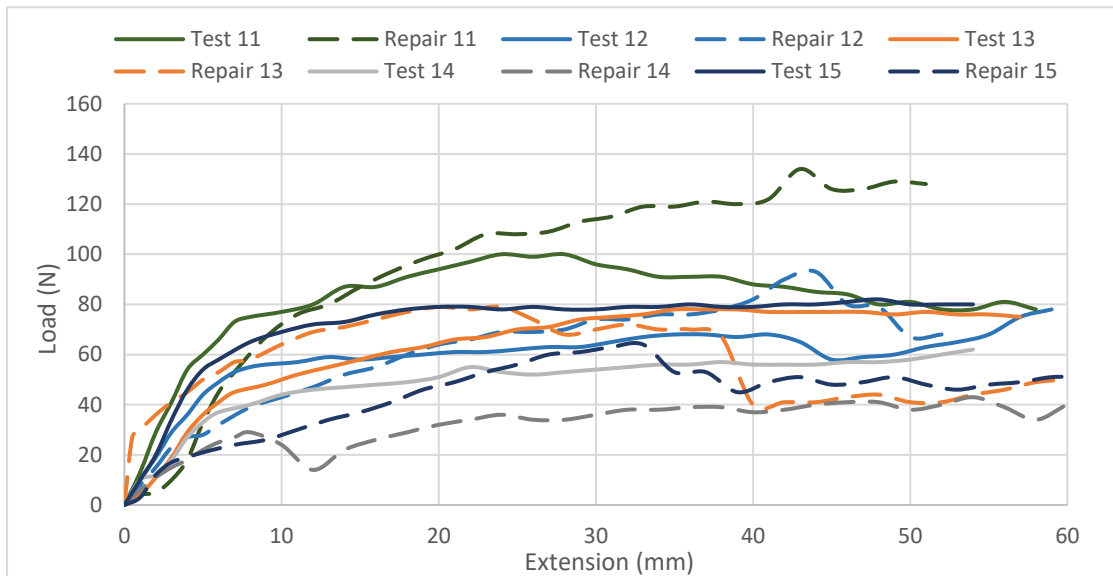
Figure 5.6: Tests of live fuchsia stems loaded and then left for 8 weeks to repair.

Figure 5.6 shows results after 8 weeks of healing, showing significant changes compared to 4 weeks. Here the reloading lines are more similar to the first loading lines, and in some cases higher. Specimens from tests 11 and 13 had the best exposure to sunlight.

Table 5.1 demonstrates the repair response of the fuchsia on the diameter of the stem. Table 5.2 compares the results from samples left for four weeks to repair with those left from 8 weeks. It is clear that even after four weeks all stems increased their diameter and there is another statistically significant increase from 4 to 8 weeks. We can also see that the difference in diameter at repaired section to diameter just below is significantly different meaning the diameter increased by more than it would have during normal growth.

Table 5.1: Diameter of stems before and after repair with diameter below the repaired site to account for growth. Specimens 1-10 were given 4-weeks to heal and specimens 11-15 were given 8 weeks to heal.

Specimen	Initial Diameter (mm)	Repaired Diameter (mm)	Diameter of stem just below wound, after repair (mm)	Difference in repaired section and initial diameter (mm)	Difference in repaired section and region below diameter (mm)
1	9	10.5	10	1.5	0.5
2	7.5	9	8.5	1.5	0.5
3	8	9	8.5	1	0.5
4	7.5	9	8	1.5	1
5	8	9.5	9	1.5	0.5
6	7.5	8.5	8	1	0.5
7	8.3	10.5	9	2.2	1.5
8	8	8.5	8	0.5	0.5
9	8.5	9	8.5	0.5	0.5
10	8	8.5	8	0.5	0.5
11	9	14.5	12	5.5	2.5
12	8	10	8.5	2	1.5
13	9	13	10	4	3
14	8.5	11	8.5	2.5	2.5
15	8.5	12.5	10	4	2.5

Table 5.2: Statistic from table 5.1 comparing results from 4 weeks of healing to 8 weeks of healing.

	Difference in repaired section and initial diameter	Difference in diameter at repaired section to diameter just below
Average (4 weeks)	1.17 mm	0.65 mm
Average (8 weeks)	3.6 mm	2.4 mm
St Dev (4 weeks)	0.568	0.337
St Dev (8 weeks)	1.387	0.548
T-Test p value	0.00028	0.000003

Figure 5.7: Specimen damaged and left to heal for 8 weeks. Callus has formed around the damaged area. Red arrow pointing to small amounts of compressive damage where the support pressed on the specimen during bending.

Figure 5.7 gives a clear visual indication of just how much plants respond to damage. The stem was subject to three-point bending at the point indicated by the red arrow. A callus has grown and formed around the damaged zone and is primarily responsible for the increased diameter. However, there appears to be no formation of the callus at the site where loading took place. The callus is an aggregation of parenchyma cells that form shortly after wounding (13). These are thin-walled living cells with relatively poor mechanical strength found in leaves, wood, bark and other tissues. In the weeks and months after the callus forms, it becomes lignified, loses its ability to divide and is often covered by the development of other tissues. The callus forms a cambium layer which has the effect of significantly increasing the diameter. The stem itself appears relatively unharmed except for the small indent which is a result of compressive damage from the support in the three-point bend test.
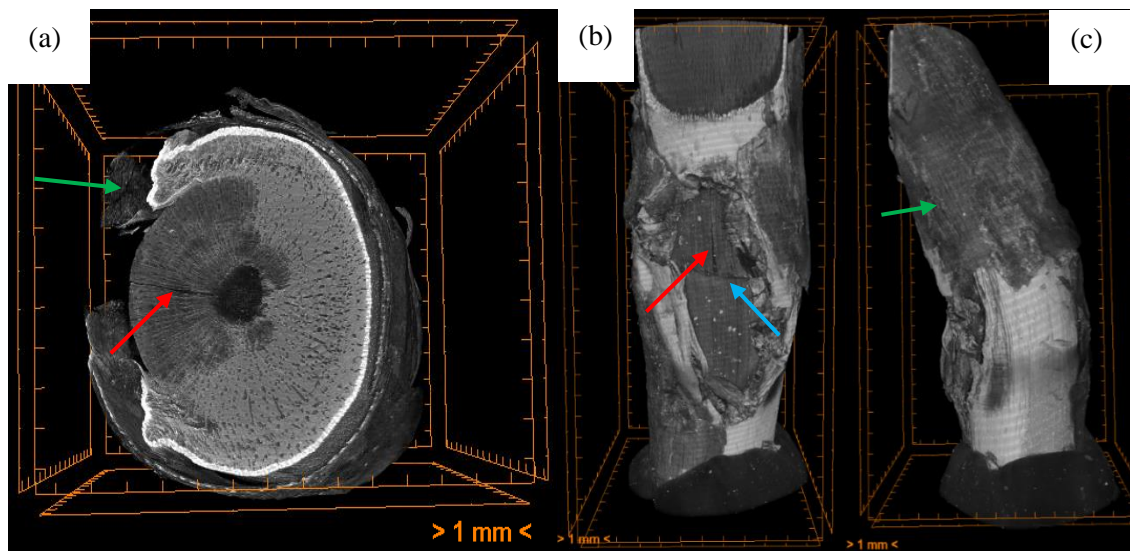
Figure 5.8: Micro CT scans of damaged fuchsia. (a) Cross sectional view, (b) Isometric view of damaged side of stem and (c) Isometric view of back of stem.

Micro CT scans were performed on a specimen which was subject to three-point bending and left to repair (figure 5.8). Loading took place at the site indicated by the green arrow. The repaired specimen shows a large build up of tissue around the damaged site when observing the cross section (Figure 5.8a, b and c). However, there is no new tissue at the exact point of loading. The build up of tissue is sometimes referred to as a wound callus consisting of undifferentiated cells. A small fissure can also be seen, indicated by the red arrows in figure 5.8a and b. The fissure seen is a result of a longitudinal crack that initiates on the compression side of the three-point bend test. This crack forms as a result of ovalisation similar to that seen in previous work (1). Ovalisation has the effect of altering the second moment of area resulting in increased tensile stresses at their circumference and splitting of the fibres. The blue arrow indicates the compressive damage that occurs on the concave side of the stem during three-

point bending. Due to limited access to laboratories during Covid-19 these scans were taken of the sample 9 months after repair had taken place. However, these months were during autumn and winter where limited growth and hence repair is likely to take place.

Toluidine blue staining provides differentiation between the different cell types. Figure 5.9 a is a damaged specimen with no repair. It has a large fissure significantly distorting its geometrical integrity. Figure 5.9b is of the same specimen which has been left for 9 months after repair as figure 5.8. The cambium has been ruptured and as a result freshly divided cells can be seen in the bulge where the black arrow is pointing. The fissure can be seen to be much smaller; this may be a result of new parenchyma cells pressing the fissure back together.
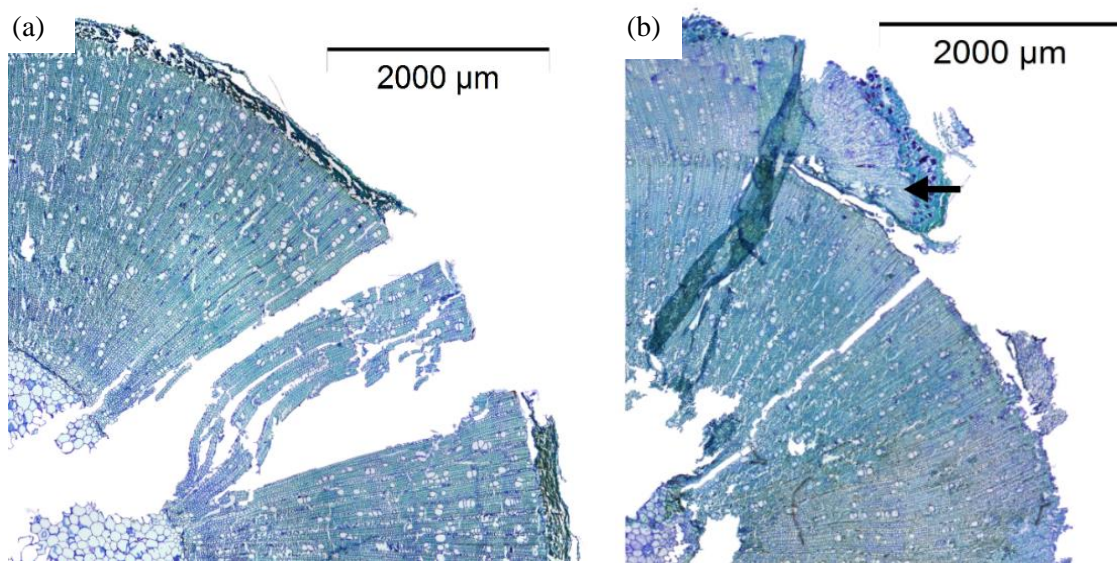
Figure 5.9: Toluidine blue staining on (a) damaged specimen (b) repaired specimen.

Figure 5.10a provides an overview of the reaction of a stem to damage and figure 5.10b an overview of how the stem repairs once damaged. Loading has occurred at the point where the fissure meets the circumference of the stem. The brown discolouration around the crack (figure 5.10a) is due to chemical inclusions in the cell walls that seals the wound and protects it from the entry of bacteria and fungi. In figure 5.10b it can be seen that this area has increased, and a visible protective layer has formed on the wound directly around the crack. The branch also demonstrates secondary thickness growth. In the area of the wound, woundwood has formed that covers the wound and forms the characteristic wound collar (which can been seen clearly in figure 5.8 of the microCT scan). Woundwood can be formed after the callus forms a cambial layer (13) or sometimes directly from the cambium after wounding. Woundwood has unique properties in that it can contain compounds toxic to fungi and a cellular structure that is highly organised when compared to a callus.
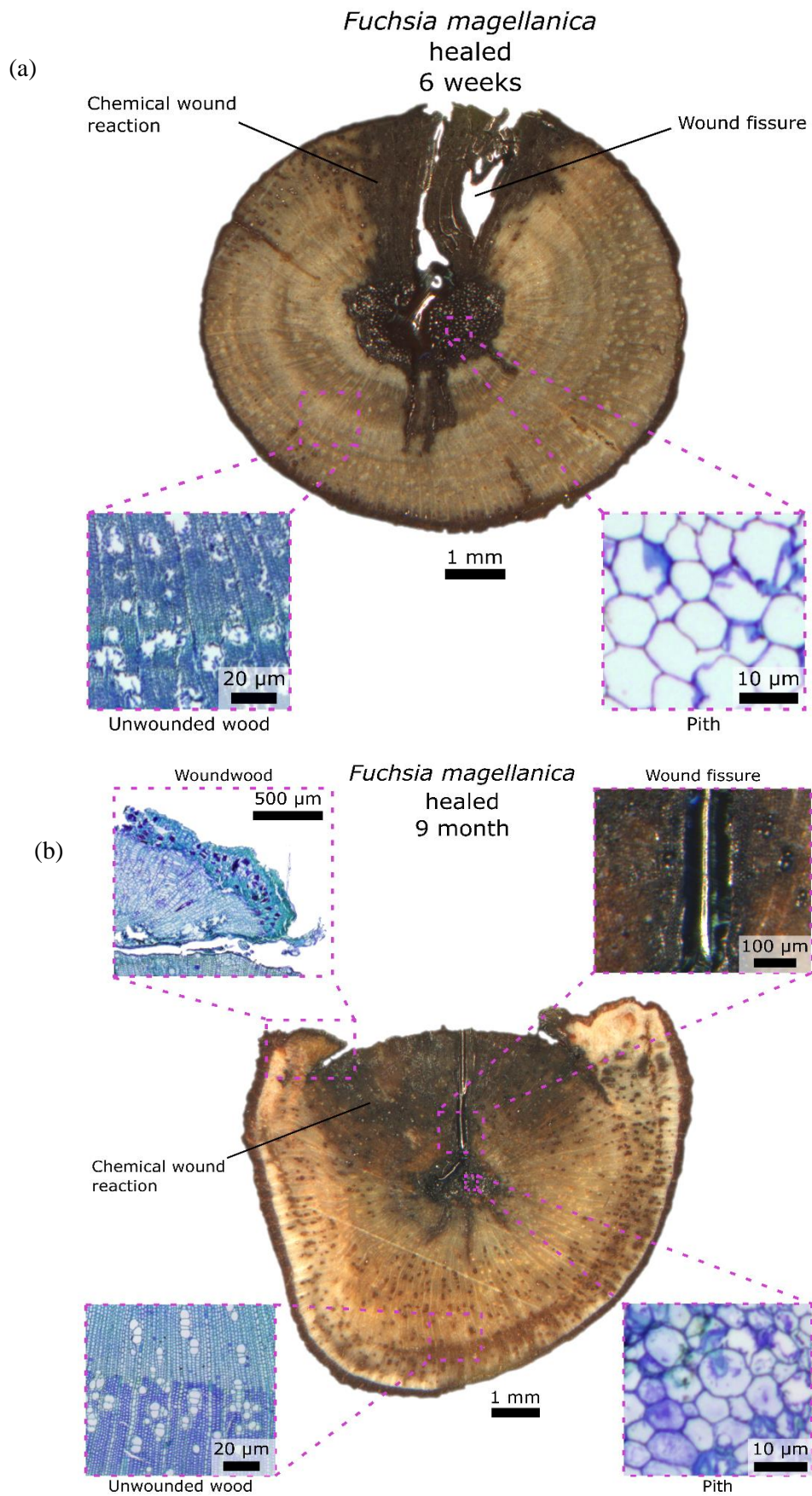
Figure 5.10: (a) Combination of binocular and stain microscopic images for (a) damaged fuchsia with no signs of healing (b) fuchsia that has demonstrated healing abilities and left for 9 months.

Figure 5.11: Effective load displacement curves adjusted from FEA correction factors on specimens left for 4 weeks to repair for (a) samples 1-5 and (b) samples 6-9

Figure 5.11 (a) and (b) focuses on specimens left for 4 weeks to repair with the correction factors applied to the initial tests to account for the new growth. As we can see, most of the stems are now weaker than they would have been if they had not been damaged.

Adjusted curves for 8 weeks of repair (Figure 5.12) demonstrate that some of the stems return close to their original maximum strength after repair. Test 5.12 grew an extra 3mm in diameter which was greater than most by a significant amount which explains the dramatic increase in load.
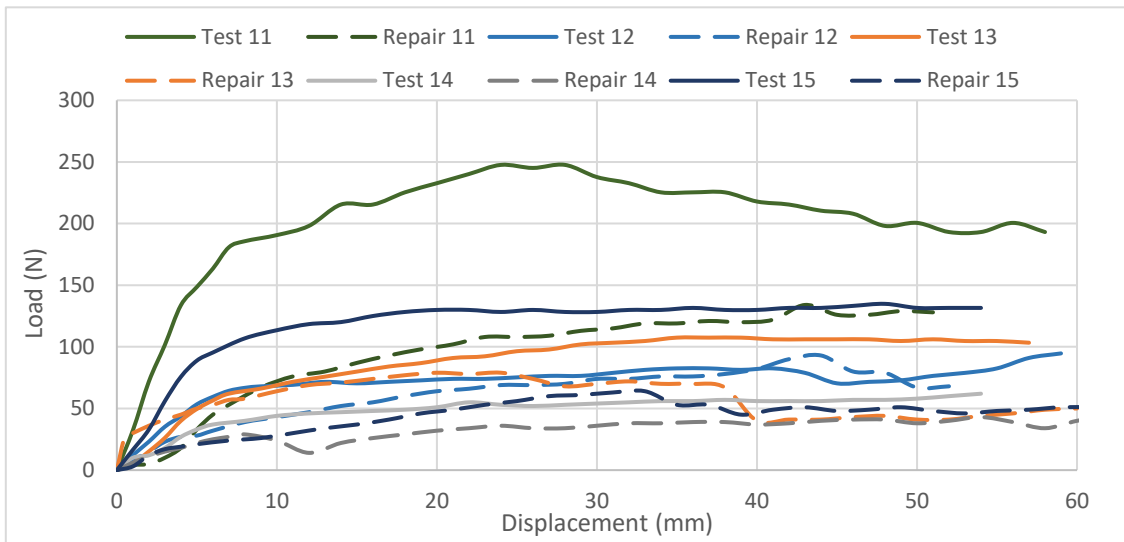
Figure 5.12: Effective load displacement curves adjusted from FEA correction factors on specimens left for 8 weeks to repair.

To adequately measure and quantify the implications of repair on mechanical properties, damage and repair coefficients of different parameters were calculated to determine what properties were restored. The coefficient made use of the same formula as equation 5.1 where the damaged specimen was compared to the repaired specimen. The following parameters were chosen as they provide an indication of how damage has affected key mechanical properties required for the survival of the stem. The initial slope is effectively the stiffness of the stem and is primarily responsible for resisting bending force from sources such as wind. The load at 30mm and maximum load aid in defining the stem's strength from yielding right through to just before compete failure. Finally, the energy is an important parameter as it accounts for both load and displacement. A plant's ability to absorb energy will likely impact its chances of survival upon sudden impact and damage. These same parameters were used when studying defect tolerance.

Table 5.3: Damage coefficients for cyclic load tests and test given 10 minutes to recover.

	Initial slope	Load at 30mm	Max Load	Energy at 40mm
Coefficient for cyclic loading comparing the first and second cycles	0.269	0.557	0.954	0.373
Coefficient for loading with 10min interval	0.462	0.645	0.697	N/A

Table 5.3 presents the damage coefficients for different parameters calculated from figure 5.4. In the cyclic loading tests, the maximum load almost returns to its original value. It must be noted that the stems had limited accessibility and the maximum load may not have been

reached. Given that definite yield points could not be accurately determined, the initial slope was calculated at 5mm extension. Considering both load and extension, energy was dramatically compromised in that the damage coefficient was significantly lower than that of other parameters. During the 10-minute resting period, stiffness was improved significantly from 0.27 to 0.46. The maximum load of the rested stem appears weaker than in the cyclic test (figure 5.4a). However, given there is only one cyclic test, it may be an exception. We expect that more cyclic tests to greater displacements would not return to the same point. All other parameters have increased given 10 minutes to recover indicating viscoelasticity is present and must be considered to play a role during the healing process. All coefficients have values lower than 1.0 which demonstrate that damage has occurred.

The FEA simulations (figure 5.4b) revealed that, despite the improved parameters as a result of viscoelasticity, the best fit to the experimental results occurred when the yield strength was reduced by 50% and the Youngs modulus by 90%.

Table 5.4: Healing coefficients for samples left for 4 weeks and 8 weeks to repair.

	Initial slope	Load at 30mm	Max Load	Energy at 40mm
Average healing coefficient (4 weeks)	0.44	0.80	0.88	0.69
Average effective healing coefficient (4 weeks)	0.35	0.65	0.72	0.56
Average healing coefficient (8 weeks)	0.73	0.95	1.01	0.84
Average effective healing coefficient (8 weeks)	0.53	0.65	0.69	0.58

Table 5.5: p values for T-tests of various parameters based on the actual, and corrected (effective) values.

T-Tests	Initial slope	Load at 30mm	Max Load	Energy at 40mm
Coefficient	0.080	0.236	0.369	0.207
Effective coefficient	0.159	0.959	0.818	0.817

Table 5.4 uses the same formula provided above (Equation 5.1) to calculate the healing coefficient of the same parameters as Table 5.3. Looking at all the parameters it is observed that 8 weeks of healing offers some improvement over 4 weeks of healing indicating that repair in fuchsia is a gradual process. However, this is not backed up by the t-tests as the p-value is greater than 0.05 for all parameters indicating further testing is needed to fully verify the claims. The p value for the slope is 0.159, which is much lower than the other three parameters and is approaching significance since this means that there is only a 15.9% chance that it's not significant. Once the correction factors are applied to take account for the new growth, the

healing coefficient is significantly reduced when compared to the initial cyclic loading tests. Lignified tissue plays a key role in providing mechanical strength to the stems. The lignin cross-links with hemicellulose and embeds the cellulose. By doing so it makes the tissue less compressible and therefore strengthens it at the same time (14). Lignification of fresh tissue occurs over months rather than weeks. Given considerably more time we would expect to see an improvement in this healing coefficient.

The initial slope (figure 5.5) demonstrates evident healing properties, especially compared to the cyclic loading. Once the correction factors are applied the values reduce but still show signs of improvement. It appears slope is the most sensitive measure of repair as it increased from 4-8 weeks by 51%. Stiffness is also correlated to the density of lignified tissue, which is limited in the repaired samples. Contrasting the images in Figure 5.10 demonstrates differences in geometry between a specimen that has self-sealed and one that has self-healed. The ovalisation of the self-healed specimen (figure 5.12b) may influence stiffness in that there is an increase in the second moment of area resisting the bending. It is reasonable to believe that this is an intentional response from the plant as similar behaviour has been seen before in trees where a bias in loading on one side of the trunk resulted in a thickening of the other side (15).

The energy absorbed can be seen to have improved, even when the correction factors were applied. The callus acts like a splint for the stem, as seen in the micro-CT scans (figure 5.10). Small cracks remain in the longitudinal orientation as well as compressive damage (figures 5.9 and 5.10). The plant's response appears unable to heal these fibres but rather keeps depositing new material around the damaged zone. The increased volume of material has the capacity to absorb more energy during loading. This new material is predominantly composed of parenchyma cells which have the capability to deform and deflect without rupture, at least not any that were observed from the microscopy. The change in geometry will also impact the energy absorbed as there are greater moments to overcome.

Figure 5.10a shows a large fissure dividing the cells from the core to the circumference which will present the stems with adverse impacts on all of the parameters discussed above. This is due to the stem deforming unfavourably during three-point bending by reducing the effective second moment of area. Figure 5.10b demonstrates that although the fissure has not yet been sealed, it can be compressed and reduced to a very fine line, significantly improving the mechanical and geometrical integrity of the stem. Given more time it is expected that this fissure would fully seal.

This study has verified that fuchsia has the capability to repair damage given sufficient time in the growth seasons of spring and summer. Specimens given 8 weeks to repair experienced significantly more growth in diameter relative to those given 4 weeks. They also appear to have improved mechanical properties, however this was not confirmed with T-tests. It can be noted that the same repair tests were attempted during the winter months and no new growth or repair was observed. Additionally, cuts were inserted half-way through the cross section of the stems, and whilst the stems did not die, they were not able to repair the damage.

5.4 Conclusions:

This study has revealed that fuchsia has the capability to repair damage in the appropriate growing season. However, it does not have the ability to fully restore all of its mechanical properties in the timeframe provided for these tests. Lignification plays an important role in complete recovery which can be a prolonged process. By analysing various parameters including diameter of the stem and data extrapolated from force/displacement curves we present an insight into understanding what type of damage is being repaired. The biggest difference between specimens with cyclic induced damage and specimens left to rest for ten minutes is the slope of the curve. This provides an indication that viscoelasticity is accountable for improvement in stiffness over short periods of time.

Specimens left for four and eight weeks to repair had an average increase in diameter of 0.65 ± 0.33mm and 2.4 ± 0.54mm respectively to the damaged sections. T-tests revealed that the repair over an eight-week period is significantly different to that of four weeks. Specimens held for eight weeks demonstrated the ability to restore 73% of their stiffness, 101% of their maximum load and 84% of the energy absorbed. This arises from a number of factors that include the sealing of fissures inflicted during initial loading, large deposits of parenchyma cells in the form of a callus and woundwood, and finally change in geometry and effective second moment of area. Once correction factors were applied the effective diameters were comparable, resulting in the specimen performance being reduced significantly. However, this does not mean self-repair was not present as a dramatic change in the shape of force displacement curves could be witnessed as well as preventing further deterioration of the stem in the interim period.

We believe that this pilot study should lead to an improved understanding of the processes involved in the damage and repair of plant materials subject to bending. This was a pilot study to develop methodologies for this kind of experiment, which is completely new. Although the study was limited to Fuchsia, we believe that the findings may be applied to other botanical

materials, albeit with caution. From an engineering standpoint the study has relevance where natural materials are used, for example in the construction industry. The findings are also important when developing artificial materials which mimic the properties which plants demonstrate. While work in this area is still in the early stages, the development of materials with improved ability to withstand cracking and to self-repair has huge implications in terms of both cost savings, longevity, and safety in a wide range of applications.

This work has some limitations in that we only considered three-point bending and sample sizes were limited due to availability. Further research in gathering more data on the repair of plant stems using different bending methods and allowing the plants more time to recover would provide a more in depth understanding of the self-repair response of plants to damage from bending.

5.5 References

1. Hone T, Mylo M, Speck O, Speck T, Taylor D. Failure mechanisms and bending strength of *Fuchsia magellanica* var. *gracilis* stems. J R Soc Interface [Internet]. 2021 Feb 17 [cited 2021 Mar 11];18(175):20201023. Available from: https://royalsocietypublishing.org/doi/10.1098/rsif.2020.1023

2. Hone T, Kelehan S, Taylor D. Fracture and repair in a bio-inspired self-healing structure. Fatigue Fract Eng Mater Struct. 2021 Dec 1;44(12):3373–83.

3. Mylo MD, Krüger F, Speck T, Speck O. Self-Repair in Cacti Branches: Comparative Analyses of Their Morphology, Anatomy, and Biomechanics. Int J Mol Sci 2020, Vol 21, Page 4630 [Internet]. 2020 Jun 29 [cited 2021 Oct 20];21(13):4630. Available from: https://www.mdpi.com/1422-0067/21/13/4630/htm

4. Paul-Victor C, Dalle Vacche S, Sordo F, Fink S, Speck T, Michaud V, et al. Effect of mechanical damage and wound healing on the viscoelastic properties of stems of flax cultivars (Linum usitatissimum L. cv. Eden and cv. Drakkar). PLoS One. 2017;12(10):1–23.

5. Wilson JW, Dircks SJ, Grange RI. Regeneration of Sclerenchyma in Wounded Dicotyledon Stems. Ann Bot [Internet]. 1983 Sep 1 [cited 2021 Oct 20];52(3):295–303. Available from: https://academic.oup.com/aob/article/52/3/295/91066

6. Busch S, Seidel R, Speck O, Speck T. Morphological aspects of self-repair of lesions caused by internal growth stresses in stems of Aristolochia macrophylla and Aristolochia ringens. Proc R Soc B Biol Sci. 2010;277(1691):2113–20.

7. Fisher JB, Ewers FW. Wound Healing in Stems of Lianas after Twisting and Girdling Injuries. https://doi.org/101086/337770 [Internet]. 2015 Oct 19 [cited 2021 Oct

20];150(3):251–65. Available from:
https://www.journals.uchicago.edu/doi/abs/10.1086/337770

8. O'Neill M, Taylor D. Repair of microdamage caused by cyclic loading in insect cuticle. J Exp Zool Part A Ecol Integr Physiol [Internet]. 2020 Jan 1 [cited 2021 Dec 16];333(1):20–8. Available from: https://onlinelibrary.wiley.com/doi/full/10.1002/jez.2329

9. Speck O, Speck T. An Overview of Bioinspired and Biomimetic Self-Repairing Materials. Biomimetics 2019, Vol 4, Page 26 [Internet]. 2019 Mar 20 [cited 2021 Oct 20];4(1):26. Available from: https://www.mdpi.com/2313-7673/4/1/26/htm

10. Lucas SS, Von Tapavicza M, Schmidt AM, Bertling J, Nellesen A. Study of quantification methods in self-healing ceramics, polymers and concrete: A route towards standardization. J Intell Mater Syst Struct. 2016 Nov 1;27(19):2577–98.

11. Cohades A, Branfoot C, Rae S, Bond I, Michaud V. Progress in Self-Healing Fiber-Reinforced Polymer Composites. Adv Mater Interfaces [Internet]. 2018 Sep 1 [cited 2021 Oct 20];5(17):1800177. Available from: https://onlinelibrary.wiley.com/doi/full/10.1002/admi.201800177

12. Diesendruck CE, Sottos NR, Moore JS, White SR. Biomimetic Self-Healing. Angew Chemie Int Ed [Internet]. 2015 Sep 1 [cited 2021 Oct 20];54(36):10428–47. Available from: https://onlinelibrary.wiley.com/doi/full/10.1002/anie.201500484

13. Callus v. Woundwood. [cited 2021 Nov 16]; Available from: www.isa-arbor.com

14. L. Salmén, "Micromechanical understanding of the cell-wall structure," C. R. Biol., vol. 327, no. 9–10, pp. 873–880, Sep. 2004, doi: 10.1016/J.CRVI.2004.03.010.

15. Mattheck C (Claus), Kubler H. Wood : the internal optimization of trees. Springer; 1997. 129 p.

Chapter 6 Conclusions, General Discussions and Future Work:

6.1 Conclusion:

Plant stems have complex structures being cellular, anisotropic and viscoelastic, whereas conventional engineering materials can be considered relatively homogeneous compared to plant stems. Fibre composites such as carbon fibre are finding more and more applications in modern engineering. Nature has evolved its fibre composite structures to be strong, light and tolerate damage without catastrophic failure. By understanding the intricacies responsible for this, I hope to inspire new structures in modern engineering materials with more impressive mechanical properties. The study was partially assisted by the Plant Biomechanics Group in the Faculty of Biology at the University of Freiburg, Germany who provided expertise in understanding the biology behind the unusual responses of these plant stems when subject to three-point bending.

This work has focused on the failure mechanisms, defect tolerance and repair of plant stems alongside the development of a bi-inspired self-healing structure. The main plant stem investigated was from fuchsia (*Fuchsia magellanica* var. *gracilis*), which was then compared and contrasted against two other species, elder (*Sambucus nigra*) and ash (*Fraxinus excelsior*). These species were chosen as they all can fail with different failure mechanisms and all had different cross-sectional tissue patterns. Various models were developed to aid in understanding the failure mechanisms and properties responsible.

The first study began with investigating the failure mechanisms and bending strength of fuchsia; three-point bending being used to simulate bending similar to that generated by wind. Fuchsia was initially chosen for the study as it was readily available and was of shrub like material on which there had been little previous work. However, it revealed itself to be a very interesting species to investigate in that it could fail with one of two different failure mechanisms, indicating its mechanical properties were almost perfectly balanced. It could fail with either a greenstick fracture or what I am calling a plastic hinge fracture. These failure mechanisms had previously been identified in other species by Ennos and van Casteren but not fully investigated. Performing microCT revealed how the stems were reacting internally to the stresses from three-point bending. While it might have been expected that the crack commenced at the point of bending, microCT showed that the crack started at the core of the

stem and penetrated outwards. This surprising novel discovery of the development of an internal crack, resulted from ovalisation and a reduction in the second moment of area. This phenomenon later provided inspiration for the self-healing structure.

Mathematical modelling made use of plastic bending theory while also taking account of this internal crack and the orthotropic properties of the stems, where the tensile strength is much greater than the compressive strength. This modelling was accurate but required the addition of a correction factor to account for the slippage that occurs on the supports during three-point bending. The correction factor was found by developing a bilinear plastic FEA model in symmetry that would mimic the three-point bending rig and fuchsia stem. The greenstick fracture was different in that a crack would initiate on the tensile side of the stem, propagate through the cross section until a point which the ratio of the transverse stresses to the tensile stresses would change and the crack would turn 90 degrees and propagate longitudinally. Staining techniques and microscopy aided in determining that the greenstick fracture would occur in denser more lignified stems.

The second study is novel in that by taking inspiration from the observed internal failure mechanisms in fuchsia stems, I developed a self-healing structure. Most studies on self-healing focus on the material rather than the structure. This is where this study is unique and novel. The self-healing mechanism used was composed of a resin and hardener system in alternating vascular channels, similar to that found in previous work. However, I designed the vascular channels so that they would replicate the vascular channels found in plant stems used for transporting food and water. The concept is that once a crack begins to propagate, resin and hardener should mix and cure, repairing the crack. A common issue with the majority of these self-healing systems that make use of a resin/hardener system is that the fluid will leak out through external cracks that occur during damage development and before the resin/hardener mix has time to cure. By making use of my previous discovery of the internal crack that forms during three-point bending, I designed a novel structure that would begin to fail with an internal crack that would propagate outwards during three-point bending. The development of an internal crack suggests that the material could heal from the inside without losing healing agents. This structure also displayed impressive energy absorption properties by deformation and fracture of cell walls. With the introduction of healing agents, the resulting structure was capable of near-perfect self-healing, that could restore its original mechanical properties, even after significant damage. A FEA simulation was able to predict the early-stage deformation and damage initiation. This paper was published by the Journal of Fatigue and Fracture of Engineering Material and Structures, 2021. The development of this self-healing structure could have a magnitude of applications for engineering materials. These include applications

where sudden failure could have catastrophic consequences for safety; situations where failure results in the item becoming unserviceable, for example when wind turbine blades delaminate, and in bioengineering applications.

While a comprehensive understanding of the failure mechanisms of plant stems during three-point bending had been achieved, little was known of how they would respond to damage. The third paper involves investigating what I'm calling defect tolerance of three different plant species, Fuchsia, Ash and Elder. Defect tolerance is a material's ability to resist the effects of damage on its mechanical properties. This study involved developing a new approach for quantifying defect tolerance by comparing plain and notched specimen parameters obtained from three-point bend tests on the three different species of plant stems. A custom-built rig ensured that consistent accurate cracks of the same shape and depth could be made in each specimen before subjected to three-point bending. The three species were compared with each other and idealised materials subjected to FEA simulations. The model made use of plastic, tough and elastic brittle hollow, and plain idealised materials. The FEA was also used to create correction factors to account for the different diameters of each specimen so that they could be normalised as if they were all 8mm and so all specimens could be compared irrespective of geometry. Microscopy and imaging techniques provided an insight into the different stems' composition and properties. The study revealed that fuchsia had the best defect tolerance, which again is likely due to its balanced failure mechanisms. All three plant species performed well compared to their appropriate idealised material counterparts. This is likely due to the complex fibrous structures which are known to be defect tolerant. The findings from this study will hopefully provide inspiration for defect tolerant modern engineering materials.

Testing on fuchsia up until this point had been in a laboratory context which does not allow for the investigation of what happens in their natural environment to the stems after the damage has been inflicted. The fourth and final study involved a pilot test to investigate the repair ability of fuchsia. This experiment is novel in that initial damage is inflicted using three-point bending on living stems rather than cutting or slicing the stems. Quantifying repair involved developing a method and formula to reduce parameters to a dimensionless figure which defines the healing coefficient. A tailor made three-point bending rig allowed testing on the plants to be performed in their natural habitat so that repair could occur naturally. Cyclic loading and testing with rest intervals of 10 minutes indicated the presence of viscoelastic properties within the stems. FEA models quantified the damage done during this period. Correction factors were calculated from FEA models, as done previously, to normalise the initial diameter of the stems to account for the natural growth that occurred during the time to repair. Repair tests were conducted on 10 specimens over 4 weeks and 8 specimens over 8 weeks. There were significant improvements

in the parameters over both time periods, indicating the presence of self-healing properties. Some samples even outperformed the initial tests after repair, including when accounting for growth. Microscopy indicated the self-sealing of the fissures and development of callus and wound wood around the damaged area. This new tissue is known to have different mechanical properties which explained the change in shape of the load displacement curve between an undamaged stem and a repaired stem. This paper has established a methodology which can be used in the future to generate publishable results.

The findings are clearly of interest to both the biologist and the engineer. A better understanding of failure, defect tolerance and repair mechanisms in natural materials can but lead to a better understanding of such mechanisms in man-made materials.

6.2 General discussion and future work

The research discussed has led to uncovering new unseen responses and insights into the mechanical behaviour of plant stems when subjected to three-point bending. The novel studies discussed above establish multiple new avenues for further examination in the field of bioengineering.

Working with organic materials is generally a formidable task as it can be challenging to obtain a sufficient number of samples in the appropriate diameters and lengths for testing as well as there being significant scatter in the data. In the first study of this thesis, I investigated failure mechanisms and bending strength of fuchsia. This revealed that the stem could fail either with a greenstick or plastic hinge fracture. In order to gain a greater insight into how density effects this, further testing could be performed to determine a specific value that would alter the failure mechanism. A unique discovery from my work was the formation of the internal crack when an external crack might reasonably be assumed. If it was possible to perform a transverse tensile test to determine the fibre interface strength, it would be possible to more accurately predict the formation of this crack.

One aspect which was not investigated in these experiments was the effects of different loading/strain rates on the three-point bend tests. The loading rate for three-point bend tests in this study were set at 40mm per min, which resulted in different failure mechanisms for different species occurring. However, altering the strain rate is likely to change the failure mechanism for each species, this is because strain rate will affect the materials' elastic properties. Plant stems in nature are subject to all kinds of bending moments, sometimes very

gradual from growth or wetting of leaves and other times very rapidly from storms. Therefore, this opens the possibility for more work to be done in this area.

The greenstick and plastic hinge failure mechanisms may provide bioinspiration for modern engineering materials where a better understanding of different failure mechanisms would assist in reducing the likelihood of catastrophic failure. A perfect application could be in the mast and boom of a ship. These are long beams subject to large bending stresses that arise from wind, similar to what these plant stems experience in nature. A controlled failure would result in the boom or mast deforming without catastrophically failing and potentially sinking the ship.

Developing a self-healing structure rather than a self-healing material is a novel concept. FE simulations have played an important role in verifying and replicating experimental results. FE analysis was particularly helpful for the work in Chapter 3 in designing a structure that would fail from the centre and propagate outwards. When the specimen was subject to compression, I could see that the greatest stresses occurred about the centre of the structure. It was assumed that the fracture was most likely to initiate at this point. However, there is room for further development if damaged development and crack propagation could be modelled. This would provide a more accurate prediction of where the crack would initiate and which direction it would propagate. This will also allow for better positioning of the resin and hardener in alternating vascular channels.

Further investigation would be required in order to identify industrial applications for this structure. Extending this structure to a long cylinder suitable for full scale bending tests would reveal its true potential for repair in bending scenarios. The self-healing structure also has the ability to employ a constant flowing system where the healing agents would be continuously circulated throughout the vascular channels. This has a magnitude of applications, especially in closed tubular structures. A perfect example is a tubular truss bridge, where structures are also subject to bending forces from wind as well by the downward forces from crossing vehicles. Constantly healing small fractures could significantly increase the lifespan and reduce the likelihood of catastrophic failure.

The biomimetic structure also demonstrated impressive energy absorption properties. Further work could be done in optimising this structure for applications where energy absorption is important. For example, crash bars at the front and rear of cars are long beams designed to absorb energy before it is transferred to the structure of the car and passengers. There is already a move to manufacture these items using porous materials. This same principle could be

applied to crash barriers on the sides of the roads. They are essentially long beams that could be designed to absorb more of the impact energy transferred from the vehicle.

Defect tolerance is an interesting concept. However, the current methodology surrounding a framework for quantifying the ability of a specimen to resist damage is relatively undeveloped. The process developed in Chapter 4 on defect tolerance of plant stems has provided a foundation for comparatively studying the ability of natural and man-made materials to resist damage. Each stem performed exceptionally well when compared to similar idealised engineering materials, in their own right. Further work could compare their performance with regards to the "cost", i.e. the total biomass in each case. For example, elder can be seen to be the weakest of the three species. However, it is significantly lighter due to its essentially hollow cross section and therefore has a good strength to weight ratio. Further investigation could also include additional notch shapes and depths to be examined. This type of further analysis may provide inspiration for the development of new material structures where strength to weight ratios are important. A potential example are structures built near earthquake zones. Utilising structures that have the capability to be defect tolerant and deflect during an earthquake could reduce the probability of the structure failing.

The work involving studying the repair mechanisms of fuchsia was performed in the Covid 19 pandemic lockdown of 2020, and therefore there were certain limitations on the availability of laboratory facilities to both develop and modify the three-point bending rig and to perform further experiments using the rig. There was also the issue that there was only time to do a limited number of tests due to the fact repair primarily occurs during spring/summer. I believe if this method was repeated using more samples then the results would be more conclusive and could be published. This could certainly be addressed in future work. From a biologist's perspective further microscopy could lead to a better understanding of the repair mechanisms in the plant stems.

As self-healing and defect tolerance are better understood, healing agents and structures can be further optimised and refined, which could have an impactful effect on modern engineering practice. A potential example is wind turbine blades and masts. Wind turbine blades are fibre composites that are subject to bending from wind, just like the plant stems. They regularly experience delamination of the layers of material in the blades which can cause catastrophic failures. Some wind turbine blades have a life span as short as 15 years and damaged and irreparable blades can be difficult to dispose of using environmentally acceptable methods. Employing a combination of self-healing and defect tolerance structures could improve their lifespan and reduce our carbon footprint. The masts are often subject to huge bending forces.

By introducing a repair system similar to that of a callus on a stem, additional support could form on the mast like a splint and provide resistance to stresses at the damaged site until the mast could be repaired.